Hydrodynamic and morphodynamic response of Perkpolder after a managed realignment

Tim de Wilde

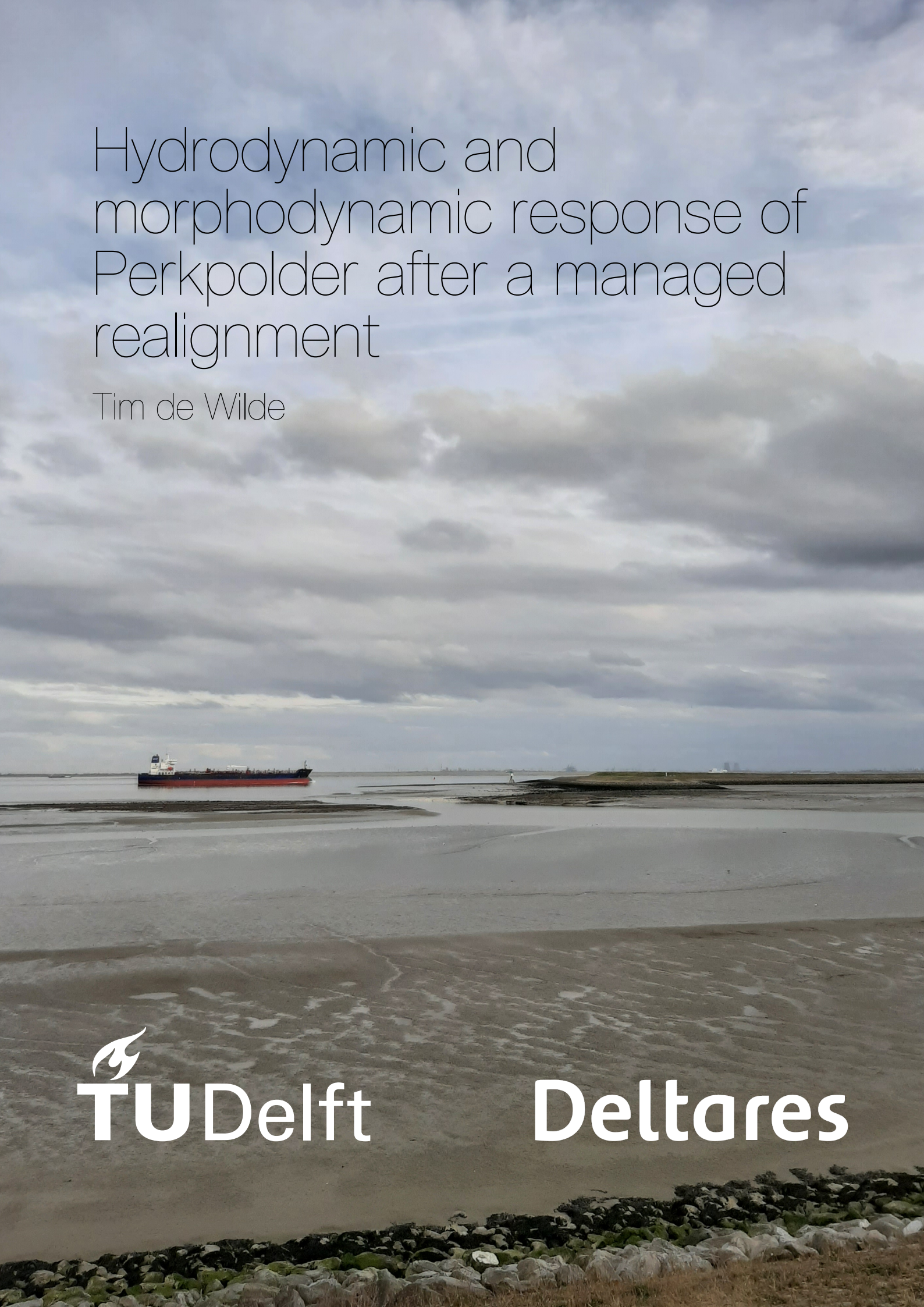

TU Delft Deltares

Hydrodynamic and morphodynamic response of Perkpolder after a managed realignment

by

Tim de Wilde

in partial fulfilment of the requirements for the degree of

Master of Science
in Civil Engineering

at the Delft University of Technology (TU Delft)
to be defended publicly on Wednesday October 5th, 2022 at 14:00.

Student number:	4449916	
Date:	Monday 26th September, 2022	
Chair committee:	Dr. ir. B.C. van Prooijen	Delft University of Technology
Thesis committee:	Dr. ir. P.L.M. de Vet	Delft University of Technology & Deltares
	Dr. D.S. van Maren	Delft University of Technology & Deltares
	Prof. dr. ir. Z.B. Wang	Delft University of Technology & Deltares

An electronic version of this thesis is available at http://respository.tudelft.nl/.

Cover: Inlet of Perkpolder, photo taken when visiting Perkpolder.

This graduation work is part of a project by a consortium consisting of HZ University of Applied Sciences, Royal Netherlands Institute for Sea Research, Wageningen Marine Research and Deltares commissioned by Rijkswaterstaat. Data presented in this thesis are sampled and provided by these institutes to enable this study.

TU Delft Deltares

Preface

This research concludes the Master of Science program in Hydraulic Engineering at the Delft University of Technology. This research has been conducted at the research institute Deltares. I am very grateful for the opportunity to perform my thesis in this environment and looking back on it, it was a very pleasent experience. The past eight months flew by and I have learned a lot during the process.

This thesis would not be possible without the help of my graduation committee. Therefore, I would like to thank *Lodewijk de Vet* for the regular help. Your constructive feedback, eye of detail and positivity were very helpful during the process. I really appreciate that you always made time when I was stuck and/or asked questions. Thank you *Bram van Prooijen* for chairing the committee and supervising the project. Moreover, thanks for the creative ideas during the different committee meetings and the feedback on the different versions of the report. *Bas van Maren*, thanks for your help during the project, especially during the calibration of the morphodynamic model. Thank you *Zheng Bing Wang* for the feedback and help in the second phase of the project, some of your comments were eye-openers for me.

Furthermore, I would like to thank the interns at Deltares for their interest, advice and especially for the coffee breaks. Moreover, I want to thank my colleagues at the Applied Morphodynamics department for their interest in my research and constructive feedback. In particular, I want to thank *Jebbe van der Werf* for the multiple fruitful brainstorms we had and the feedback on my report. I look forward to keep working at the department!

Lastly, I want to thank my family and friends for the support and enthusiasm. I had a great time, not only during graduation, but during the past seven years studying in Delft.

Tim de Wilde
Delft, September 2022

Summary

A managed realignment is the landward relocation of a flood defence to re-establish tidal exchange on formerly reclaimed land. In a managed realignment, the newly formed intertidal area acts together with the realigned dike as a nature-based flood defence system. In this thesis, the focus is on the managed realignment of Perkpolder, a former polder located in the south of Zeeland (The Netherlands). This realignment serves as nature compensation for the dredging activities in the Western Scheldt. The realigned area contains an intertidal flat which facilitates ecological services.

In 2015, creeks and a deeper lying pond were excavated. After these preparations, the dikes were breached to connect the polder to the Western Scheldt. Previous research on the managed realignment focused on the initial morphological response of the realignment site. However, the main processes leading to the observed morphological change were not fully unravelled. For example, the temporal variability of measured net sediment transport through the inlet of Perkpolder could not be explained. Furthermore, the contribution of the former intertidal area in front of Perkpolder (frontal entrance area) and the Western Scheldt to the total sediment budget in Perkpolder was not known. Lastly, managed realignments are a relatively new measure. Therefore, understanding the development of Perkpolder provides valuable information for future realignment projects.

To this end, a combination of different data sources (sediment samples, flow velocities, turbidity measurements and bathymetric data), together with a hydrodynamic model of the Western Scheldt and a morphodynamic model of Perkpolder are used to interpret the response of Perkpolder after the managed realignment.

Bathymetric data composed of LIDAR, multibeam and single-beam measurements shows three main developments in Perkpolder: (1) erosion of the frontal entrance area, the inlet and the seaward side of the creeks, (2) infilling of the creeks landward of the first bifurcation and (3) sedimentation on the intertidal area and even more sedimentation of the pond. By comparing the temporal evolution of the bed levels of the frontal entrance area with measured concentrations at the inlet of Perkpolder, it can be concluded that the frontal entrance area acted as a finite source of sediment that eroded quickly in the first years and increased sedimentation within Perkpolder during these years.

The higher sedimentation rate of the pond is partially explained by the larger disequilibrium resulting from the large depth of the pond. Moreover, the inlet of Perkpolder was initially excavated to MSL, in the first year a deep and narrow entrance channel eroded. Over the first few years, the inlet developed into a wider and shallower entrance channel. Since the inlet was above low water in the first year, the entrance channel blocked the flow during low water levels. This led to a longer period of low velocities in the pond and subsequently a small period with high velocities creating more sediment transport and more time to settle. If the goal of the realignment is to trap sediment (e.g. as solution for the excess of sediment in the Ems estuary), a pond combined with the inlet substantially above MLW is beneficial.

Concentration measurements show that a high tidal range leads to smaller and negative trapping efficiencies (net import divided by the total amount of imported sediment). The morphodynamic model of Perkpolder confirmed this trend. Adding wind and wave effects in the model of Perkpolder created more temporal variability in trapping efficiencies. Therefore, it is expected that wind and waves have an important contribution to the trapping efficiency of a managed realignment. However, no net export could be simulated using the model.

Creeks convey water and sediment to the intertidal area, therefore the configuration of creeks is an important design aspect for managed realignments. Different creek lay-outs are tested using the morphodynamic model. When creeks are set-up too small, the water flows directly over the intertidal area leading to erosion at the seaward side of the intertidal area and smaller accretion rates on the intertidal area. Moreover, converging creeks fit better with the decreasing conveying capacity and therefore lead to less deposition of sediment inside the creeks.

New realignment projects can profit from the research at Perkpolder. Bed shear stresses of the initial proposed layout of Perkpolder gives a clear indication if the creeks are setup correctly. Furthermore, an estimate of the initial sedimentation can be based on the accretion rate of other intertidal areas within the estuary. Since realigned areas are often more sheltered and have a lower elevation, accretion rates may be higher. Moreover, not only the forcing of the estuary, but at the same time the availability of different sediment sources and the initial bathymetry shape the morphodynamic response of the realignment site. Therefore, it is recommended to measure the bathymetry for a sufficient long period (e.g. 10 years after the realignment) to get grip on the mechanisms shaping the morphodynamics at these areas.

Contents

Nomenclature

List of Acronyms

Abbreviation	Definition
ADCP	Acoustic Doppler Current Profiler
BSS	Bed Shear Stress
D3D	Delft3D
DGPS	Differential Global Positioning System
DET	Dynamic Equilibrium Theory
E	East
ETM	Estuarine Turbidity Maxima
FM	Flexible Mesh
HW	High Water
LIDAR	Laser Imaging Detection And Ranging
LW	Low Water
N	North
NAP	Normaal Amsterdams Peil (Dutch datum line)
MHHW	Mean Higher High Water
MHW	Mean High Water
MLLW	Mean Lower Low Water
MLW	Mean Low Water
MSL	Mean Sea Level
OBS	Optical Back Scatter
RD	Rijksdriehoekscoördinaten (Dutch coordinate system)
S	South
SLR	Sea Level Rise
TS	Tidal Storage
W	West
WS	Western Scheldt

List of Symbols

Symbol	Definition	Unit
A_{eq}	Equilibrium cross sectional area	$[m^2]$
a	Depth of reference concentration	$[m]$
c	Concentration at a distance y of the bed	$[g/L]$
c_a	Reference concentration at a distance $y = a$ of the bed	$[g/L]$
H	Tidal range	$[m]$
h	Water depth	$[m]$
L_{basin}	Basin length	$[m]$
L_{tide}	Tidal wave length	$[m]$
P	Tidal Prism	$[m^3]$
R_0	Rouse number	$[-]$
u_*	Shear velocity	$[m/s]$
U_e	Critical velocity for erosion	$[m/s]$
U_d	Critical velocity for deposition	$[m/s]$
w_s	Settling velocity	$[m/s]$
y	Vertical distance above bed	$[m]$
y_0	Depth of uniform flow	$[m]$
z	Elevation of intertidal area above MLW	$[m]$
δ	Vertical accretion rate of intertidal area	$[cm/yr]$
κ	Von Karman constant	$[-]$

Symbol	Definition	Unit
ρ	Density of water	$[kg/m^3]$
ρ_s	Density of sediment	$[kg/m^3]$
τ_0	Bed shear stress	$[N/m^2]$

List of Figures

List of Tables

1

Introduction

1.1. Background

In 1995 the Dutch and Flemish government signed a treaty concerning the second extension and deepening of the Western Scheldt to the port of Antwerp. Part of this treaty was compensation of nature in the Western Scheldt, this was worked out in the program 'Natuurcompensatie Westerschelde' (Ministerie van V&W, 2008). Moreover, in 2003 the Western Scheldt tunnel was opened, which made the ferry service between Kruiningen and Perkpolder obsolete. Therefore new plans were developed for the entire area of Perkpolder which included a large intertidal area as part of the 'Natuurpakket Westerschelde' (Paiva et al., 2019; Verbeek, 2005). Both packages contribute to the realignment of Perkpolder from farmland to intertidal area.

The main goal of transforming Perkpolder to intertidal area is nature compensation, this realignment project creates marshes and intertidal flats that are under pressure in the Western Scheldt and the entire world (Chen et al., 2016; Paiva et al., 2019; Sistermans et al., 2004). The main reasons for the global decrease in intertidal areas are land claim, erosion and/or coastal squeeze (Lotze et al., 2006; Mazik et al., 2010). It is important to keep these intertidal areas, since tidal flats facilitate intense biological activity (Barbier et al., 2011; Widdows et al., 2004). This includes generation of benthic micro algae, which is the primary source of food for microbial and benthic species (Herman et al., 2001). Moreover these locations have a protective function for the flood defences behind the tidal flat. The tidal flats break waves and reduce run-up on the dike itself, therefore the height of these flood defences can be reduced (Willemsen et al., 2020). Moreover, the salt marshes lower breach impact by confining the breach size when engineered defences have failed (Zhu et al., 2020).

The construction of Perkpolder started with improving the secondary dikes of the polder, such that these dikes fulfil the requirements for a primary sea defence. Moreover creeks and a pond were excavated to guide the water to the intertidal area (Paiva et al., 2019; van Ginkel, 2019). In June of 2015 the dikes were breached and from that moment the basin would be flooded twice a day from the Western Scheldt. To give an overview of the realignment,

(a) 2013 **(b)** 2019

Figure 1.1: Aerial photographs of Perkpolder. Retrieved from: Atlas van Zeeland (aerial photo of 2013 and 2019).

Figure 1.1 shows the polder in 2013 before the construction of the realignment and in 2019, four years after the opening of Perkpolder.

1.2. Relevance of the research

Currently, coastal managers face the need for coastal dike adaptation to anticipate for the foreseen sea level rise induced by climate change (Nicholls et al., 2018; Oppenheimer et al., 2019). In the coming decades, efficient and environmentally sustainable dike reinforcement methods are required to ensure the same level of safety from coastal flooding (Hinkel et al., 2014; Vousdoukas et al., 2020). Moreover, European policy prioritises nature-based solutions for these reinforcements (European Commission, 2021). Therefore, managed realignment is a promising climate change adaptation measure besides the traditional dike reinforcements (Esteves, 2014; Temmerman et al., 2013; Zhu et al., 2020).

Before the start of the realignment project, it was known that the precise morphological development of this polder could not be predicted up front (Boersema, 2015). A lot of research is dedicated to understand the behaviour and predict the fate of intertidal areas (Friedrichs, 2011; Friess et al., 2012; Kirwan et al., 2016). Also in the Western Scheldt the behaviour of intertidal areas has been researched, e.g. by de Vet et al. (2017). At the same time, realignment projects arise all over the world, for example in Japan, the United Kingdom, Germany, France, Belgium, Bangladesh and the Netherlands (Dixon et al., 2008; van den Hoven et al., 2022; Warner et al., 2018; Yamashita, 2021). Therefore, understanding the driving processes at Perkpolder can give more knowledge about the development of intertidal area after a managed realignment.

At Perkpolder several measurement campaigns were planned by Boersema (2015) in order to understand the hydrodynamic and morphodynamic response of Perkpolder after the alignment. From the measurements and modelling until 2018, already some valuable insights about the initial response of Perkpolder are discovered and published in Paiva et al. (2019) and Brunetta et al. (2019). However, still a lot is unknown about the intertidal area of Perkpolder. The sediment transport at the inlet shows temporal changes that are unresolved. Furthermore it was concluded that the eroded sediment at the former intertidal area in front of Perkpolder (frontal entrance area) had a different grain size than the accreted sediment at the intertidal area (Brunetta et al., 2019; Paiva et al., 2019). The relative contribution of the frontal entrance area and Western Scheldt to the sediment budget is thus not yet known. Until now only the initial response, directly after opening of Perkpolder is investigated. Different processes can play a role after a few years. Moreover, it is unknown how the polder will develop over time and in which pace the intertidal area will accrete.

1.3. Goal and research questions

Section 1.2 highlighted the main knowledge gap that is the basis of this thesis, namely that a lot of processes at Perkpolder are not fully understood. Moreover, when the response of Perkpolder is known, this can give more information for realignment projects in general. This has been described in the research goal:

Determine the main processes and driving conditions that steer the hydrodynamics and morphodynamics at Perkpolder in order to understand the evolution and optimise future realignment projects.

This is a broad research goal and in order to achieve this goal, the first research questions will focus on understanding the development of the intertidal area of Perkpolder. From section 1.2 it became clear that the temporal fluctuations and the origin of the sediment were still unknown. Therefore these knowledge gaps have been rewritten as research questions.

(1) What drives the temporal variability in suspended sediment import and export in the basin of Perkpolder?

(2) What is the contribution of the frontal entrance area and Western Scheldt to the sediment accretion at Perkpolder?

The next step is to determine the (potential) accretion rate of Perkpolder. Perkpolder has been designed to become a salt marsh and therefore the bed level should grow to high water and in the future it should be able to adapt to rising sea levels.

(3) What is the accretion rate potential of Perkpolder and what processes dominate this?

The last research question will address the second part of the research goal, namely use the knowledge gained in Perkpolder to understand how realignment projects evolve and optimise the design of general realignment projects. This research will therefore not only be focused to Perkpolder, but will be an extra tool in the design of future realignment projects.

(4) What processes and (initial) conditions determine the growing capacity of intertidal areas after a managed realignment?

1.4. Research approach and thesis outline

Based on the case study of Perkpolder the research questions are analysed in this thesis. Therefore, first, the relevant literature is presented in Chapter 2. The theoretical concepts explored in Chapter 2 are the basis for the data analysis and model studies. In order to acquire the results, a range of measurements (e.g. bed levels, sediment samples, flow velocities and suspended sediment concentrations) is analysed. Moreover, two separate models evaluate respectively the hydrodynamics and morphodynamics of Perkpolder. Chapter 3 shows the methodology which includes the study site, available data and set-up of the two models.

Chapter 4 to Chapter 7 presents the combined results of the data analysis and modelling studies. First, Chapter 4 gives an overview of the measured geomorphology of Perkpolder, this includes yearly bed levels, sediment samples and sediment cores. These results are used as basis to present the morphological development in Chapter 5. This chapter shows how Perkpolder and its different sub-areas changed temporally and spatially. To increase the understanding of the morphological development, the sediment transport through the inlet is analysed and connected to the morphological development of different areas at Perkpolder. Furthermore, the driving processes and the temporal changes are analysed, this is presented in Chapter 6. Chapter 7 shows how different scenarios alter the morphological evolution of Perkpolder. This is done to create an enhanced understanding of Perkpolder, furthermore the scenario study creates insights of the morphological development of realigned areas.

The discussion presented in Chapter 8 links back to the acquired results and takes a broader perspective how the lessons learned in Perkpolder gives insight in the morphological development of realigned areas. The main conclusions established for the four research questions will then be given in Chapter 9. Lastly, Chapter 10 shows recommendations for further research and new realignment projects.

2

Theoretical background

Section 2.1 gives a general introduction to managed realignments. Section 2.2 presents a process-based classification for different coastal systems. This classification is used to dive into tidal basins in Section 2.3 including the Western Scheldt estuary and tidal flats in Section 2.4. Lastly Section 2.5 shows the sediment transport processes relevant for this study. This includes the asymmetry of the tide, lag effects and a special focus on sedimentation within realignment sites.

2.1. Managed realignment

Managed realignment is the landward relocation of flood infrastructure to re-establish tidal exchange on formerly reclaimed land (Bridges et al., 2021; French, 2006). In a managed realignment, intertidal areas and saltmarshes can be combined with the realigned dike to create a nature-based flood defence system where flood levels are reduced and ecosystem services like recreation are provided (van den Hoven et al., 2022; van Wesenbeeck et al., 2014).

In order to create a realignment site, the old seaward dike will be lowered, breached or removed (Esteves, 2014). Moreover, regulated exchanges like pipes or sluices can be used to bring the water to the realigned area (Beauchard et al., 2011). In Perkpolder the old seaward dike was breached along a transect of $350\ m$. By breaching the seaward dike, regular inundation and transport of sediment is possible to the low-lying land between the old seaward dike and the landward relocated dike. In general the landward relocated dike can newly be build or was already part of an existing dike system. In Perkpolder the realigned dike was a landward dike that has been reinforced to conform to the standards for a primary sea defence (van Ginkel, 2019).

The old seaward dike blocked sediment transport to the land, thereby limiting accretion. Due to the realignment the low-lying land will receive sediment and the low-lying land will increase its elevation (Syvitski et al., 2009; Temmerman et al., 2013). This raised land helps in flood protection (e.g. Battjes et al. (2000)) and can eventually serve as temporary farmland again (Zhu et al., 2020). The land use switch is described by the concept 'transitional polder' where a former polder is opened to tidal flow and therefore experience accretion, the raised land could potentially be turned to farmland again (Belzen et al., 2021; De Mesel et al., 2013; Weisscher et al., 2022; Zhu et al., 2020).

2.2. Classification of coastal systems

In order to create a distinction between the different coastal systems that are analysed in this study, a process-based classification as determined by Bosboom et al. (2022) is used. This divides typical coastal morphologies based on two criteria. The first criterion is how important fluvial sediment (river input) is for shaping the coastal system. The second criterion is if the sediments are primarily reworked by waves or tides (wave dominance or tide dominance). The classification is shown in Figure 2.1.

Managed realignment areas restore the natural foreshore, the foreshore consists mostly of mudflats and saltmarshes (Liu et al., 2021; Schuerch et al., 2018). When realigning Perkpolder a relatively sheltered tidal basin is created and is therefore classified as a tide dominated tidal flat with no fluvial input (Paiva et al., 2019). Perkpolder is connected to the Western Scheldt, which is classified as an estuary due to the river input of the Scheldt river and the forcing of the tide (Pritchard, 1967).

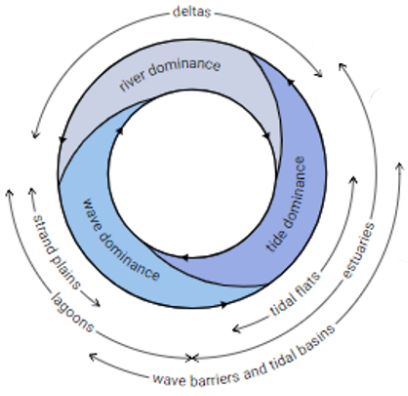

Figure 2.1: The relative influence of fluvial, wave and tidal processes classifies coastal features. Figure retrieved from Bosboom et al. (2022).

2.3. Tidal basins

Section 2.2 shows that a tidal basin is primarily a tide dominated coastal system. However depending on the location, fluvial input and waves can significantly alter the morphological development (Bosboom et al., 2022). This section starts with two important aspects of tidal basins, namely the storage capacity of short basins and the morphological development of the inlet. Moreover, the Western Scheldt estuary is analysed such that the interaction between the realigned area of Perkpolder and the Western Scheldt is fully understood.

2.3.1. Characteristics of tidal basins

General characteristics that are important for the understanding and development of Perkpolder are described in this section.

Short basins

Short basins have a basin length that is much smaller than the wavelength of the forcing waves, for Perkpolder, the forcing wave is a tidal wave ($L_{basin} \leq \frac{1}{20} L_{tide}$ (Bosboom et al., 2022)). Since Perkpolder is an intertidal area, the water depth is small compared to the tidal wavelength, the shallow water celerity is used to calculate the tidal wavelength. An average water depth of $1\ m$ has been assumed and the period of the M_2 component of the tide has been chosen as representative period. This leads to a tidal wavelength in the order of $140\,km$ while Perkpolder is $1.2\ km$ long, therefore the short basin approximation is valid for Perkpolder.

Since Perkpolder is a short basin, the water level at Perkpolder will instantaneously follow the water level in the Western Scheldt near Perkpolder. Therefore the discharge is calculated using the tidal storage approach (Bosboom et al., 2022). Using the hypsometric curve of Perkpolder and the water level variations the discharge is calculated as shown in Equation 2.1.

$$Q(t) = A(z) \cdot \frac{dh}{dt} \tag{2.1}$$

This procedure has already been validated using a five day measurement campaign in which flow velocities at the inlet were measured and compared with the calculated discharge of the tidal storage approach (Paiva et al., 2019).

Equilibrium cross-section of the inlet

Using empirical relationships, the stability of geometric properties of the channels and flats of tidal basins is described. These geometric properties are linked to hydrodynamic conditions. Watt (1905) has first discovered the dependence of the spring (maximum astronomical) tidal prism to the inlet cross-sectional area. This has been elaborated by O'Brien (1931, 1969) to Equation 2.2.

$$A_{eq} = C \cdot P^q \tag{2.2}$$

This equation is valid for large estuary mouths, bays and tidal lagoons. The coefficient q is in the order of 1 and C is in the range of $10^{-4} - 10^{-5}\ m^{-1}$ (the unit depends on the coefficient q). A certain combination of values for C and q is only valid for a set of inlets with the same sediment characteristics, wave conditions and tidal conditions. However Jarrett (1976) has determined a fit for multiple types of inlets, which is shown in Equation 2.3.

$$A_{eq} = 1.576 \cdot 10^{-4} \cdot P^{0.95} \tag{2.3}$$

2.3.2. The Western Scheldt

The Western Scheldt as shown in Figure 2.2 has a lot of influence on the hydro-morphodynamics of Perkpolder, therefore the hydrodynamic conditions and sediment characteristics will be presented in this subsection.

Figure 2.2: Western Scheldt and river Scheldt. Adapted from: Scheldecommissie (2019).

Hydrodynamic conditions

The Western Scheldt is an estuary, which is tide-dominated with a meso- to macro-tidal regime according to the classification of Dyer (1973). The tidal range increases from $3.8\ m$ at Vlissingen to $5.2\ m$ at Antwerp (de Vet et al., 2017). The amplification of the tidal range is due to convergence, shoaling and partial reflections within the Western Scheldt. From the 1970's until 2020 the tidal range shows a clear increase in the Western Scheldt (Wang et al., 2019). This is due to engineered interactions, e.g. dredging activities in the Western Scheldt in which the channels were deepened (van Kessel et al., 2011; Wang et al., 2002). The Western Scheldt is funnel-shaped with a lot of local variations, the average width is $6\,km$ at Vlissingen to $2-3\,km$ near Bath. The width-averaged depth decreases from $15\ m$ at Vlissingen to $3\ m$ near Gent (Wang et al., 2002).

The duration of the falling tide exceeds that of the rising tide, creating a flood-dominant system (Jeuken, 2000). The tidal asymmetry increases with the amplitude of the tide, therefore the asymmetry is larger during spring tides, than during neap tides (Wang et al., 1999). Due to deepening of the channels in the past 50 years, the flood dominance has decreased (Wang et al., 2002).

The mean tidal prism at Vlissingen is $2.2 \cdot 10^9\ m^3$ and $0.2 \cdot 10^9\ m^3$ at the Dutch-Belgium border. The mean river outflow is about $120\,m^3/s$ (Wang et al., 2002). Based on the ratio of the salt water of the tide and the fresh water at the river outlet, during high river discharges the estuary is partially mixed between Rupelmode and Hansweert and is well-mixed between Vlissingen and Hansweert (Bolle et al., 2010). For lower river discharges the entire Western Scheldt is well mixed. Significant changes in the salinity are found over a spring-neap cycle and during winter and summer. The salinity is higher during the summer and during spring tides, than during winter and neap tides (van Kessel et al., 2011).

(Suspended) sediment in the Western Scheldt

Mud is transported via the North Sea and the river Scheldt to the Western Scheldt. The marine mud originates from the English Channel and the Flemish Banks. Fluvial mud originates from the Scheldt catchment area and material eroded from muddy beds. The fluvial mud supply is depended on the discharge of the Scheldt river and it has been found that 90% of the mud has been discharged in less than 10 % of the time, during high water discharges (Verlaan, 1998). Since the discharge of the Scheldt river is in the order of 1/1000 of the tidal prism, the fluvial sediment input is almost negligible (De Vriend et al., 2011).

The human interventions (Delta works) in the past and the dynamic conservation of the coast by sand nourishment's influences the sediment exchange between the estuary and the coasts. The sediment (sand) balance of the Western Scheldt is mainly determined by the import-export at the mouth of the estuary and dredging works in the estuary. Since the 1980's the approximate constant import rate started to decrease, even becoming a net export. Taking into account the sand mining and the relative sea level rise, it is concluded that the Western Scheldt is becoming deeper (De Vriend et al., 2011). This is backed up by Dam et al. (2017) who discovered a general export

of sand in the Western Scheldt which is visible in an expansion of the channels and import of mud which is seen in the deposit of mud in bars and side channels. This changing system influences the residual sediment transport, which is related to the tidal asymmetry which in turn drives the morphological development of the estuary (Wang et al., 2015).

The sediment concentrations in the Scheldt estuary show variations on different time scales as listed below (Fettweis et al., 1998; Temmerman et al., 2003b; van Kessel et al., 2011). However, this gives not a complete picture, very local and stochastic changes in sediment supply can occur due to for example storms (Zhu et al., 2019).

- Flood-ebb tide (M_2 and M_4),
- Spring-neap tide,
- Seasonal variations depending on differences in river discharge and erosion in the river,
- Decades, possibly resulting from climate change or changes in sediment supply.

These conclusions are backed up by Van Der Wal et al. (2010), who used remote sensing and in-situ techniques to estimate the suspended particle matter in the Western Scheldt and found three profound dependencies as shown in Figure 2.3. The suspended sediment concentration is higher in the winter than in summer and higher during spring tide than neap tide. Lastly over a diurnal cycle, the suspended sediment is overall higher during low water than during high water.

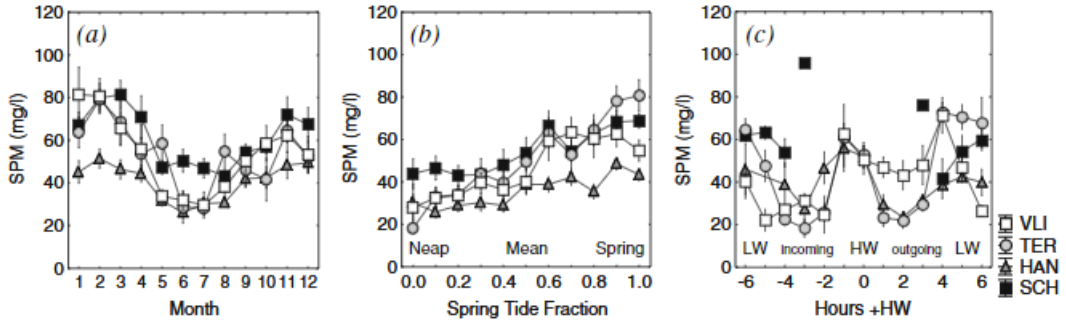

Figure 2.3: Suspended sediment concentration on four stations at different time scales, i.e. (a) over a year, (b) over a neap-spring cycle and (c) a semi-diurnal tidal cycle. Station names: Vlissingen (VLI), Terneuzen (TER), Hansweert (HAN), Schaar van Ouden Doel (SCH) (Van Der Wal et al., 2010)

2.4. Tidal flats

Since Perkpolder consists largely of intertidal area (Paiva et al., 2019), it is important to understand the basic morphodynamics of these intertidal areas. Tidal flats undergo spatiotemporal changes, that need to be captured in order to understand the fundamental processes leading to erosion or accretion of the tidal flat. The temporal changes can be very short-term, e.g. the response of the tidal flat under a storm (de Vet et al., 2020), but also tidal changes, seasonal changes and decal changes (Friedrichs, 2011).

2.4.1. Longitudinal profile

The morphological response of intertidal systems to tidal waves and wave-induced forcing over various timescales can be described by Dynamic Equilibrium Theory (DET). DET assumes that tidal flat morphological equilibrium is achieved when the maximum bed shear stress (BSS) is uniform over space, ensuring zero net sediment transport (Friedrichs, 2011; Pritchard et al., 2002; Roberts et al., 2000). This has been backed up by experiments done in the Western Scheldt in which the bed shear stress has been measured at multiple intertidal areas (Hu et al., 2018). However, it is important to realise that this conceptual model contains not yet all the variations seen in practise.

The longitudinal profile of the tidal flat, determined from dynamic equilibrium theory, indicates the main hydrodynamic forcing and morphodynamic response of the tidal flat. This is summarised in Figure 2.4, where the analytical solutions are shown for the equilibrium profile for a hydrodynamic forcing of only tides or only wave (Friedrichs, 2011). Small waves, large tides and sediment import are three main drivers that all favour a convex-up tidal flat profile. Whereas large waves, small tides and sediment export favour a concave profile (Kirby, 2000). Furthermore, a larger tidal range is significantly correlated with greater convexity. The suspended sediment concentration plays an important role, when the available suspended sediment concentration is larger, the profile will extend more seaward (Friedrichs, 2011).

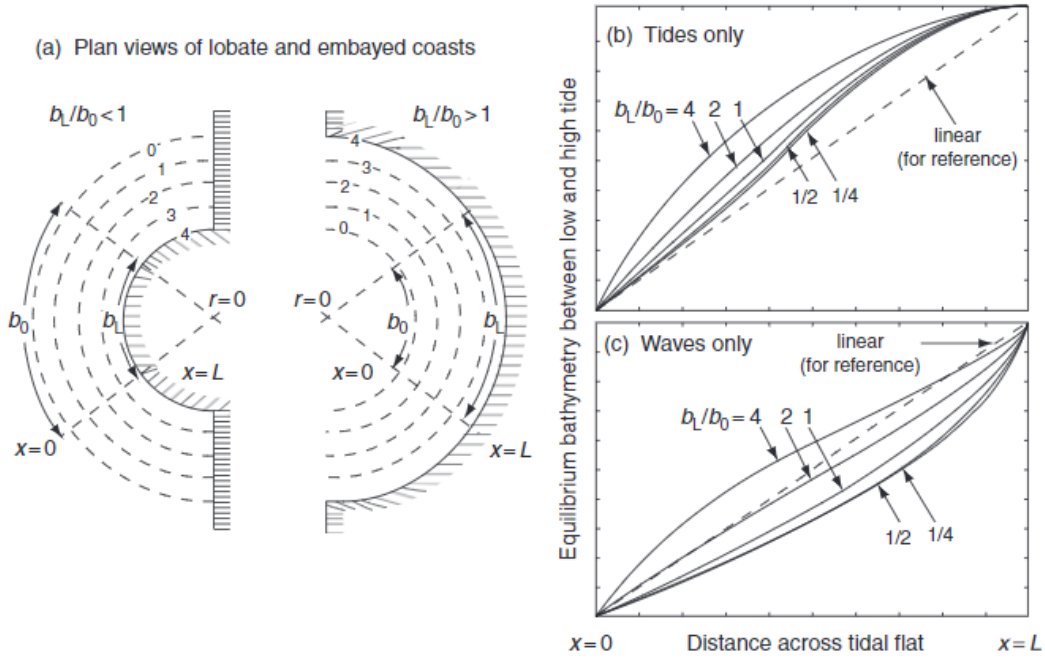

Figure 2.4: (a) Schematic plan view of lobate and embayed tidal flat coastline. The contour lines 1-4 indicate arbitrary elevations between high and low water. Analytical solutions for equilibrium profiles between low and high water for (b) tides only and (c) waves only. Retrieved from: Friedrichs (1996).

2.4.2. Adaptation to sea level rise

Tidal flats erode or accrete to an equilibrium profile in the long term, in this equilibrium these flats tend to develop near high water level. However when the hydrodynamic conditions change, for example due to sea level rise, also the equilibrium situation changes (Allen, 2000; Friedrichs, 2011; Hu et al., 2015). Several feedback mechanisms between plant growth, geomorphology and hydrodynamic forcing allow marshes and tidal flats to actively resist effects of sea level rise (Kirwan et al., 2010; Kirwan et al., 2013).

As determined in Friess et al. (2012) there are four main contributors to intertidal surface elevation. These are tectonic, geomorphological and biological processes.

1. Surface elevations change due to deep tectonic processes like large-scale isostatic adjustment in response of the last glacial maximum can decrease or increase the surface elevation (Shennan et al., 2002).
2. Moreover, vertical accretion is controlled by long-term sediment availability and accumulation. This is split up in two important conditions, namely the sediment supply and the sediment trapping and consolidation by vegetation. Sediment supply on a small scale is a function of intertidal surface elevation. Lower surfaces are inundated more frequently and therefore have more sediment deposition and thus more accretion in the long term (Kirwan et al., 2016; Van Wijnen et al., 2001). On a larger scale, sediment should be inputted to the system from rivers, cliff erosion or the reworking of offshore sediment. Sediment trapping is mainly determined by vegetation, the vegetation can attenuate tidal flow velocity and wave height, such that sediment particles fall out of suspension increasing the deposition. Moreover vegetation reduces resuspension, since the tidal flow velocities are reduced. Different type of vegetation and their root systems can also alter the trapping efficiency of the sediment (Morris et al., 2002).
3. Expansion of the soil due to organic matter accumulation by below ground productivity, such as root biomass and organic matter production, contribute to the vertical growth of the intertidal area. The biomass accumulation can be critical for the marsh drowning rate and survival (Best et al., 2018).
4. Subsidence of the soil will have a negative impact on the surface elevation.

2.4.3. Intertidal areas in the Western Scheldt

A study to assess the morphological development of intertidal areas in the Western Scheldt is performed by de Vet et al. (2017). Although the morphological evolution changed per location and is determined to be site-specific, general trends could be found for the Western Scheldt. It was discovered that sudden changes in area and volume (Middelplaat Oost (F4) and Ossenisse (F7)) correspond with dredging and dumping activities in the Western

Scheldt (de Vet et al., 2017). Despite the non-uniform long-term evolution of the WS flats, the aggregated average intertidal height, weighted with respect to the area of each flat, increased from $-0.12\ m$ *NAP* around 1955 to $+0.45\ m$ *NAP* in 2014. This implies an average increase in height of almost $1\ cm$ per year with an absolute deviation of $0.5\ cm$ per year.

At some tidal flats the average height increases and at the same time the surface area of the tidal flat decreased (e.g. Middelplaat West (F3), Molenplaat (F6) and Hoge platen (F1)). Tidal flats needs lateral and horizontal accommodation space in order to sustain sea level rise (Kirwan et al., 2016). This is also seen at other locations in the Netherlands and the United Kingdom, which are both countries with a lot of dykes and infrastructure that limits the landward retreat of intertidal areas (De Vriend et al., 2011). In both countries a general horizontal retreat of these areas up to several meters per year has been observed. However the vertical accretion rate of the intertidal areas were similar to SLR (Van der Wal et al., 2008).

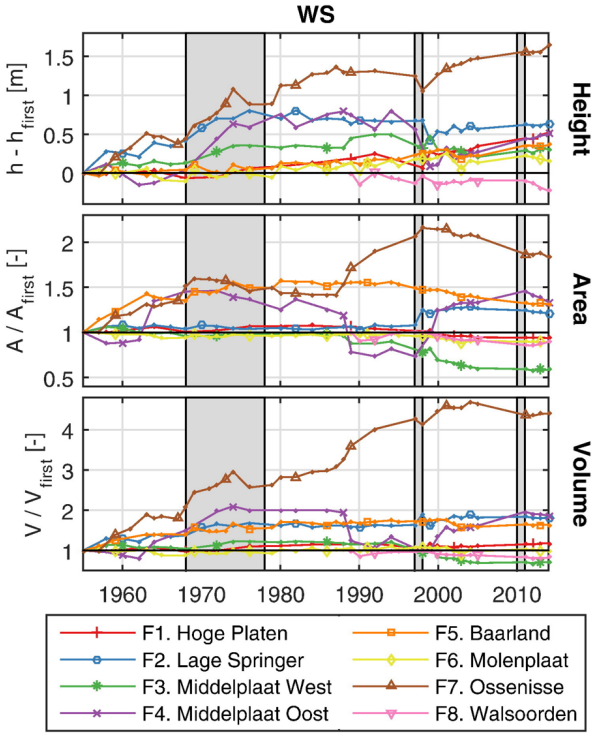

Figure 2.5: Morphological development of tidal flats in Western Scheldt. The vertical grey boxes on the background indicate the deepening projects in the WS. Adapted from: de Vet et al. (2017).

2.5. Sediment transport processes

The focus in this section is to understand the mechanisms forcing sediment transport. In this thesis the focus lies on barotropic processes and not on baroclinic (density currents), as established in Neves (1995) the baroclinic processes are of secondary importance with respect to the barotropic processes for the Western Scheldt. Two main barotropic mechanisms will be analysed, namely sediment transport by asymmetries of the tide and sediment transport due to lag effects. Moreover the last subsection will dive into sedimentation in realignment sites.

2.5.1. Asymmetry of the tide

To analyse the sediment transport due to asymmetry of the tide a Eulerian frame of reference is used. Different tidal constituents, especially the shallow water overtides, create asymmetry in the vertical tide (Dronkers, 1986; Ridderinkhof, 1988). Depending on the water level signal and the bathymetry of Perkpolder, the velocity signal is also asymmetric. Coarse sediment is more sensitive to asymmetries in maximum velocity (Bosboom et al., 2022). The residual transport takes place in the direction of the highest peak velocity. An indication for the maximum peak velocity is the duration of the flood period of the water level signal, a shorter flood period correspond to higher velocities during flood and therefore landward transport.

Fine sediment is more sensitive to asymmetries in the duration of slack, also called acceleration/deceleration asymmetry (Groen, 1967). Tides with a longer slack around high water than low water favour sediment transport landward, since there is more time for sediment to settle after high water. Figure 2.6 shows a case for which the

flood slack is longer than the ebb slack. Fine sediment needs time to respond to the new hydrodynamic forcing, since the adaptation time scale is inversely proportional to the settling velocity. Intertidal areas will by definition have a longer slack after flood, because there is generally no water present during the slack after ebb (Friedrichs, 2011).

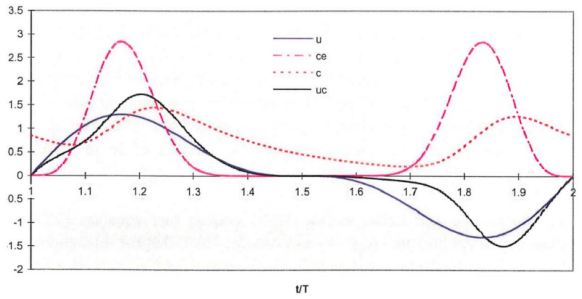

Figure 2.6: The result of asymmetries in the duration of slack on fine sediment transport. Retrieved from: Wang et al. (1999).

2.5.2. Resuspension by waves

Erosion of sediment by small-amplitude waves has been identified as a process of major importance for morphodynamics of tidal flats (Friedrichs, 2011; Green et al., 2007; Green, 2011; Green et al., 2014; Talke et al., 2008). On tidal flats wave growth is limited by both shallow depths and the fetch length which varies throughout the tidal cycle. Nevertheless, even during fair weather conditions, bed-shear stresses are enhanced by small-amplitude waves, which can be crucial for the sediment dynamics of shallow channels and tidal flats (Green, 2011). Tidal velocities may be insufficient to exceed the threshold of motion, this can be overcome by the contribution of these small waves (Gatto et al., 2017).

2.5.3. Lag effects

From studies already performed in the 1950s, spatial (lagrangian) asymmetries, called lag effects have been identified to cause sediment transport (Postma, 1961; Van Straaten et al., 1957). The energy required to mobilise fine cohesive sediment particles from the bed is much larger than the energy needed to bring and keep them in suspension. Moreover, since cohesive particles are very small, the time scale to mix the particles over the water column is much smaller (~minutes) than the settling time (~hours) (Van Maren et al., 2013). Thus, lag effects cause asymmetries of the sediment particle's trajectory under a periodically reversing flow. Classically these lag effects contribute in landward transport of the sediment particle over a tidal cycle (Gatto et al., 2017). Four types of lag effects are classified in this thesis, namely settling lag, threshold lag, scour lag and entrainment lag.

Settling lag is the distance a particle can travel when the flow velocity has fallen below the critical shear stress for erosion (Van Maren et al., 2013). A sediment particle is entrained when the flow is above U_e (critical velocity for erosion) at that location, when the flow velocity decreases to below U_d (critical velocity for deposition), the particle starts to settle. However, during settling, the particle is still transported horizontally before hitting the bed. When hydrodynamic conditions are uniform (Fig. 2.7a), the sediment particle is re-entrained by a water parcel originating closer to land and the ebb-trajectory mirrors the flood directory. Due to differences in the flow field (Fig. 2.7b), bed level differences (Fig. 2.7c) or water level differences (Fig. 2.7d) the particle can have a net landward or seaward movement. If the velocity of the driving water parcels reaches below the erosion threshold, the sediment particle will not be resuspended, this condition is called **threshold lag** (Gatto et al., 2017).

Settling lag is further enhanced by **scour lag** when the condition that $U_e > U_d$ (the erosion threshold is larger than the deposition threshold) is introduced. Physical mechanisms increasing the critical velocity for erosion with time are self-weight consolidation, bed strengthening by diatom mats and/or drying of intertidal areas (Van Maren et al., 2013). Figure 2.7e shows the net landward transport of a sediment particle by a lower deposition threshold than erosion threshold and a damped velocity field.

Entrainment lag is the time needed for the particle to cross the bed-load layer and be lifted up in the water column after it has been picked up from the bed, so after the critical erosion threshold has been reached (Nichols, 1986). When crossing the bed-load layer, the movement is dominated by flows in the near-bed layer instead of depth mean or flows higher up (Dyer, 1997).

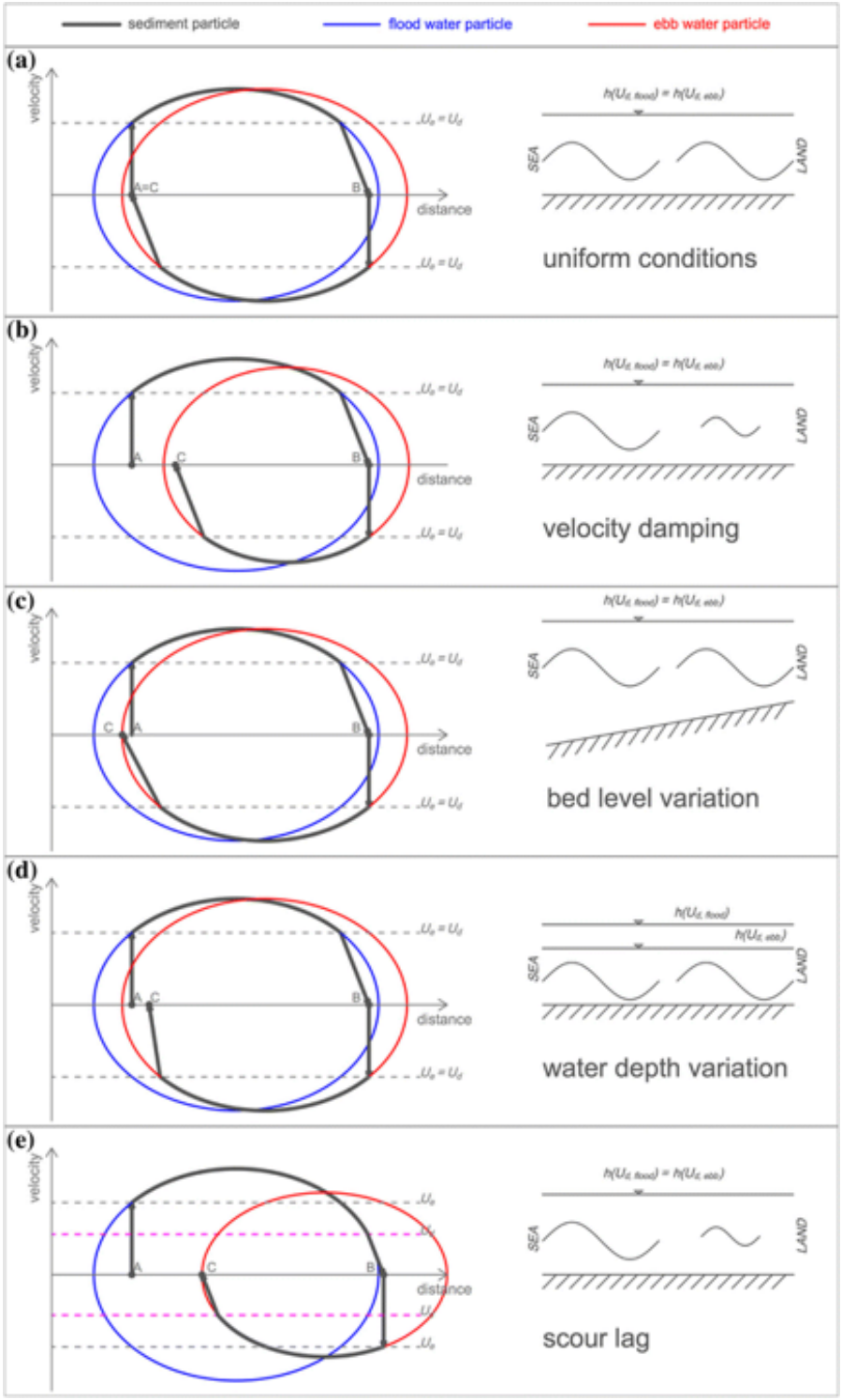

Figure 2.7: Settling lag (panels a to d) and scour lag (e) mechanisms. Figure retrieved from Gatto et al. (2017). The x-axis represents the streamwise distance from the inlet, the y-axis represents the velocity of the sediment (water) particle. The dotted lines are the threshold velocities for erosion and deposition. A different sub-mechanism is illustrated in each panel. Retrieved from: Gatto et al. (2017)

2.5.4. Sedimentation of realignment sites

In order to investigate the morphological development of Perkpolder after the managed realignment, it benefits from morphological research performed in other realignment sites. Differences will be expected due to different circumstance in e.g. available suspended sediment, tidal range, wave and wind conditions. However in this way the response of different realignment sites is compared with Perkpolder. In general rates of land-level rise range from a few millimetres to tens of centimetres per year and level off over time as the inundation period decreases

(Morris, 2012; Temmerman et al., 2003b). In managed realignment sites in the UK elevation changes are in the order of several cm/yr (e.g. Tollesbury: $2.3\ cm/yr$ (Garbutt et al., 2006); Orplands: $2.5cm/yr$ (French, 2006); Norhey Island: up to $4.9\ cm/yr$ (Research, 1998); Paul Holme strays: $10\ cm/yr$ (Clapp, 2009)).

Close to Perkpolder, the dyke of the Sieperda polder in the Western Scheldt was breached due to a severe storm in 1990 (Eertman et al., 2002). Since then the tidal influence returned to the polder. The polder was only closed of from Saeftinge since 1966, therefore bed levels were relatively high. The levees of the creeks accreted with a relatively constant $8\ cm/yr$, the floodplains had an initial sedimentation of $3\ cm/yr$, this decreased to $1.5\ cm/yr$ for the next three years after which it increased to $4cm/yr$ when vegetation was developing (Eertman et al., 2002).

For the Western Scheldt, a model study has been performed by Weisscher et al. (2022) to investigate the morphological developments of transitional polders in the Western Scheldt. The inlet width and geometry of the transitional polder affected the net import of sand and mud. A smaller inlet width increases flow velocities at the inlet up to a point where the friction of the inlet width becomes a limiting factor. The managed realignment of Alkborough with a $20\ m$ inlet limits tidal exchange and input of sediments (Wheeler et al., 2008). Moreover, transitional polders with complete dike removal experienced weaker tidal exchange flows and significantly less sand import. As for mud, the distance to the inlet strongly correlated with mud deposits, because these areas have weaker tidal flows that favour net mud deposition, which is also seen in Eertman et al. (2002) and Jongepier et al. (2015).

The realignment site near Freiston Shore is located on the East side of the English coast, behind a mud/sand flat. Land claim and rapid saltmarsh retreat had led to the deterioration of the embankments (Rotman et al., 2008). The site is $66\ ha$ with three $50\ m$ entrances, where an artificial creek network was excavated. The initial sediment accretion is most evident in the vicinity of the breaches due to the reworking of sediment from creek and breach excavation (Rawson et al., 2004). Moreover accretion varied widely over the site with an inverse relationship between elevation and sediment deposition (Brown et al., 2007; Rawson et al., 2004). Moreover Rotman et al. (2008) indicates that the majority of the accreting material is derived from the established saltmarsh in front of the breached embankment. Other sources are the sand/mud flat seaward of the saltmarsh and the breached sea wall.

2.6. Key points

- Managed realignment systems are nature-based flood defence systems, where flood levels are reduced and ecosystem services are provided. The main reason to realign Perkpolder was nature conservation. Part of the dike has been breached to connect Perkpolder to the Western Scheldt.
- The Western Scheldt has higher suspended sediment concentrations in the winter than in summer and higher concentrations during spring tide than neap tide. Over a diurnal cycle, suspended sediment concentrations are higher during low waters than during high waters. This will be matched to measured concentrations at the inlet of Perkpolder.
- The intertidal areas in the Western Scheldt have a general increase in height of almost $1\ cm$ per year. This will be compared with accretion rates of the intertidal area of Perkpolder.
- Asymmetry of the tide and lag effects are main drivers in sediment transport in intertidal areas. Net landward transport by asymmetry of the tide is due to higher peak velocities during flood than ebb or longer high water slack than low water slack. Lag effect cause net landward transport due to differences in flow field, bed level and/or water level.
- Managed realignment sites experience in general land-level rise from a few millimetres to tens of centimetres per year and level off over time as the inundation period decreases.

3

Methodology

In this study the managed realignment site Perkpolder acts as case study. Therefore the methodology starts with an introduction to the study site Perkpolder in Section 3.1. Section 3.2 continues with the presentation of the available data in Perkpolder. Moreover a hydrodynamic model of the Western Scheldt in Delft3D Flexible Mesh evaluates the currents and water levels at Perkpolder. The set-up and validation of this model are shown in Section 3.3. Lastly a morphological model that encloses Perkpolder, a bathtub model, is used in this study. The set-up and schematization of this model is shown in Section 3.4.

3.1. Study site: Perkpolder

Figure 3.1 shows the map of the Netherlands, with in the southwest the Western Scheldt. On the south side of the Western Scheldt (Zeeuws Vlaanderen) Perkpolder is located, which is the study site for this research. This section presents the size of Perkpolder and some general characteristics.

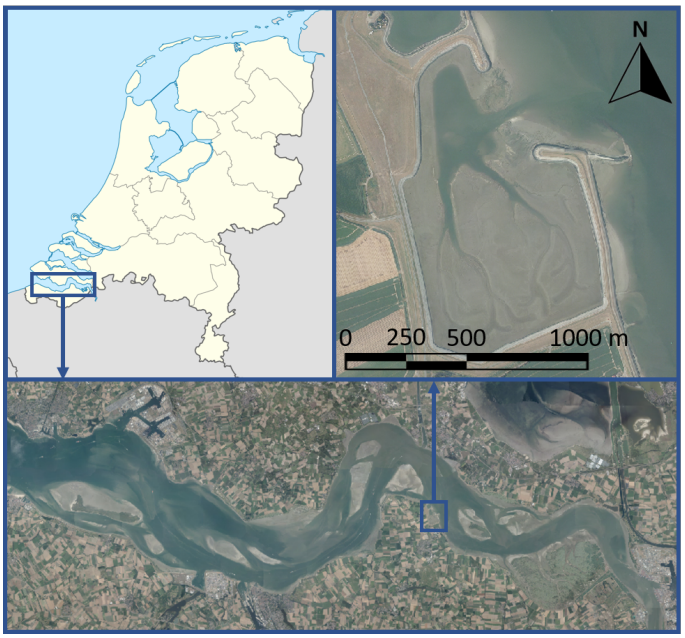

Figure 3.1: Map of the Netherlands, aerial photo of the Western Scheldt and aerial photo of Perkpolder. Retrieved from: Atlas van Zeeland (aerial photo of 2019)[1].

Since June 2015 Perkpolder is opened along a transect of $350\ m$ and has a direct connection with the Western Scheldt. The polder is approximately $700\,m$ wide and $1200\,m$ long, leading to a total area of $70\,ha$. Before opening the polder was used for agriculture, but has been opened to create intertidal area as part of a nature compensation program for the deepening to the Western Scheldt. The realigned area consists of a deeper lying area in the north

[1] https://kaarten.zeeland.nl/map/atlasvanzeeland

and an intertidal area in the south connected by creeks that were excavated before opening.

The tidal datums as shown in Table 3.1 give an indication of the water levels at Perkpolder. The tidal range falls between $2.6\ m$ during neap tides and $6.0\ m$ during spring tides with an average tidal range of $4.6\ m$. This corresponds with a general macro tidal regime at Perkpolder. Winds are primarily coming from the southwest (as shown in Figure 3.2a) and wind velocities are on average higher in the winter than during the summer as concluded from Figure 3.2b.

Table 3.1: Tidal levels at Walsoorden during measurement period of 2015 to 2019.

Tidal Level	**Value [m *NAP*]**
Mean Higher High Water	2.65
Mean High Water	2.58
Mean Sea Level	0.18
Mean Low Water	-2.03
Mean Lower Low Water	-2.15

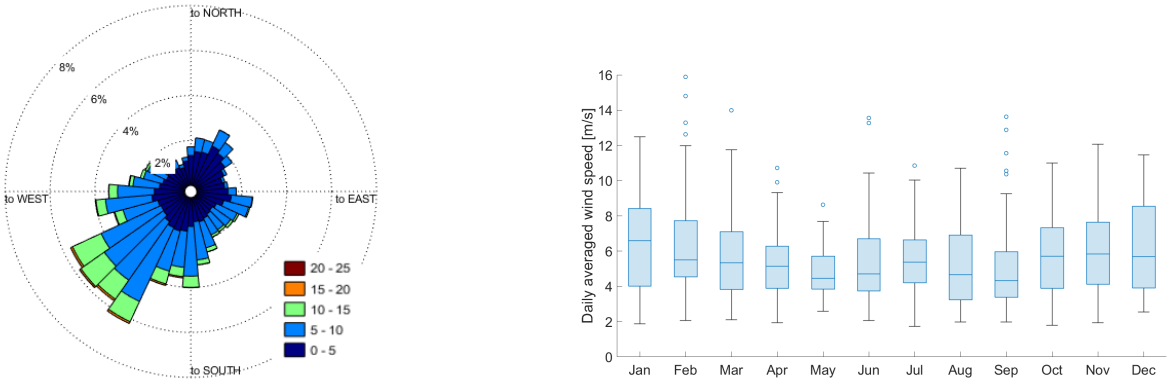

(a) Wind rose

(b) Box plot of daily averaged wind speed

Figure 3.2: Wind conditions at Hansweert during 2016 and 2017.

These hydrodynamic and meteorological conditions lead to peak velocities in the order of ~$1\ m/s$ in the main channel of the inlet and at the beginning of the creeks. On the intertidal area peak velocities are found in the order of ~$0.2\ m/s$. Average suspended sediment concentrations of ~$1\ g/L$ have been measured near the inlet. The sediment distribution is spatially very heterogeneous, but an average grain size of $45\ \mu m$ is found, which correspond to silt.

3.2. Available data

This section presents the relevant data that is measured in and near Perkpolder. This data is collected by different institutes, namely Rijkswaterstaat, the Royal Netherlands Institute for Sea Research (NIOZ) and HZ University of Applied Sciences. Multiple measurement stations of Rijkswaterstaat that measure hydrodynamic and meteorological properties are located close by Perkpolder as shown in Figure 3.3, these stations have a measurement interval of 10 minutes.

There are no measurements of waves at Walsoorden, only at the station of Hansweert and the Overloop van Valkenisse. The downside of these wave measurements is that these measurement stations are respectively 5 and $8\,km$ from Perkpolder. Due to the geometry of the Western Scheldt, the energy from waves coming from the North Sea will not reach until Perkpolder (Chen et al., 2005). However, locally generated waves will still be generated in the Western Scheldt, the downside of the Hansweert measurement station is that the waves that are generated locally will differ significantly between Perkpolder (at the South) and Hansweert (at the North) (Willemsen et al., 2022). Therefore only a qualitative consideration of waves near Perkpolder is made based on wind data.

Several measurement campaigns have been organised to measure hydrodynamic, morphodynamic and ecological properties of Perkpolder. Table 3.2 shows a subset of these measurements which are used in this research. Figure 3.3 shows the locations of these measurements. This consists of three types of bathymetric data, namely yearly

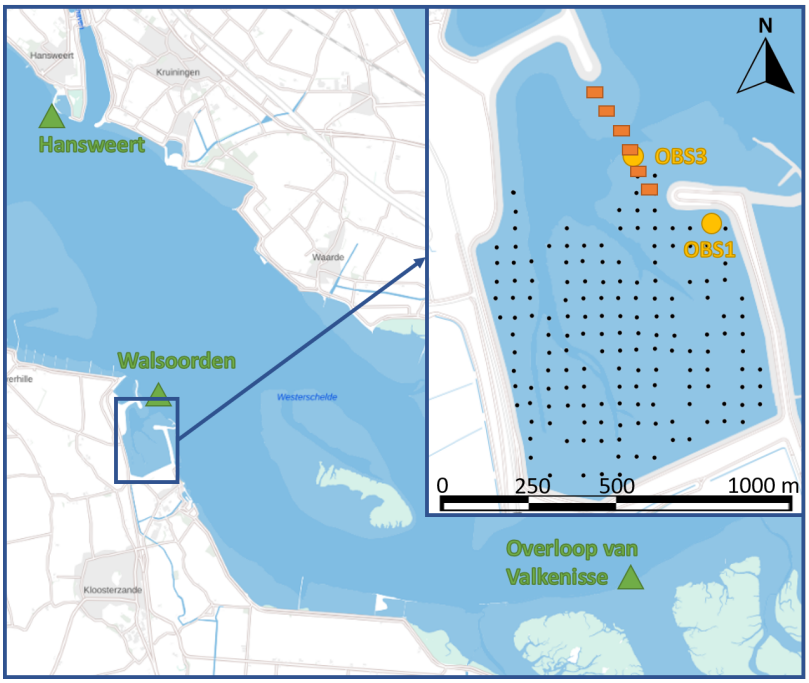

Figure 3.3: The location of Rijkswaterstaat measuring stations are shown in green triangles, the location of the two Optical Back Scatter sensors are shown in yellow circles, the locations of the six flow velocity sensors are shown in red rectangles and the location of the bed sample locations are shown in black. Viewing from North to South the velocity sensors are named MP0101 to MP0106.

measured LIDAR and vaklodingen data and multibeam measurements that are measured four times a year. Moreover, six ADCP measurement devices measured the flow velocity in the entrance for 6 days, this data is used to validate the hydrodynamic model. At two locations the turbidity of the flow is measured to get an indication of the suspended sediment concentration at these locations. Sediment samples of the top layer ($3\ cm$) of the intertidal area of Perkpolder are analysed by the NIOZ. Furthermore, multiple sediment cores have been taken in Perkpolder in the last sixty years, which gives an indication of the history and depth profile of the subsurface.

Table 3.2: Performed measurements at Perkpolder in the period 2015-2024.

Type	Measuring equipment	Data type	Resolution	Date	Frequency
Morphology					
Bed elevation	LIDAR	Grid data (x,y,z)	2 m x 2 m	2015 - 2024	1 / yr
Bed elevation (without shallow intertidal area)	Multi-beam	Grid data (x,y,z)	1 m x 1 m	2015 - 2024	4 / yr
Bed elevation	Vaklodingen	Grid data (x,y,z)	25 m x 25 m	2015 - 2024	1 / yr
Hydrodynamic					
Flow velocity at the inlet	Aquadopps	Flow velocity	6 points / 400 m (Figure 3.3)	25-11-2015 - 01-12-2015	1 / 10 min
Sediment concentration					
Suspended sediment concentration	Optical Back Scatter (OBS)	Turbidity	2 locations	16-09-2016 - 06-03-2017	1 / 5 min
Soil properties					
Sediment characteristics	Samples	-	200 locations / 50 ha	2016 - 2019, 2021	1 / yr
Sediment characteristics	Samples	-	15 locations	2016 - 2018, 2020	4 / yr
Sediment profile	Cores	-	20 locations	-	-

For ecological purposes much more data is available, such as species numbers (e.g. benthic communities or birds), but this lies beyond the scope of this research. Morris et al. (2002) shows the importance of vegetation for the morphodynamic response, however from aerial photos (e.g. Figure 1.1) vegetation is not yet present at this intertidal area and the effects of vegetation are therefore not included in this research.

3.3. Hydrodynamic model

To analyse the hydrodynamics at Perkpolder and the interaction with the Western Scheldt, an existing Delft3D Flexible Mesh model is used. This model is set up by de Vet et al. (2022) to determine the impact of groynes on the hydrodynamics near Knuitershoek and Baalhoek. The benefit of this model is that it covers the entire Western Scheldt from Vlissingen towards the Dutch-Belgium border. Therefore current interactions between Perkpolder and the Western Scheldt are taken into account. Section 3.3.1 will show the grid, depth profile and setup of the model. Since Perkpolder lies between Knuitershoek and Baalhoek, it is expected that the results will match reality, however this will still be proven in Section 3.3.2.

3.3.1. Grid schemetization and model setup

The full model setup is found in de Vet et al. (2022) of which a close up of the grid around Perkpolder is shown in Figure 3.4. From the regular grid in the Western Scheldt a transition is made to the triangular grid in Perkpolder by using two grid refinements. The resolution increases from approximately $60\ m$ to $15\ m$ within Perkpolder. Furthermore, Figure 3.4 shows the inserted observation points, observation cross section and thin dams.

Figure 3.4: Refinement of the grid at the area of Perkpolder. Two mesh refinements are included to move from the regular grid to the triangular grid in Perkpolder. The red lines show the thin dams that represent the groynes. The pink line is an observation cross section to determine discharges. The eye icons represent observation points: the six locations close to the entrance are the locations of the six ADCP sensors and the observation point outside of Perkpolder corresponds with station Walsoorden.

Figure 3.5a and 3.5b show the computational domain of the Western Scheldt for respectively the bathymetry of 2016 and 2018. Using the LIDAR, multibeam and vaklodingen data the bathymetry of Perkpolder is available for every year from 2015 to 2021. Therefore five model runs have been setup using a combination of the bathymetry of the Western Scheldt of 2016 and 2018 and the bathymetry of Perkpolder from 2015 to 2021. Moreover, for 2015 to 2017 the initial bathymetry has been altered slightly to create a clear entrance channel. Since the grid size of Perkpolder is still in the order of $15\ m$ and the bathymetry is interpolated between these grid points, this is too coarse to reproduce the narrow entrance channel in the entrance of Perkpolder during the first years. Therefore the bathymetry has been adapted to create a realistic entrance channel.

At the entrance of Vlissingen a water level and velocity boundary condition is imposed. For the boundary condition

Table 3.3: Initial bathymetry of Western Scheldt model runs

Name	Bathymetry Perkpolder	Bathymetry Western Scheldt	Alteration of entrance channel
RUN004-15	2015	2016	Yes
RUN004-16	2016	2016	Yes
RUN004-17	2017	2016	Yes
RUN004-18	2018	2018	No
RUN004-19	2019	2018	No
RUN004-20	2020	2018	No
RUN004-21	2021	2018	No

at the Belgium-Dutch border, a discharge condition is applied. The boundary conditions are derived from the Waqua DCSMv6-SUNOv4-Kf model (Zijl et al., 2015; Zijl et al., 2013) which encloses the Southern North Sea. The calibration procedure is described in de Vet et al. (2022) and will not be repeated. A summary of the most important model parameters is given in Table 3.4. Salinity has not been taken into account, since the domain of interest is located in the upper meters of the estuary, where density effects do not play a large role.

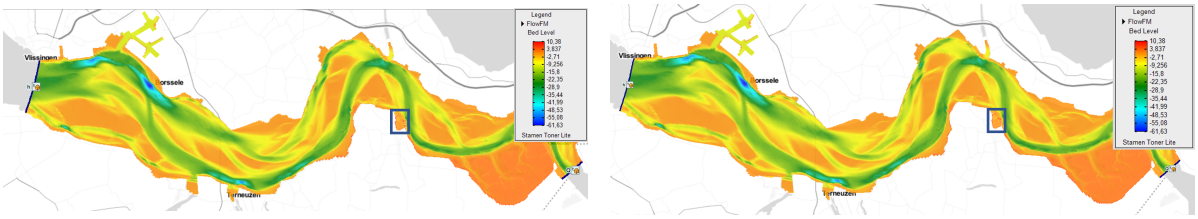

(a) 2016 **(b)** 2018

Figure 3.5: Initial bed level of the Western Scheldt for the model runs of 2016 and 2018. The blue enclosed area is Perkpolder.

Table 3.4: Model parameters for the model.

Parameter	Value	Unit
Maximum computational time step	30	s
Maximum courant number	0.7	$-$
Density of water	1000	kg/m^3
Density of air	1.2	kg/m^3
Friction coefficient (Manning)	0.024	$s/m^{1/3}$
Horizontal eddy viscosity	1	m^2/s
Vertical eddy viscosity	$5 \cdot 10^{-5}$	m^2/s
Threshold depth for drying and flooding	0.0001	m
Wind drag coefficient (Smith & Banks)	0.00063 0.00723	$[-]$

3.3.2. Validation

The model of 'Buitendijkse Maatregelen' is calibrated for Knuitershoek and Baalhoek, Perkpolder lies between these two places and therefore the results are expected to match reality. Still, waterlevels, velocities and discharge at Perkpolder of the model are validated with measurements. First, the water levels at station Walsoorden are compared with the model results, the error between the model results and measurements is quantified using:

1. Bias: the mean difference between the model results and the measurements. This is an indicator for the net deviation of the model.
2. RMSE: root-mean-squared-error, the square root of the mean of the difference between the model results and measurements squared. This is an indicator for the variance of the deviation.
3. uRMSE: unbiased root-mean-squared-error, the same as the RMSE after subtraction of the bias. This is an indicator for the variance of the deviation without an effect of the bias.

The validation of the water levels, flow velocities and discharge is performed in Appendix A. It was concluded that the water levels at station Walsoorden were in very good alignment with a bias equal to $-0.0058\ m$, the RMSE and uRMSE are equal to $0.067m$. With a tidal range in the order of $4.6m$, the water levels are accurately reproduced.

Besides the water levels it is important that the flow velocities and directions show good similarities with reality. Therefore the flow velocities of the model are compared with ADCP measurements. Since there are no ADCP measurements of flow velocity during the simulation period (25-8-2016 to 25-9-2016), the flow velocities are compared based on the tidal range. Since the flow velocities are measured in november 2015, the closest measured bathymetry of march 2016 (RUN004-16) is compared with the ADCP measurements. Also the discharge at the entrance of Perkpolder is compared with the discharge computed from the ADCP measurements and the tidal storage approach described in Section 2.3.1.

The detailed results of the comparison of flow velocities and discharges is shown in Appendix A. The discharge through the entrance shows a reasonable alignment with the ADCP measurements and tidal storage approach. However, it is found that the difference in model simulations, tidal storage approach and ADCP measurements have a physical origin. In the first year, the deepest part of the entrance channel was still higher than low water. Therefore part of the tide the flow was blocked, while the water levels kept changing outside of Perkpolder. After blocking of the flow, the water levels in Perkpolder needed to catch-up during the remainder of the tide, thereby increasing peak flow velocities. The tidal storage approach does not take this phenomena into account, since it assumes a direct feedback between the discharge in the entrance and the water level change. This phenomenon has been elaborated in Appendix B. Concluding, the discharge from the Western Scheldt model is modelled correctly and is line with both ADCP measurements and the tidal storage approach.

Lastly the flow velocities at Perkpolder show many similarities with the measured ADCP data, although there are some differences in peak velocity. This has the same physical reason, namely that in the first year the entrance is partially blocking the flow. Overall, the hydrodynamics at Perkpolder are accurately reproduced and the Western Scheldt model corresponds with the measurements.

3.4. Morphodynamic model

The 'Buitendijkse maatregelen' model is only calibrated and validated for hydrodynamics. Furthermore, the downside of such a large model for morphodynamics at Perkpolder is that it is hard to control and calibrate a large model for a relatively small domain of interest. To achieve the right conditions at Perkpolder would take a lot of effort. Lastly an error has already been found in the velocity field near the grid refinement boundaries (as shown in Appendix A), this will lead to unrealistic sedimentation and erosion patterns close to the region of interest.

Therefore another modelling approach has been used for the morphodynamic model. A local (bathtub) model of Perkpolder containing only the polder area until the entrance of the basin is set up in Delft3D 4. The boundary conditions are imposed at the entrance of Perkpolder. The main advantage of such a model is that it is easily understood and controlled. A scenario study is performed in which initial and boundary conditions are altered in order to understand the response of Perkpolder in different circumstances.

3.4.1. Grid schemetization and model setup

The Delft3D 4 model is depth-averaged (2D) and takes only sediment transport into account. Wind and wave forcing is not taken into account, except for one of the scenario runs. In order to capture the morphological effects within the creeks and at the same time keep a reasonable simulation time a grid size of $5\,m$ was chosen. In order to keep the Courant number below 1, a time step of $0.1\,min$ has been applied for which the model is proven to be stable. The grid is build up out of square grid cells, the grid is oriented in such a way that the entrance consists of a single row of grid cells as shown in Figure 3.6. The bathymetry of 2018 has been used for the base case, since the area has already matured and especially the entrance area is deeper and wider than the initial bathymetry. One representative month from the 25th of August to the 25th of September is simulated (see Appendix F for more information about the representative month). The cumulative erosion and sedimentation is scaled to obtain the yearly cumulative erosion/sedimentation.

The hydrodynamic calibration has been fully based on the water levels and flow velocities of the Western Scheldt model. This model has been validated (see Appendix A) and therefore the water levels and spatial velocity field will be matched to this model. The full calibration and validation procedure is shown in Appendix C. Concluding, the discharge through the entrance and the water levels in Perkpolder are sufficiently reproduced by a single water level boundary condition and the parameters shown in Table 3.5.

The spatial velocity field shows good similarities with the Western Scheldt model, however it differs close to the boundary condition. Since the boundary condition consists of prescribed water levels, the flow can enter Perkpolder only perpendicular to the boundary condition. In reality, the flow enters Perkpolder from the north due to the currents in the Western Scheldt. This leads to a spatially different velocity field during rising water levels as shown in Figure 3.7.

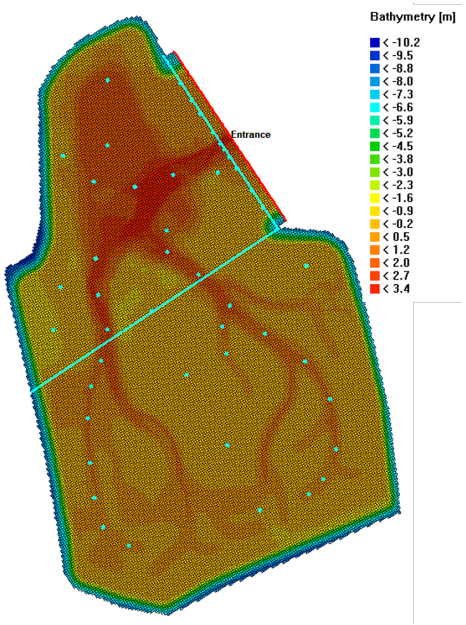

Figure 3.6: Grid of the bathtub model of Perkpolder, the bathymetry of 2018 is plotted in this grid. Legend shows depth with respect to NAP, so red areas are the deepest parts of Perkpolder. The boundary condition is applied at the red line named Entrance. The blue lines are observation cross sections and the blue points are observation points within Perkpolder.

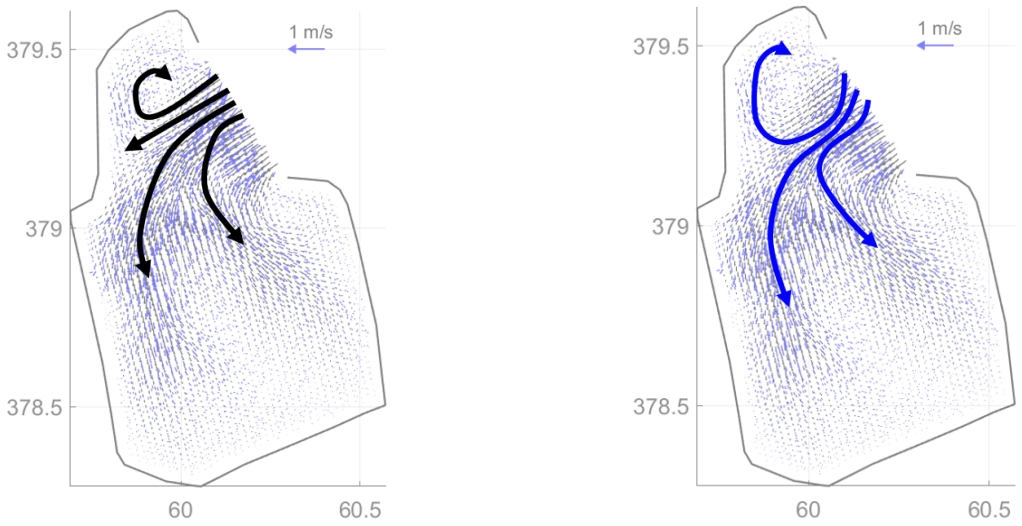

(a) Bathtub model

(b) Western Scheldt model

Figure 3.7: Main flow directions of the bathtub model and Western Scheldt model at LW + 4.5 hr.

Two main differences are found between the bathtub model and the Western Scheldt model as shown in Figure 3.7. First, the eddy observed in the north of Perkpolder is smaller in the bathtub model. Moreover, in the Western Scheldt model, the flow is squeezed after the entrance since the flow is coming more from the North instead of perpendicular to the entrance. This phenomena is not observed in the bathtub model and will probably lead to differences in sedimentation and erosion of Perkpolder. A more detailed explanation of the effects is shown in Appendix C. However, the differences in flow field do not limit the value of this model, as long as these considerations are included in the interpretations of the results.

To calibrate the morphodynamics of the bathtub model, three types of sediments are used. Table 3.5 shows the different sediment types and the properties. The bottom of the model consists of a mixture of sand and mud (mud - base). In order to mix the sediments over the bottom layers, the model has a spin-up time of a week where only the bottom layers mix and the bed level is unaffected. When this spin-up time was not included high erosion rates were found near the entrance and at the beginning of the creeks.

The mud applied at the boundary, consisting of suspended sediment from the Western Scheldt, is called mud - entrance. The difference between the two mud types is the critical shear stress for erosion. In order to represent the consolidation of the mud that is present in Perkpolder, the critical shear stress for erosion is increased for the mud - base. When the consolidated mud (mud - base) is entrained and in suspension, it will have the same properties as the mud applied from the boundary condition, with a lower critical shear stress for erosion. This cannot be modelled in Delft3D 4, therefore the depth efficiency of the mud - base is set to 0 and mud - base cannot settle. In this way it is prevented that sediment eroded from mud - base settles at low dynamic areas in Perkpolder, creating layers at these locations that are difficult to erode. Since the erosive volume of mud - base is small compared to the accreting volume of mud - entrance, this assumption is valid. The magnitude of the critical shear stress for erosion are based on van der Vegt et al. (2021).

The mud concentration at the boundary is created artificially and based on OBS measurements. A linear trend is imposed between the water levels at station Walsoorden and the measured concentrations as shown in Figure 3.8. The concentrations are obtained from the OBS measurements as shown in Appendix D. If the water level was lower than $1\ m + NAP$, a background concentration of $0.2\ g/L$ has been used (for more details see Appendix D). This does not match with the trend line at $1\ m + NAP$, so there is a discontinuity in the concentration at the boundary. Since the concentration is calibrated using a linear calibration curve, the trend line is scaled in order to match the mean sediment flux through the entrance as shown in Figure 6.6a. Best results were acquired when the trend line was scaled with a factor of $\frac{3}{4}$. In the remainder of this report this factor will be called *magnitude factor mud entrance*.

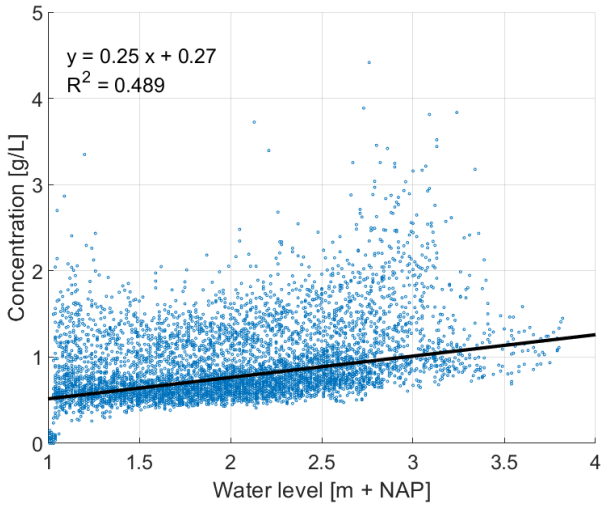

Figure 3.8: Relation between water level and measured suspended sediment concentrations.

As discussed, limitations of the bathtub model are arising due to the use of a 2D model (instead of 3D), the forcing of the boundary condition, the type of sediments used and the exclusion of wind and wave forcing. The wind and wave forcing will be investigated using a scenario run in which the wind and wave forcing is applied. Local redistribution of mud-base will not be taken into account, since settling is not possible for this type of mud. Moreover, sand is not included in the boundary condition. However, the benefit of scenario studies is that this will be compared to the base run and when knowing the limitations of the model, the right conclusions can be drawn.

3.5. Key points

- The foundation of the data analysis are bathymetry data and concentrations at the inlet of Perkpolder. Bathymetric data is combined from LIDAR, multibeam and vaklodingen data to obtain a complete bathymetric profile of Perkpolder. The concentration measurements are calibrated from turbidity measurements and post-processed, e.g. outliers are removed (see Appendix D).
- The hydrodynamics (water levels and currents) at Perkpolder are derived from a validated Delft3D Flexible Mesh (depth averaged) model that models the entire Western Scheldt from Vlissingen to the Dutch-Belgium border (see Appendix A). Therefore current interactions between the Western Scheldt and Perkpolder are included in the model. The model is still relatively coarse ($\sim 15\ m$) inside Perkpolder, therefore it should be used as indication of the flow velocities inside Perkpolder.
- A 2D model of Perkpolder until the entrance (thus excluding interactions with the Western Scheldt) is setup to analyse the morphodynamics at Perkpolder. The model has been calibrated and validated for hydro-

Table 3.5: Model parameters for Delft3D 4 bathtub model.

Module	Parameter	Value	Unit
Flow	Computational time step	0.1	*min*
	Density of water	1000	kg/m^3
	Friction coefficient (Manning)	0.022	$s/m^{1/3}$
	Horizontal eddy viscosity	1	m^2/s
	Horizontal eddy diffusivity	1	m^2/s
	Threshold depth for drying and flooding	0.01	m
	Reflection parameter (boundary condition)	1	s^2
Morphology	Morphological scale factor	1	-
	Spin-up interval until start of changes in bed composition	720	*min*
	Spin-up interval until start of changes in bed level	10800	*min*
	Sediment - Sand		
	Sediment type	sand	-
	Specific density	2650	kg/m^3
	Median grain size (D_{50})	150	μm
	Dry bed density	1600	kg/m^3
	Initial sediment thickness	0.4	m
	Sediment - Mud entrance		
	Sediment type	mud	-
	Specific density	2650	kg/m^3
	Settling velocity	$1.0 \cdot 10^{-5}$	m/s
	Critical bed shear stress for sedimentation	1000	N/m^2
	Critical bed shear stress for erosion	0.5	N/m^2
	Erosion parameter	$1 \cdot 10^{-4}$	$kg/m^2/s$
	Dry bed density	500	kg/m^3
	Initial sediment thickness	0	m
	Sediment - Mud base		
	Sediment type	mud	-
	Specific density	2650	kg/m^3
	Critical bed shear stress for sedimentation	1000	N/m^2
	Critical bed shear stress for erosion	1.0	N/m^2
	Erosion parameter	$1.3 \cdot 10^{-4}$	$kg/m^2/s$
	Dry bed density	500	kg/m^3
	Initial sediment thickness	1.0	m
	Depth efficiency	0	-
Underlayers	Transport layer thickness	0.1	m
	Number of underlayers	5	-
	Thickness of underlayer	0.1	m

and morphodynamics. Using three types of sediment (sand and two types of mud), the morphological development of Perkpolder is described. This model is applicable for scenario runs, where differences are compared with the base run to see how the morphological development of Perkpolder would be altered in a specific scenario.

4

Historical reconstruction of Perkpolder

This chapter presents part of the results of the data analysis with a focus on the geomorphology of Perkpolder. First of all, in Section 4.1 the historical context of Perkpolder is shown. Next, the initially excavated lay-out and bed levels after the managed realignment are shown in Section 4.2. Moreover sediment samples are taken from the bottom, these measurements are shown in section 4.3. Lastly in section 4.4 sediment cores are presented for different locations within Perkpolder to show the sediment characteristics of the bottom until a depth of approximately $5 - 10\,m$. The results from this chapter provides insights for the morphological development of Perkpolder.

4.1. Historical context

Knowing the history of Perkpolder is necessary to create a complete view on the morphological development of this area. Figure 4.1 shows a map of Zeeland with the embankment of the different polders. The polders surrounding Perkpolder (and thus also Perkpolder) are all embanked before 1300. Moreover, the bed level will be very low with respect to the current MSL.

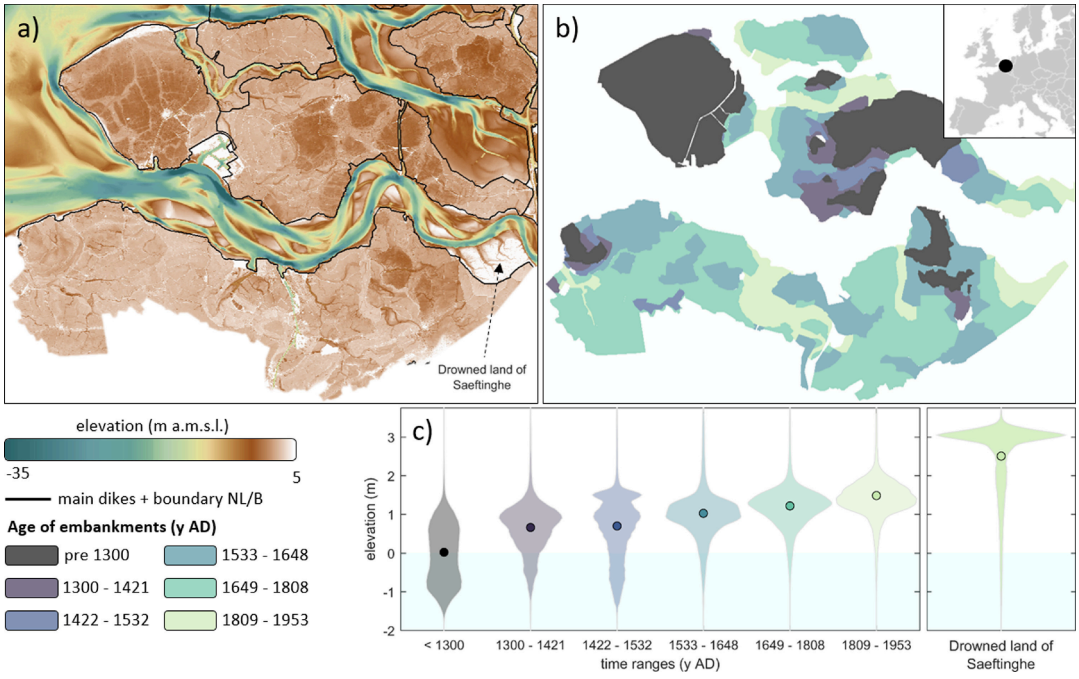

Figure 4.1: Overview of land reclamations along the Western Scheldt Estuary. (a) Map of bed elevation of the area near the Western Scheldt Estuary. Note that the highest bed elevations along the estuary are found outside the main dikes (exluding the barrier coast and the harbour near the estuary mouth). (b) Age of embanked areas along the Western Scheldt Estuary. Uncoloured regions represent unreclaimed land. The geographical location is given in an inset. (c) Violin distribution plots of bed elevations split per age of embankment, showing older polders have a lower bed elevation than younger ones. For reference, an unembanked salt marsh named "Drowned Land of Saeftinghe" is shown for comparison, which has a much higher bed elevation. Retrieved from: Weisscher et al. (2022).

Furthermore, when comparing maps from different time periods, the dyke layout did not change between 1850

and 2015. The dyke layout first showed up in maps from 1850 (Figure 4.2a) and stayed until 2015, when the dyke was removed over a length of $350\ m$ to create the entrance of the managed realignment (Paiva et al., 2019). The soil beneath this dike is thus subjected to consolidation for at least 165 years.

(a) Perkpolder in 1850 **(b)** Perkpolder in 1925 **(c)** Perkpolder in 2022

Figure 4.2: Maps of Perkpolder showing evolution from 1850 to 2022. Retrieved from: Atlas van Zeeland (historical maps of 1850; 1925 and map of 2022)[1].

4.2. Bed levels

The morphological lay-out of Perkpolder is not the same as the bathymetry of the original farmland. To enlarge the conveying capacity of the water to the intertidal area, creeks were excavated (van Ginkel, 2019). The initial proposed lay-out is shown in Figure 4.3 which includes a deeper excavated area and three different type of creeks. The deeper lying area was initially excavated to MLW, around $-3.0\ m$ *NAP*, this was done on purpose to create a sub literal ecosystem (de Kramer, 2008; van Ginkel, 2019). Type 1 of the creeks were the largest type of creeks with a bottom depth of $-1.50\ m$ *NAP* and a bottom width of $10.0\ m$. Type 2 creeks consisted of a bottom depth of $-1.25\ m$ *NAP* and a bottom width of $5.0\ m$. Lastly, type 3 creeks had a bottom depth of $-1.00\ m$ *NAP* and a bottom width of $2.5m$ (van Ginkel, 2019). The slope of the creeks was the same for all type of creeks, namely $1:20$.

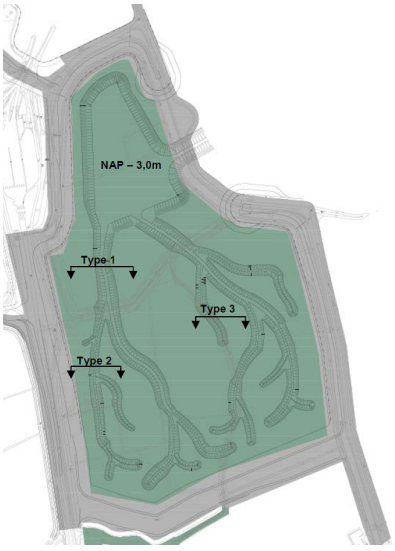

Figure 4.3: Initial layout for Perkpolder with the type of creeks at each location in Perkpolder. Retrieved from: (van Ginkel, 2019)

[1] https://kaarten.zeeland.nl/map/atlasvanzeeland

Three types of bathymetry data are available to determine the morphological development of Perkpolder, namely vaklodingen, LIDAR and multibeam data. As shown in Table 3.2 the multibeam data has a frequency of 4 times per year, while the LIDAR and vaklodingen data has a yearly measurement interval. The multibeam data only contains data of deeper lying areas, therefore bathymetry data for low-lying intertidal area is available once every year. Moreover the grid size of the vaklodingen data is $25 \times 25\,m$, while LIDAR and multibeam have more detailed measurements, so vaklodingen will only be used if LIDAR and multibeam do not have coverage. The LIDAR and multibeam data are combined based on the date of measurement that is closest to each other. In Figure 4.4 the bed levels in each year are shown from the start of the realignment in 2015 until the most recent LIDAR measurements in 2021.

The vaklodingen data set has a vertical accuracy of $50\,cm$ (2σ) (Wiegmann et al., 2005). This is mostly attributed to interpolation errors. The LIDAR data is slightly more accurate, approximately $30\,cm$ (2σ) (Marijs et al., 2004). The multibeam has an accuracy in the same order as the LIDAR measurements (Dix et al., 2012). Since this research averages the measurements over large number of grid cells, the cumulative interpolation error averages out and the accuracy increases considerably. Marijs et al. (2004) shows that systematic errors can still be present, however the error is in the order of $10\,cm$. Moreover, for the LIDAR data the exact measurement date is not known. The 2016 data set is measured in March 2016 and thus it has been assumed that for the following years the LIDAR is also measured in March. Due to this inaccuracy trends over multiple years are very reliable, but deviations between years can take place.

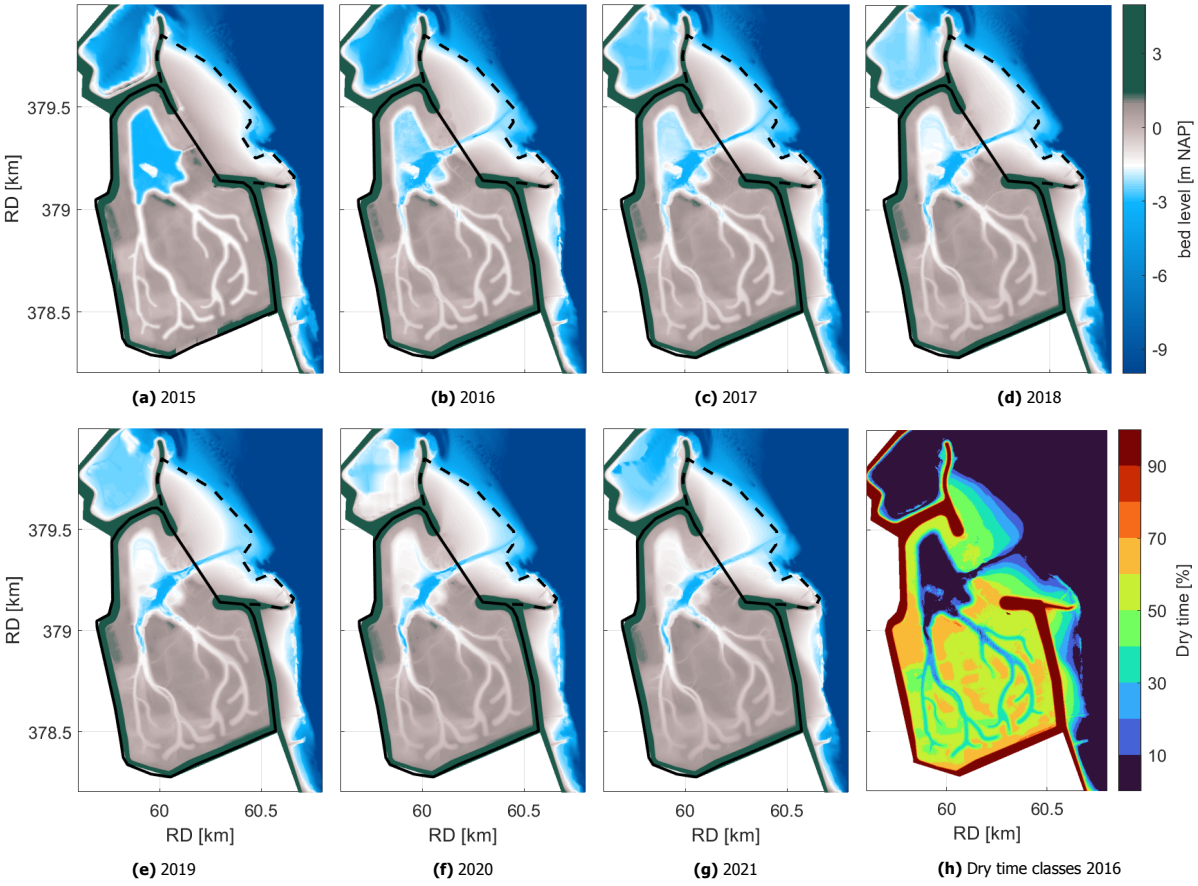

(a) 2015 **(b)** 2016 **(c)** 2017 **(d)** 2018

(e) 2019 **(f)** 2020 **(g)** 2021 **(h)** Dry time classes 2016

Figure 4.4: Bathymetry of Perkpolder from 2015 to 2021 for every year ((a) to (g)). LIDAR data is used as base and missing data is filled up with multibeam and vaklodingen data. The outline of Perkpolder is shown as a solid black line and the frontal entrance area of Perkpolder is enclosed by the dotted black line. Dry time classes for the bathymetry of 2016 are shown in (h) based on the water levels at Walsoorden in 2013.

Perkpolder is divided in three subareas, namely the frontal entrance area which is enclosed by the dotted black line in Figure 4.4. The frontal entrance area ends at the main channel of the Western Scheldt. Furthermore, Perkpolder (enclosed by the solid black line in Figure 4.4) is divided into two areas, namely the pond and the intertidal area. The pond is defined as the part of the polder that is constantly under water. For this criteria an exposure duration (dry time) of less than 10 % was chosen. As seen in Figure 4.4h, this corresponds with the dark blue area. The depth for this criterion is $-1.88\,m$ *NAP*. The rest of Perkpolder will be called the intertidal area, this encloses thus

the entire area south of the pond and surrounding the pond. The morphological behaviour of these three areas will be investigated in Chapter 5.

4.3. Sediment samples

Sediment samples have been collected from the top three centimetre of the bed (Paiva et al., 2019). This has been done for two sets of sediment samples. 200 sediment samples have been taken yearly over the entire intertidal area of Perkpolder, moreover 15 sediment samples have been collected with a frequency of four times a year (Paiva et al., 2019). For all these sediment samples the bulk density, water content, mud depth, median grain size and mud content have been determined.

In Figure 4.5 the median grain size (D_{50}) of sediment samples taken from the upper bed is shown from 2016 to 2020 for the intertidal area of Perkpolder. The data presents yearly averaged properties. It is important to realise that the sediment samples consist of imported sediment if the bed level accreted. If a location eroded, the sediment sample consists of material that was already present at Perkpolder and this is different than material entering Perkpolder.

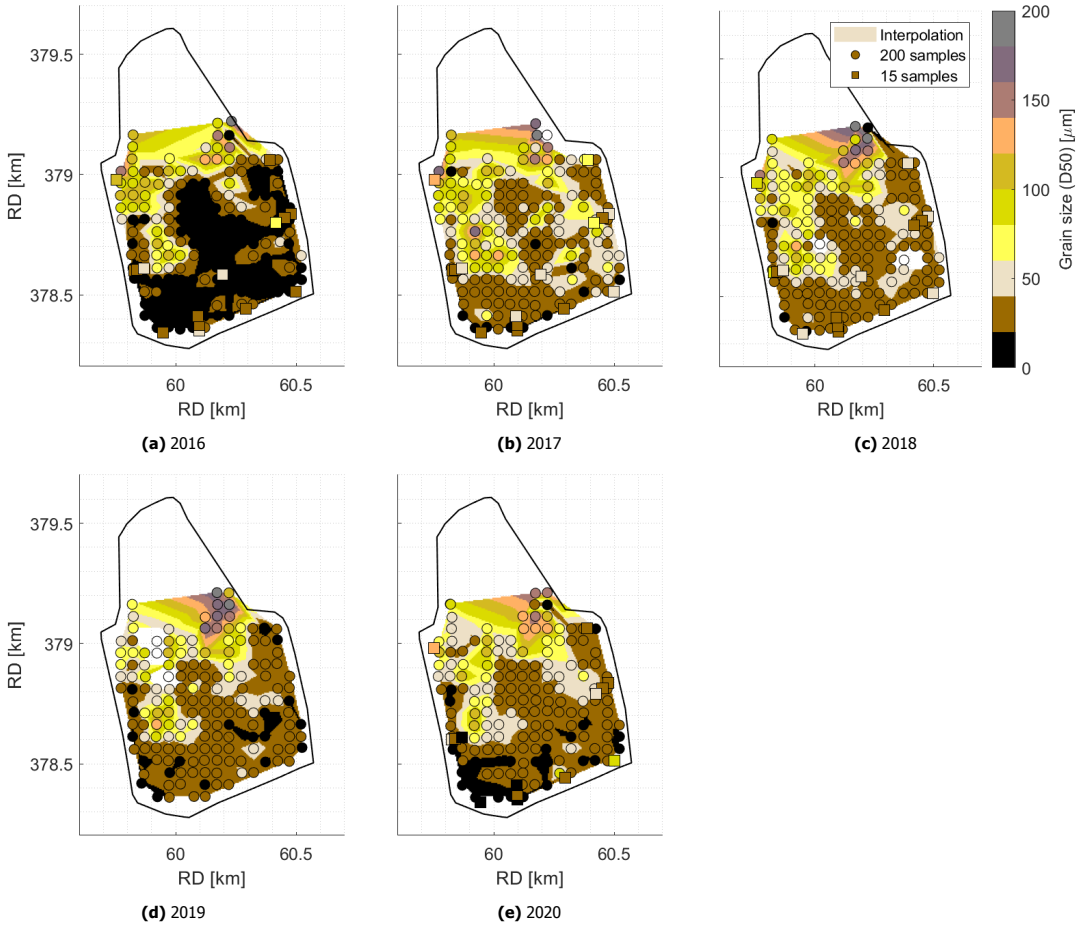

Figure 4.5: Bed level composition measured from a yearly 200 sample measurement campaign and a 15 sample measurement campaign that was performed four times a year. The 15 sample campaign was averaged for each year. The 200 sample campaign is interpolated to see the overall distribution of sediment in Perkpolder. White areas are areas with no available data.

When comparing the spatial distribution of the median grain size with Figure 4.4, it is observed that the creeks have on average a larger median grain size than the rest of the intertidal area. Coarse sediment settles in higher hydrodynamic energetic conditions (the creeks) than fine sediment that is transported as suspended sediment to the flats (Grabemann et al., 2004). The fines are transported in suspension across the flat and settle in the upper part when slack tide occurs (Brunetta et al., 2019). The largest grain size is approximately $150\ \mu m$ to $200\ \mu m$ and is found near the inlet, which correspond with sandy material (Doeglas, 1968).

It is striking that the average grain size in 2016 is much lower than other years on the intertidal area. Furthermore, from 2017 to 2020 general trends are found, which do not correspond to the 2016 data set. Therefore the

hypothesis is posed that the data set of 2016 consists largely of material that was present at Perkpolder before the opening of the managed realignment. From 2017 to 2020 a general fining of the grain size is observed at locations near the dyke ring. In the same period, the ends of the creeks are filling up with fine sediment and the average grain size decreases at these locations.

4.4. Subsurface cores

Besides the sediment samples of the top layer of Perkpolder, cores give insight in the depth profile of the bottom of Perkpolder and the history of Perkpolder as shown in Figure 4.6 and 4.7. The cores date between 1961 and 2021 and tell a coherent story about the subsurface of Perkpolder.

Cores close to the dyke show a sand layer starting around a meter below NAP to two or three meter above NAP. This is possibly material which is part of the dyke. Furthermore, almost everywhere in Perkpolder the average profile is the same, namely a clay layer of a few meters, then a peat layer and then again a clay layer. Below the clay layer sometimes a sand layer is visible. Erosion can slow down when the peat layer is reached since peat layers have on average significant higher critical erosion stresses than clay (Tuukkanen et al., 2014). The peat layer is located on a depth of around $-2\ m$ *NAP* to $-3\ m$ *NAP* as seen in Figure 4.6c and 4.6d.

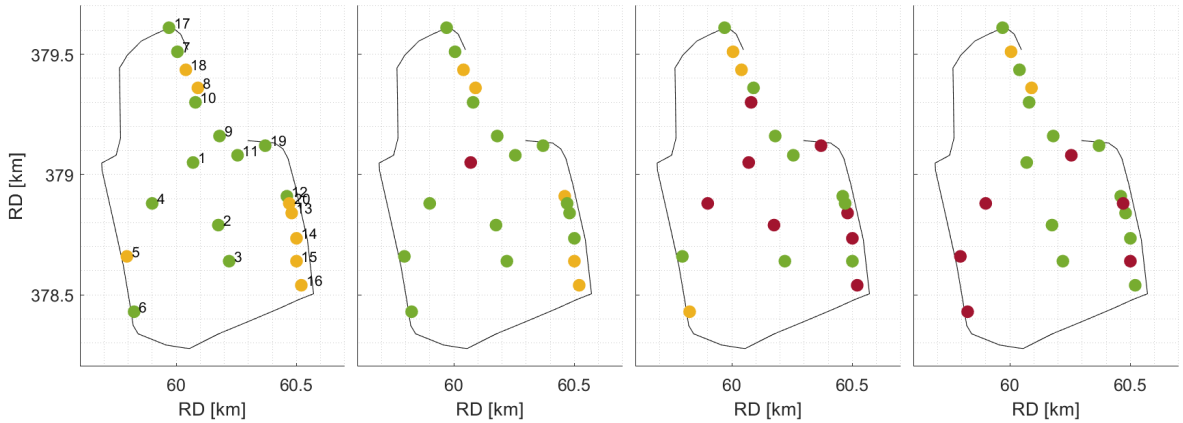

(a) Depth $0\ m$ *NAP* **(b)** Depth $-1\ m$ *NAP* **(c)** Depth $-2\ m$ *NAP* **(d)** Depth $-3\ m$ *NAP*

Figure 4.6: Sediment type at a depth of 0, -1, -2 and -3 m NAP from sediment cores. Green, yellow and red cores correspond with respectively clay, sand and peat at the indicated depth. Retrieved from: DINOloket.

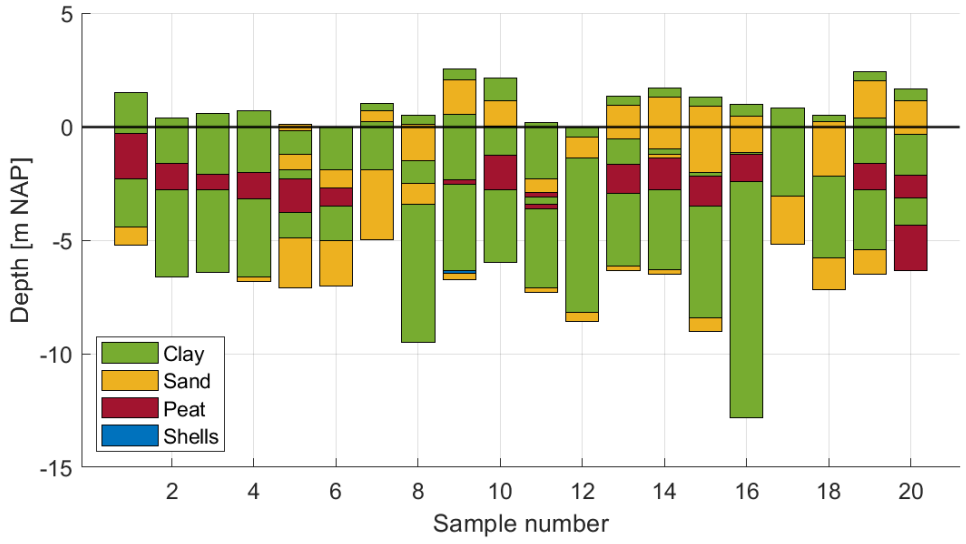

Figure 4.7: Overview of all sediment cores, the numbers correspond with the numbers in Figure 4.6a. Retrieved from: DINOloket.

4.5. Key points

- Perkpolder has been embanked since 1300, therefore bed levels of Perkpolder are relatively low compared to the current MSL. Moreover, the location of the primary dike surrounding Perkpolder has not been changed for at least 165 years, leading to consolidation of the bottom below the current inlet.
- Bathymetry data from different data sources is combined to obtain a yearly bathymetry profile of Perkpolder. Three different areas are distinguished, namely the frontal entrance area, a deeper lying pond inside Perkpolder and an intertidal area. Each area has its own morphological development.
- Sediment samples from the top bed layer indicate that the average grain size of the intertidal area is decreasing over time, mainly due to accretion. Moreover, the creeks have on average a higher median grain size than the surrounding intertidal area.
- Sediment cores of the bottom of Perkpolder show that Perkpolder mostly consists of clay material with an underlying peat layer around $-2\ m$ *NAP* to $-3\ m$ *NAP*, this layer is in general more difficult to erode.

5

Measured morphological development

This chapter presents the morphological development of Perkpolder and its subsystems. First the morphological development of the entire area is presented and analysed in Section 5.1. The frontal entrance area is analysed in section 5.2, the evolution of the inlet cross section is shown in section 5.3 and lastly the morphological behaviour of the creeks is presented in section 5.4.

5.1. Perkpolder

The bed level changes shown in Figure 5.1 are determined from the difference in bed level between two consecutive years (Figure 4.4). On a subsystem level, it appears that the pond and intertidal area are accreting every year, however the pond shows more accretion than the intertidal area. The hypsometric curve in Figure 5.2b confirms this behaviour in which the lowest lying areas (pond) have the most sedimentation. This has also been concluded in Paiva et al. (2019) where was suggested that the pond could act as buffer for the intertidal area and that accretion rates in the intertidal area could increase when the pond has reached its equilibrium situation. This hypothesis cannot be tested with this data, since the pond has not yet reached an equilibrium. The frontal entrance area on the other hand has an overall erosive character.

Figure 5.1 shows very high sedimentation and erosion rates in the main channel of the Western Scheldt, moreover this differs per year. These changes in the channel will not be evaluated in this thesis, however this may affect the frontal entrance area of Perkpolder. The edge of the frontal entrance area is defined in such a way that these major temporal changes of the main channel are not included in the frontal entrance area.

The harbour north of Perkpolder shows a sedimentary trend, however in two years the bed level decreased (Figure 5.1d and Figure 5.1f), this is because of dredging activities[1]. The influence of the adjecent harbour on the sediment balance at Perkpolder will not be investigated. Since there is a groyne seperating the frontal entrance area with the harbour basin, it is assumed that interactions between these two systems are limited.

The creeks are eroding at the beginning of the channels (near the pond) and are accreting more landward, inward of the intertidal area. Moreover, the channel located in the frontal entrance area is deviating each year. For example, the bed level change from 2018 to 2019 (Figure 5.1d) shows that the channel has accreted in northern direction and eroded in southern direction. This is probably caused by the interaction with the main channel of the Western Scheldt which is also changing very much. However, when looking at the overall change from 2015 to 2021 (Figure 5.1g), a clear eroding trend is observed for the channel. All these areas and subsystems will be investigated in more detail in the next sections.

The total bed level change of Figure 5.1g is compared with the model results from the Delft3D FM model. The model results are presented as fraction of the tides that have a maximum (peak) flow velocity lower than $0.3\,m/s$, this represents how sheltered a certain area is. To achieve an accreting area, sediment from a source should be available and transported to the location of interest. At this location the sediment can settle and shouldn't be re-entrained. Figure 5.1h gives an indication how well sediment is trapped at a certain location. This is in line with the sedimentation and erosion patterns shown in Figure 5.1g. In the pond two areas with low peak velocities which are circled in red match with large sedimentation patterns in the pond. For the creeks different processes play a role, since accretion is observed at part of the creeks where also high flow velocities occur.

[1] https://www.omroepzeeland.nl/nieuws/10816843/toch-baggerwerk-in-haven-perkpolder

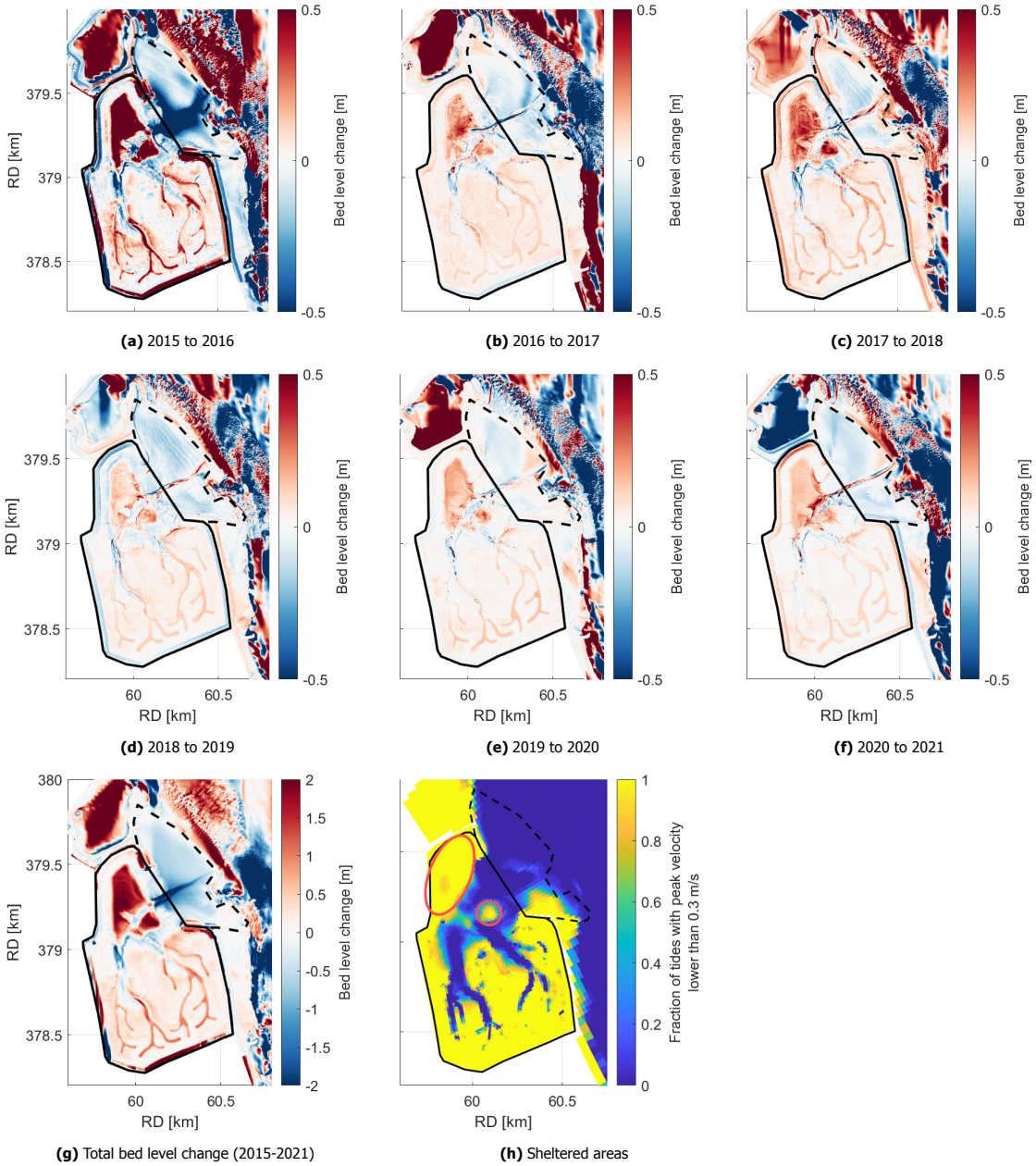

Figure 5.1: Bed level changes between 2015 and 2021 for every year ((a) to (f)) and the total bed level change over this period (g). Note that the colour range differs in (g). Figure (h) shows the results from the Delft3D FM model of the fraction of the tides with a peak velocity less than 0.3 m/s.

Figure 5.2a shows the average bed level change of certain areas in Perkpolder. The frontal entrance area and the pond faced a similar trend: in the first year the accretion rate for the pond and the erosion rate of the frontal entrance area were relatively high. From 2016 a change in trend is found and a lower, however still a respectively accreting and eroding trend is discovered for the pond and frontal entrance area. Table 5.1 shows the yearly accretion rate from June 2015 to March 2016 and the yearly accretion rate (from a linear fit) from March 2016 to March 2021. The average bed level increase for the period of 2016 to 2021 for the intertidal area ($3\ cm/yr$) matches the initial accretion rate of the Sieperda polder in the Western Scheldt (Eertman et al., 2002). The data suggests that an equilibrium position is not yet reached.

In general, when a system moves to a new equilibrium position, the changes are largest in the starting years and will decrease towards the new equilibrium position (Bosboom et al., 2022). However, in this case, there are more factors playing a role. The initial sedimentation of the pond is very high, namely a factor 4.4 higher than the mean sedimentation rate of the next years. This is more than the intertidal area, which has a factor 2.3 between the first year and the next years.

Table 5.1: Rate of change of bed levels for different (sub)areas of Perkpolder from June 2015 to March 2016 and from March 2016 to March 2021.

(Sub)area	Rate of change bed levels: Jun-2015 to Mar-2016 [m/yr]	Rate of change bed levels: Mar-2016 to Mar-2021 [m/yr]
Frontal entrance area	-0.27	-0.04
Pond	0.61	0.14
Intertidal area	0.07	0.03
Perkpolder (= pond + intertidal area)	0.13	0.04

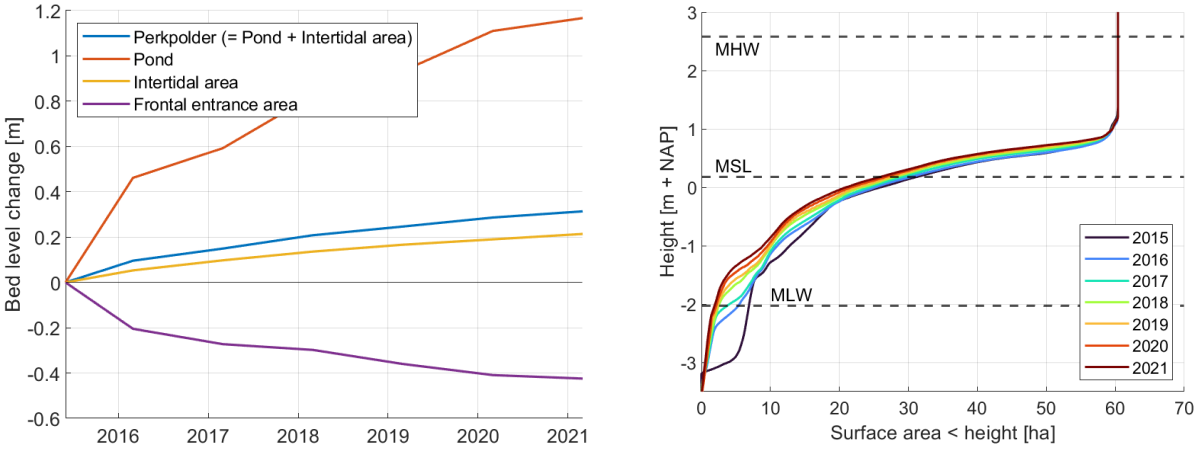

(a) Erosion/sedimentation over time for different areas of Perkpolder with June 2015 as reference.

(b) Hypsometric curve of Perkpolder.

Figure 5.2: Morphological evolution of Perkpolder.

In order to connect the realignment site with the Western Scheldt, the dykes were removed for $350\,m$, however no deep entrance channel was excavated, therefore the deepest part of the entrance was above MLW. As established in Appendix B, this lead to the situation that part of the tide the water was blocked by the entrance (see Figure 5.3b). From 2016 onward the entrance channel eroded deep enough to convey water even during low water levels. Figure 5.3a shows the most important differences between the first year and the next years. The slack time in the first year is much longer than the next years, therefore more sediment can settle. This settling takes primarily place in the pond, since the intertidal area has already dried up, before the water was blocked. Moreover the peak velocity during rising water levels is much higher than the next years, therefore more sediment could be imported to Perkpolder.

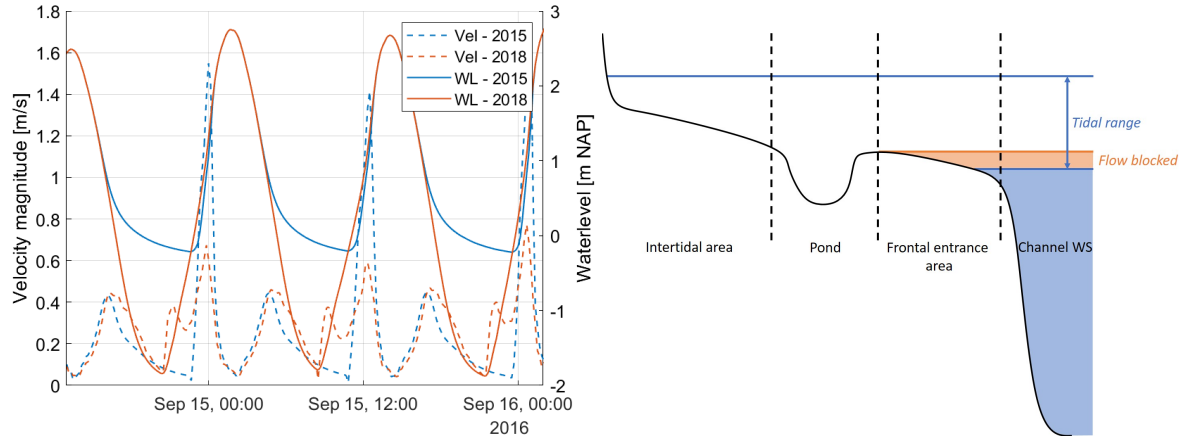

(a) Modelled velocities and water levels in pond resulting from the Delft3D FM model with bathymetry of respectively 2015 and 2018.

(b) 2D schematic showing the effect of the entrance blocking the flow.

Figure 5.3: Effect of the entrance blocking the flow.

5.2. Frontal entrance area

Before the opening of Perkpolder in 2015, the frontal entrance area was an intertidal area located between two groynes. This former intertidal area is now also conveying water to Perkpolder, potentially becoming the ebb tidal delta for the basin. To understand the frontal entrance area, not only the changes after the realignment will be investigated, but also the development of the intertidal area between 1950 to 2015. This sheds light on the sediment availability and helps explain the current morphological development.

Figure 5.4 shows on the left the difference of the minimum bed level measured between 1950 and 2015 and the bed level of 2015, on the right the difference between the minimum bed level measured between 1950 and 2015 and the bed level of 2021 is shown. Between 1950 and 2015 in general sedimentation occurred at the intertidal area as seen in Figure 5.6a. Between 2015 and 2021 an erosive trend is visible. The white areas show areas on the frontal entrance area that reached the minimum elevation of the period 1950 to 2021. In Figure 5.4b more white areas are visible than in Figure 5.4a. The hypothesis is that these areas may erode less, since this material is already a long time present on the tidal flat and not deposited in recent years. Results from the subsurface cores show that deeper lying areas have layers that are more difficult to erode. This hypothesis is tested using the bed level change between 2015 and 2021.

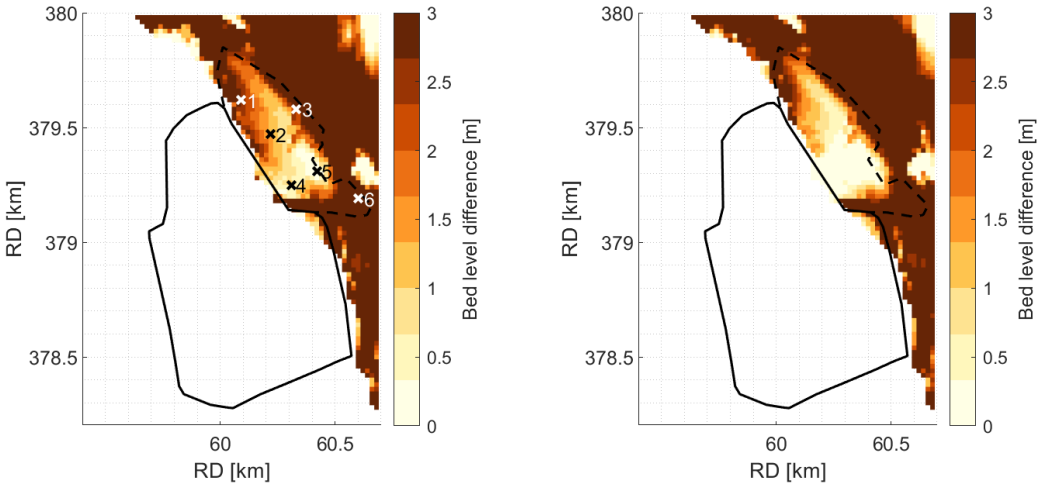

(a) 2015 **(b)** 2021

Figure 5.4: Difference between minimum bed level measured between 1950 and 2015 of the vaklodingen data set and the bed level of 2015 in Figure 5.4a, the same is shown for the bed level of 2021 in Figure 5.4b. Differences below $0\ m$ (erosive areas) are cut off at $0\ m$. This is an indication of the sediment availability at these locations. Location 1-6 in Figure 5.4a corresponds with the time series shown in Figure 5.6a.

To investigate the frontal entrance area erosion after the realignment in more detail, circles are considered to evaluate different areas of the frontal entrance area as shown in Figure 5.5. In location 1 (top of Figure 5.5) close by the dyke (radius of 50 and $100\,m$), the frontal entrance area is eroding in a smaller pace than further away from the dyke. This erosive trend continues until 2021. Location 2 of Figure 5.5 shows the erosion in the centre of the frontal entrance area. The circle with a radius of $50\ m$ shows the erosion of the inlet, which is very rapid in the first years and stabilises after 2018. Overall it is observed that the erosion stabilises from 2020. When comparing this with Figure 5.4b, it is observed that the sediment availability in this part of the frontal entrance area is less than near location 1 of Figure 5.5. This does not mean that there is no sediment that can erode, but there is no sediment deposited since 1950 which may erode more easily than sediment that is present for a long time at a certain location. In location 3 the same behaviour as location 2 is visible.

Besides the yearly LIDAR data, also multibeam data is available for the frontal entrance area up to four times a year. This gives the possibility to look more detailed in time to the bed level change. Figure 5.6b shows the bed level change for the frontal entrance area for all the multibeam measurements. Since multibeam is measured from a boat, the areas with a small depth are not captured, these are filled up with the yearly LIDAR data. Figure 5.6b shows that the bed level change is not constant in time, but changes throughout the year. High erosion rates are found initially (June 2015 to December 2016) to create capacity to convey the water in and out of Perkpolder. After the initial response, the erosion rate differs in time, in 2016 a relatively constant erosion rate is observed that stabilises in 2017. From 2021 a change in trend is found and the frontal entrance area erosion seems to stabilise.

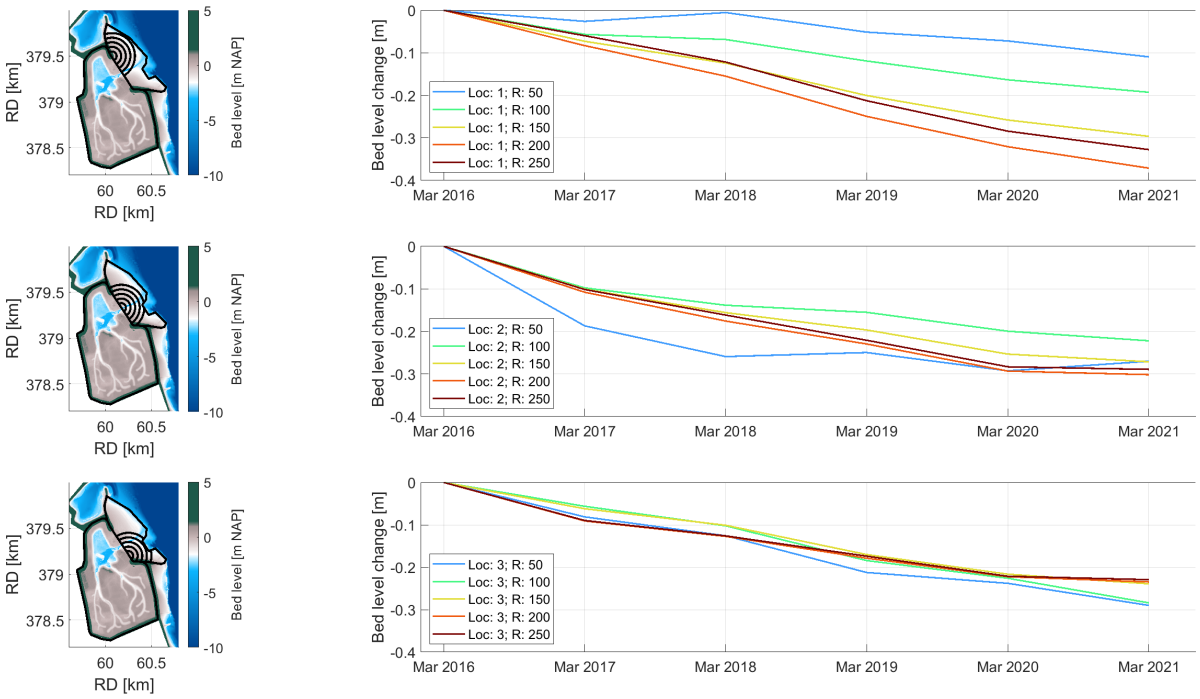

Figure 5.5: Erosion rates of frontal entrance area for different location within the frontal entrance area and different radii of the circles.

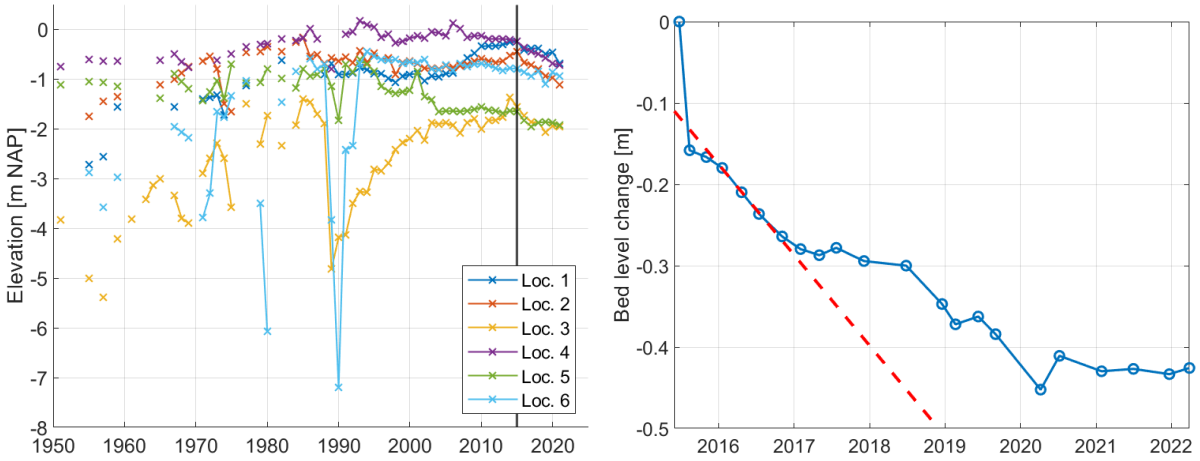

(a) Temporal evolution of frontal entrance area for 6 locations using vaklodingen data set (locations shown in Figure 5.4a). The black line indicates the moment of the managed realignment.

(b) Bed level changes of the frontal entrance area as defined in Figure 5.1 using multibeam data filled up with LIDAR data. For 2016 the trend line is shown, to show the difference with the initial response in 2015 and the response from 2017 onward.

Figure 5.6: Temporal evolution of frontal entrance area.

5.3. Inlet

$350\,m$ of the former dyke was breached to create the inlet of the realignment area. The morphodynamic evolution of the inlet is described in this section. According to maps dating back to 1850 (see Figure 4.2a) the dyke was already present at that time. The soil below the dyke will thus be consolidated for at least 165 years. Moreover, some remains of the old dyke are visible due to erosion of the frontal entrance area as shown in Figure 5.7. This will lead to difficult to erode areas close by the inlet.

To analyse the morphodynamic development of the inlet, a transect is considered as shown in Figure 5.8. The inlet first deepened, which created a deep and narrow entrance channel. Over time, this channel is widening and the area next to the narrow channel is eroding. The largest erosion took place between 2015 and 2016. Close to the southern dyke (located at $300\,m$ of the transect) a new, small entrance creek is developing.

To quantify how the inlet changed, the cross sectional area below MSL is calculated in Figure 5.9a. The inlet

(a) Close up of remains of the old dyke in the entrance area of Perkpolder. Photo taken during field trip to Perkpolder.

(b) Top view of inlet from aerial photograph in 2019. Old dyke layout from 1850 is shown in black contour lines and the location of remains of the old dyke is shown in orange. Retrieved from: Atlas van Zeeland.

Figure 5.7: Remains of old dyke near the inlet.

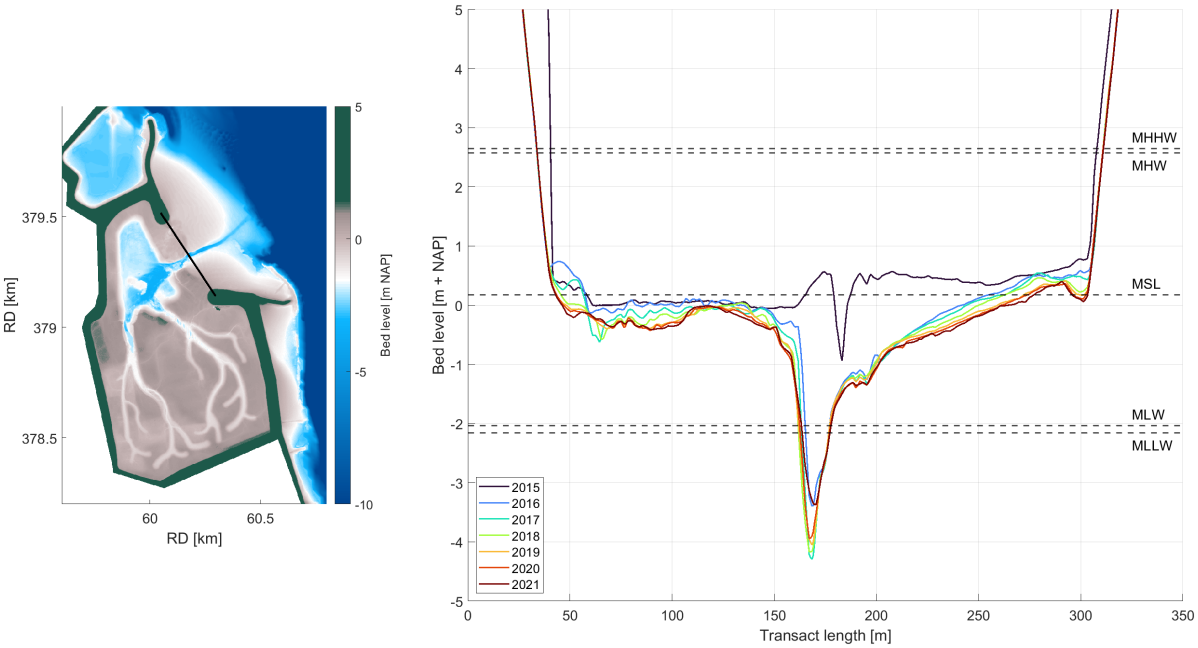

Figure 5.8: transect of the inlet to show the morphological development of the inlet over time.

eroded rapidly in the first year, and after that kept eroding at a lower pace. The stabilising trend indicates that almost an equilibrium cross section is reached. The equilibrium cross sectional area as defined by Jarrett (1976) is close to the current cross sectional area. As established in Section 5.1 Perkpolder is accreting, therefore the tidal prism will decrease every year. It is expected that in the long run with sedimentation of Perkpolder the inlet will become smaller.

The maximum depth of the entrance channel over time is shown in Figure 5.9b. The inlet deepened at first as shown in Figure 5.9b to far below MLLW until 2017. After that the depth of the inlet stabilised and since 2020 a decrease in channel depth is observed. At the same time, the cross sectional area kept increasing, therefore the channel became wider instead of deeper. It is striking that the channel eroded locally far below MLLW, this indicates that the soil at parts outside the main channel would not erode easily. A reason for this could be heterogeneous consolidation, for hundreds of years a dyke was placed above the current inlet, therefore the soil has been consolidated. Since consolidation processes will not be exactly the same for the entire area, therefore heterogeneity in consolidation could explain why only a small section of the inlet eroded to large depths. Secondly a lot of remains from the original dyke (type of remains shown in Figure 5.7a) have been found near the inlet area as shown in Figure 5.7b. This debris may prevent erosion of the area close to the debris, therefore the flow could

be squeezed through the narrow entrance channel.

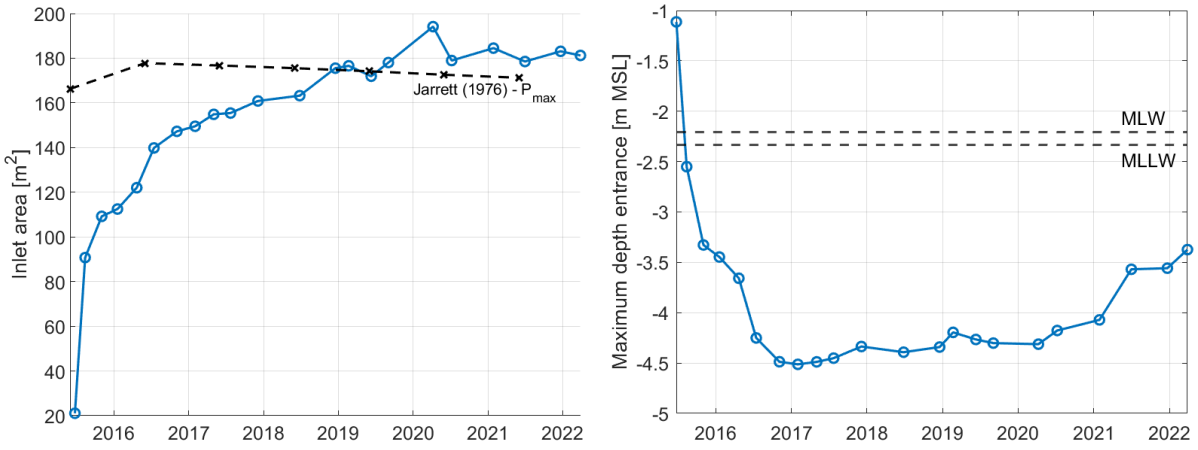

(a) Evolution of cross sectional area below MSL (0.19 m NAP) over time. The black line indicates the equilibrium area calculated from Jarrett (1976) using the maximum tidal prism. The maximum tidal prism is calculated from the Delft3D FM model for the years 2015 to 2021.

(b) Morphological evolution of deepest location of the entrance channel.

Figure 5.9: Morphological evolution of the inlet.

5.4. Creeks

There has been a lot of morphological activity in the creeks. Transects are considered through certain sections of the creeks to understand how these creeks changed over time. Figure 5.10 shows the morphological change over time, the data of 2015 shows the initial creek layout that was excavated. The initial layout consisted of three types of creeks as shown in Figure 4.3 (van Ginkel, 2019). Close to the pond the creeks were too small and therefore eroded a lot throughout the years. Especially for the creek on the west side a lot of erosion is observed, partly due to bend scour. Moreover, more inland, the creeks were too large and accreted as seen from the bottom transect in Figure 5.10. Not only the depth of these creeks changed, but also the slope of the creeks changed. For the accreted creeks, the slope became smaller over time.

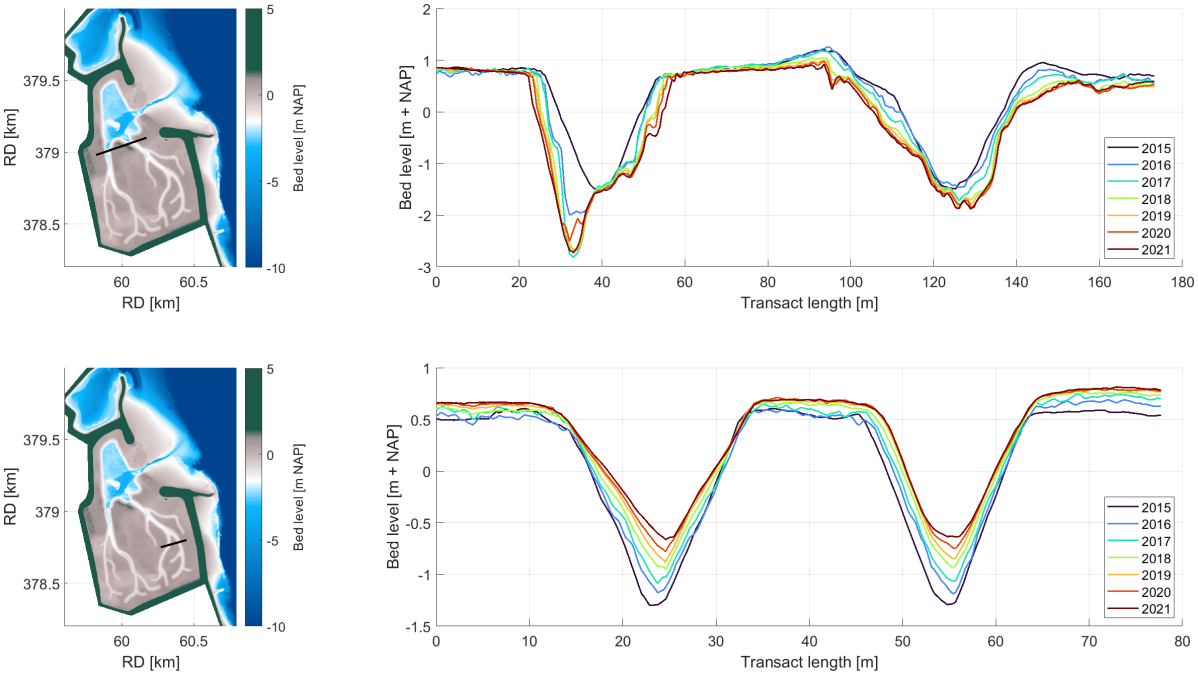

Figure 5.10: Measured transects through two sections at the intertidal area, one close by the pond and one more landward on the intertidal area.

Figure 5.11 shows the main hydrodynamic and morphodynamic developments of the creeks in longitudinal direction. Although the creeks are followed as best as possible, some measurement locations are more inward in a bend and some located more outward. This gives some local changes in bed level, grain size and flow velocity, therefore the focus lies on the general trend seen in the graph and not on explaining every peak.

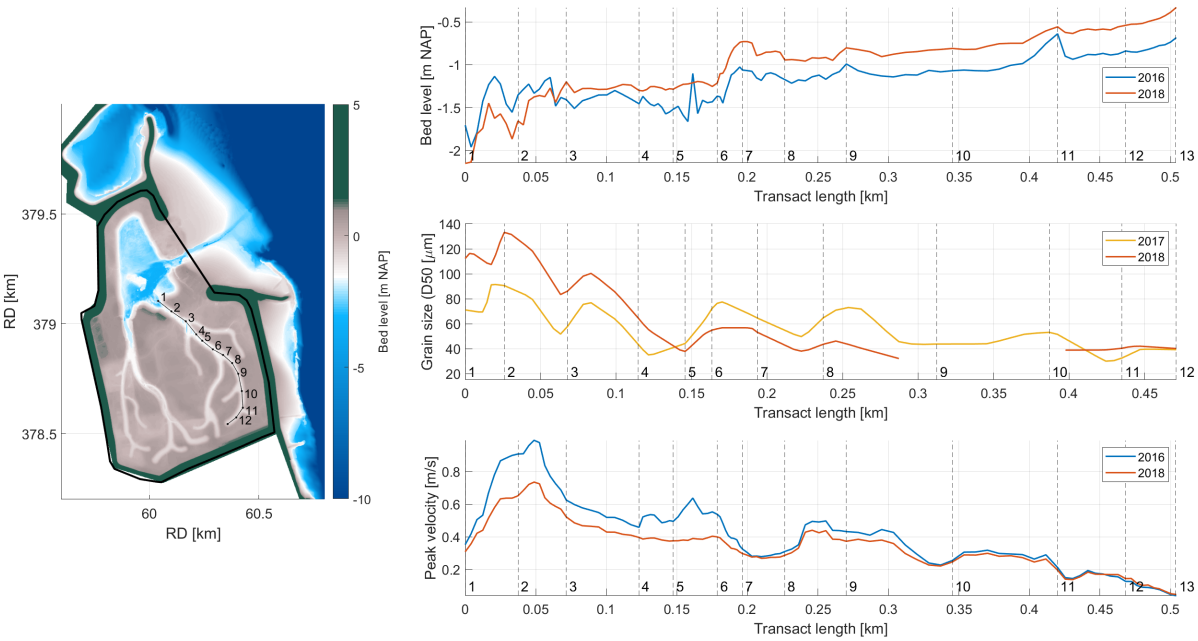

Figure 5.11: Longitudinal transect through creek. The top figure shows the measured bed level of this creek. The middle figure shows the measured average grain size along the creek transect. The bottom figure shows the modelled magnitude of the peak flood velocity. The model run is performed for 2016 and 2018, so therefore these two years are compared.

As observed in Figure 5.11, the creeks have been eroding before the main creek bifurcates (until location 3). After the bifurcation the creeks have been accreting. This correspond with a gradual coarsening of the sediment before the bifurcation (in eroding areas) and a fining of the sediment after the bifurcation. Before the bifurcation, sediment from the bed becomes exposed that has a larger grain size. After the bifurcation the fining of sediment indicates that the material that settles in the creeks is generally finer than material already present.

The peak velocities of the creeks are generally lower after the bifurcation. Moreover, a decay is found in peak velocity between location 1 and 12. This corresponds with the decreasing amount of water that needs to be conveyed to the intertidal area. The peak velocities before the bifurcation are decreasing from 2016 to 2018, this is due to erosion and therefore enlargement of the creeks. The peak velocities at the end of the creeks did not change between 2016 and 2018 while the bed level increased during 2016 and 2018. This means that the velocities could accommodate sediment, however, not so much that the peak velocities will decrease further. This could also be explained by a decreasing tidal prism due to sedimentation of Perkpolder, therefore less water needs to be conveyed to the intertidal area. These findings show in addition to the general sedimentation/erosion patterns, that the creeks are designed too small in the beginning (before the bifurcation) and too large after the bifurcation.

5.5. Key points

- The pond and intertidal area of Perkpolder are both accreting, the accretion rate of the pond is significantly higher. The frontal entrance area is generally eroding.
- All areas of Perkpolder have a significantly higher erosion or accretion rate in the first year, than during the next five years. The pond has an accretion rate 4.4 times higher than in the next years, the intertidal area accretes in the first year 2.3 times more. The erosion rate of the frontal entrance area is a factor 6.5 times higher than in the following years. This is partially explained by the higher disequilibrium in the first year.
- In the first year the entrance was excavated to MSL, therefore blocking the flow during part of the tide. This lead to a longer period of low velocities inside the pond in which sediment could settle. Moreover, this lead to higher peak velocities, creating more import of sediment into Perkpolder.
- The frontal entrance area erodes more in the north than in the south, this matches with sediment deposits from 1950 to 2015. Areas in the north had more deposition between 1950 and 2015 than areas in the south.

The areas in the south eroded below the elevation of 1950 and this may result in layers that are more difficult to erode as seen in Chapter 4.

- The inlet converges to an equilibrium area, which is close to the equilibrium area found by Jarrett (1976). The inlet eroded first to below MLLW, after that the depth decreased and the inlet became wider and less deep.
- The creeks eroded at the beginning and accreted for the remainder of the creeks. This coincided with a general fining of the creeks where sediment was accreting and a coarsening of the creeks, where erosion took place.
- There is a decay in peak velocity along the longitudinal distance of the creeks, due to the decreasing conveying capacity of the creeks.

6

Sediment transport through entrance

This chapter connects the morphological development of Perkpolder and the frontal entrance area by determining the sediment transport through the entrance. In Section 6.1, the flood and ebb dominance of Perkpolder is considered, which is an indication whether sediment is imported or exported into the system. In Section 6.2 the OBS measurements are presented. From these OBS measurements the sediment transport through the inlet is calculated in Section 6.3 and related to different hydrodynamic and meteorological properties to understand the temporal variability. Lastly a sediment balance using the measured bed levels and transport through the entrance is shown in in Section 6.4

6.1. Sediment transport mechanisms

This section gives an indication of the flood dominance of Perkpolder, which is an indication for landward sediment transport. Moreover, the effect of a changing flow field on lag effects is considered in this section. The hydrodynamic conditions for the years 2016 and 2017 have been evaluated, this time period was chosen since the suspended sediment concentration was measured from September 2016 to March 2017.

When looking at Figure 6.1a, the rising time of water levels is generally smaller than the falling time, which indicates that flood velocities are higher than ebb velocities (Jeuken, 2000). This is backed up by modelling results in Figure 6.1b, in which the average flood peak velocity is divided by the average ebb peak velocity. The red areas show a higher peak flood velocity than peak ebb velocity and therefore flood dominance. Figure 6.1b shows that Perkpolder is almost fully flood dominant, except for the entrance channel and frontal entrance area. This means that the tidal signal favours sediment import into Perkpolder (Dronkers, 1986). As addition, Figure 6.2b shows the asymmetrical and flood dominant velocity profile found in the pond and creeks. At the same time the ebb dominance of the inlet and frontal entrance area shows that probably sediment is also transported to the Western Scheldt.

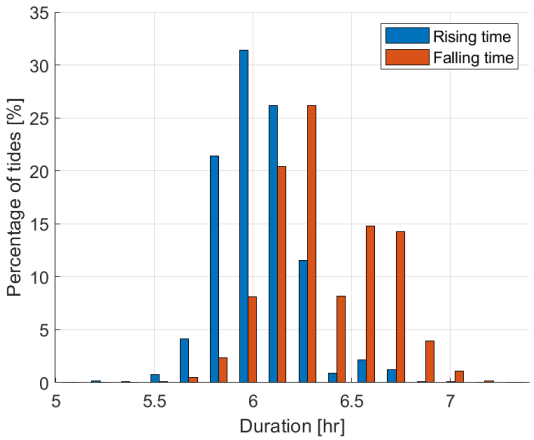

(a) Percentage of tides that a certain rising and falling time is observed from the 2016 and 2017 water levels.

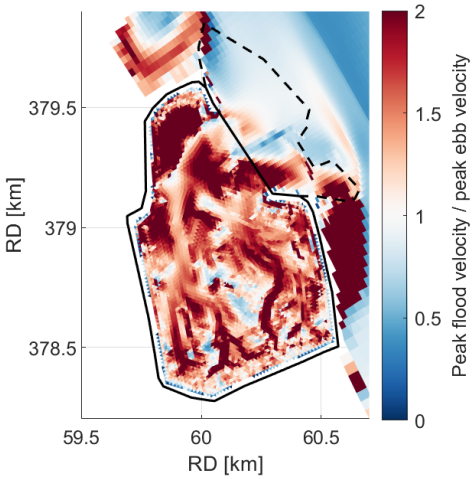

(b) Average peak flood velocity divided by average peak ebb velocity the bathymetry of 2016. This is an indication for ebb dominance (blue) and flood dominance (red).

Figure 6.1: Determination of flood dominance of Perkpolder.

As described in Section 6.1, lag effects are important for the transport of fine sediments. Lag effects cause asymmetries of the sediment particle's trajectory under a periodically reversing flow, classically leading to net landward transport of sediment Gatto et al. (2017). Figure 6.2a shows that the average peak velocity is decreasing in landward direction. This yields both for velocities in the creeks and outside the creeks, this is an indication that scour lag with decreasing velocities in landward direction may contribute to net landward transport of fine sediment (see Figure 2.7b). Moreover, Figure 4.4h shows that a large part of Perkpolder is under water during flood and above water during ebb (if dry time > 10%), creating automatically a longer flood slack time and thus enhanced import of fine sediment. This is visible in Figure 6.2b, where the creek and intertidal area have run dry at low water (LW).

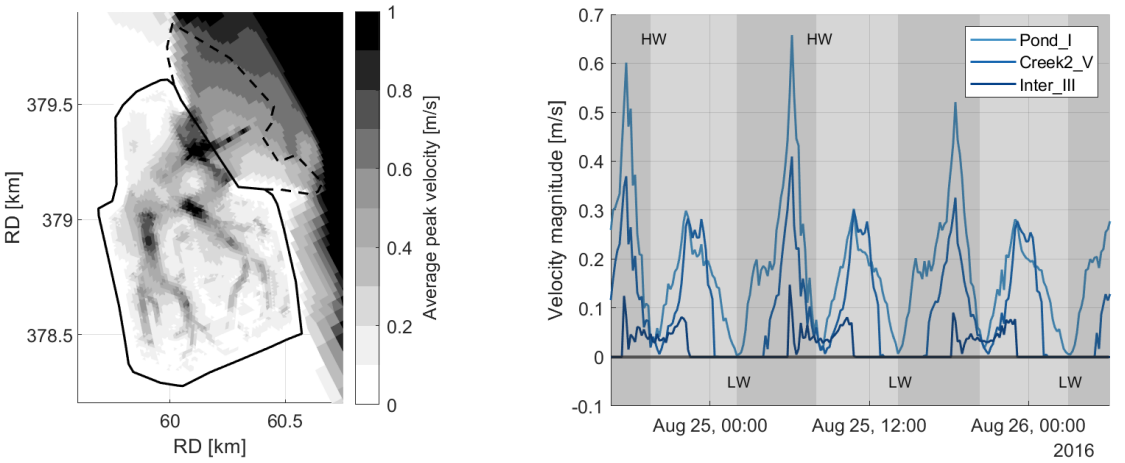

(a) Average peak velocity for model run of 2016 bathymetry.

(b) Velocity profile at different locations. The dark grey background indicate rising water levels and thus inflow of water, the light grey background represents falling water levels and thus outflow of water.

Figure 6.2: Spatial and temporal velocity characteristics.

6.2. OBS measurements

Two OBS sensors were placed in Perkpolder to determine the suspended sediment concentration. These devices measure the back scatter from emitted light waves, this is a measure for the turbidity of the flow (Fondriest Environmental, Inc, 2019). At two locations turbidity measures have been performed as shown in Figure 3.3, near the entrance channel of Perkpolder and behind the dike ring at the intertidal area of Perkpolder. In this way the measurements are compared between two locations at the polder.

The calibration procedure for both data sets is shown in Appendix D. A linear calibration line has been chosen as optimal fit for the OBS measurements, however there are multiple factors that need to be kept in consideration. For example that the sediment type used in the calibration consists of bed material and not suspended sediment (i.e. coarser material). Moreover the devices have been removed multiple times from the water to be cleaned or to change the batteries. This influences the results, therefore the most important conclusions are based on trends of the OBS measurements and less on the precise values.

The results of the OBS measurements are summarised through a box plot in Figure 6.3. This gives an indication of the mean and spreading of the concentrations in Perkpolder. In the period September and October the mean concentration is significantly higher than during the winter months (December, January, February). It is striking that the average concentration is much higher in the autumn than the winter and this is opposing to literature (e.g. Van Der Wal et al. (2010) and van Kessel et al. (2011)).

To get an indication of the magnitude, the OBS measurements are compared with suspended sediment concentrations in the Western Scheldt and other intertidal area located in the Western Scheldt. This is shown by the black lines in Figure 6.3. Van Der Wal et al. (2010) and van Kessel et al. (2011) found that the magnitude of the suspended sediment concentration in the channel of the Western Scheldt is between $50 - 100\,mg/L$ with maxima of $200\,mg/l$. The mean suspended sediment concentration in Figure 6.3 lies around $1 - 2\,g/L$, so this is an order of magnitude larger. In other intertidal areas in the Western Scheldt (peak) suspended sediment concentrations have been measured with concentrations in the order of several g/L (Guo et al., 2018). Zhu et al. (2019) measured at Kapellebank an average SSC of $0.5\,g/L$, which is in the same order of the mean OBS concentrations found during the winter. This however does not explain the higher concentrations found during autumn of 2016 (September

and October).

Figure 5.6b shows that the frontal entrance area of Perkpolder does not erode evenly over time, this is temporally changing. When comparing Figure 5.6b with the time period of the OBS measurements, a comparison is made. Between 2016 and 2017 a change in trend is found in the bed levels of the frontal entrance area. During 2016 the frontal entrance area was eroding in a much higher pace and this pace decreased in winter 2017. The same trend in mean concentration is observed in Figure 6.3 where concentrations are higher in autumn 2016 than winter 2017.

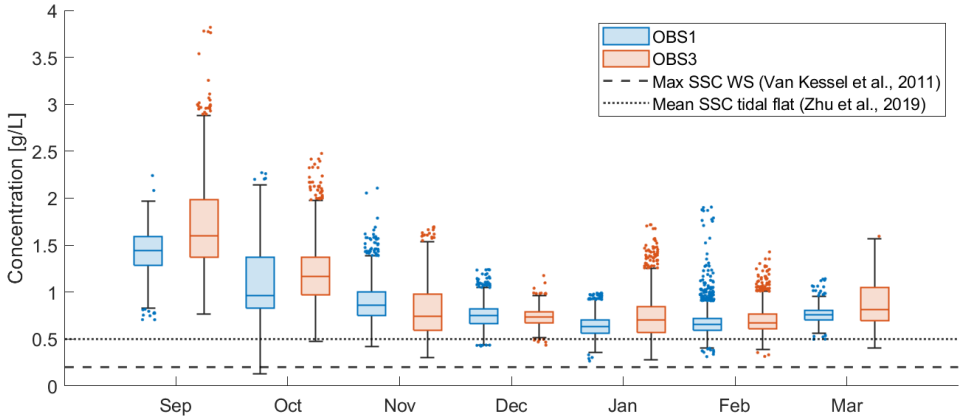

Figure 6.3: Box plot of concentration of OBS1 and OBS3 concentrations with a moving average of 0.5 hrs.

Concluding, the box plot of suspended sediment concentration (Figure 6.3) and the erosion rates of the outer delta (Figure 5.6b) indicate that the frontal entrance area is a potential source with a limited amount of sediment. In order to test this hypothesis, sediment should be stirred up at the frontal entrance area. Three main causes have been identified that can lead to high bed shear stresses and thus stirring up of sediment.

1. **High tidal range.** During spring tides the rate of change in water level is larger (see Appendix F), therefore higher flow velocities are created, which in turn create higher bed shear stresses than tides with a small tidal range (neap tides).
2. **Wind generated waves.** The frontal entrance area is not sheltered by dikes as Perkpolder and therefore waves, generated by wind in the Western Scheldt can stir up sediment.
3. **Ship generated waves.** The main channel of the Western Scheldt is close by the frontal entrance area, therefore ship generated waves can stir up sediment. The importance of ship generated waves on erosion of intertidal area has already been established by Huisman et al. (2010) and Aldershof (2020) for the Western Scheldt. No data is available to substantiate this.

As established in Section 2.3.1, the tidal storage approach is valid for Perkpolder, with this method the cross section averaged velocities at the inlet are calculated. Figure 6.4 shows that there is not a direct correlation between mean velocity during import and mean concentration during import ($r = 0.219$). However, it is striking that high concentrations occur only when the mean velocity is high (larger than $0.3\,m/s$). Figure 6.4a show that these high velocities occur only during a high tidal range (larger than $4.5\,m$). So a high tidal range does not directly lead to high concentrations, but high concentrations occur only during high tidal ranges. By combining Figure 6.4a and Figure 6.4b follows that a combination of high tidal ranges and sometimes high wind velocities (more than $5\,m/s$) create high suspended sediment concentrations. Therefore spring tides and sometimes the extra influence of wind waves is necessary to obtain high concentrations. This corresponds with the hypothesis that locally stirred up sediment from the frontal entrance area contributes to the total suspended sediment concentration. This is also seen in other realignment sites, where an intertidal area in front of the realignment becomes a source of sediment for the realignment (Rotman et al., 2008).

Since this analysis is mainly focusing on fine sediments, the suspended sediment concentration does not directly follow the hydrodynamic forcing. As shown in Figure 2.6, lag effects take place with a certain adaptation time scale (depending on the settling velocity) (Wang et al., 1999). Therefore direct comparison between concentration and velocities is not correct. In order to minimise this effect, the mean velocity during rising water levels is calculated and the mean concentration during rising water levels.

6.3. Sediment import and export

The sediment flux through the inlet is shown in Figure 6.5, since the concentrations are not measured during a full tidal cycle a background concentration is applied when no measurements were performed. Figure 6.5 shows

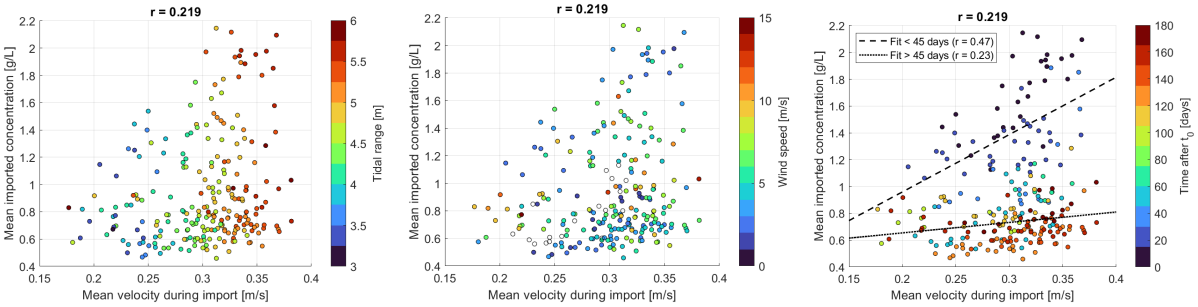

(a) Tidal range **(b)** Wind velocity **(c)** Time after first measurement

Figure 6.4: Scatter plot of cross mean section averaged velocity at the inlet during import of water correlated with the mean concentration during import of water. The colour scale indicates (a) the tidal range; (b) the mean wind velocity during the tide and (c) the time after the first measurement. A linear fit and correlation coefficient has been determined for the first 45 days and measurements taken after 45 days.

that different background concentrations leads to almost the same end result. From Figure D.1 and Figure D.2 the background turbidity was established to lie around 150 *RFUB*, this is close to $0.2\ g/L$ therefore this is used in the remainder of the analysis. Concluding, the sediment transport is mainly into Perkpolder, however there is a strong temporal variability and there is sometimes even net export of sediment. Furthermore it is deducted that high concentrations in suspended sediment (found in september and october as seen in Figure 6.3) lead to large import and export during that period.

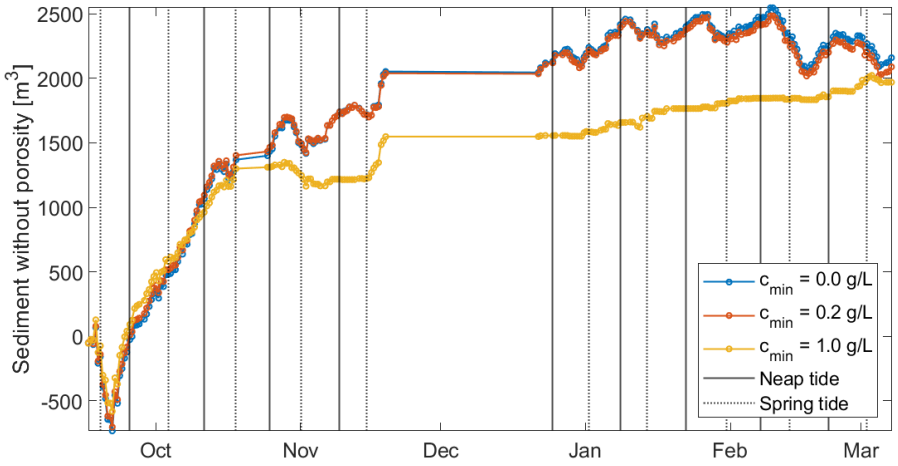

Figure 6.5: Total sediment import/export through inlet using different background concentrations of 0, 0.2 and 1.0 g/L. (Dotted) black lines show the spring and neap tides. The discharge has been matched to the model simulations.

To investigate the temporal variability, a distinction between net importing and net exporting tides is made. All the net importing and net exporting tides are plotted around high water of the respective tide and then averaged as shown in Figure 6.6. The net importing tides have a quickly rising concentration profile which results in a higher mean concentration during rising water levels. After high water the concentration profile peaks for net exporting tides, while the concentration stays constant for net importing tides. The concentration profile of net importing tides and net exporting tides shows more deviations after HW than before HW. Therefore, although the differences are subtle, the main difference in net importing and net exporting tides seems to be the response of Perkpolder and not the concentration during rising water levels.

The net exporting tides have generally a larger flood and ebb discharge and correspond to spring tides (Figure 6.6b). The sediment transport as shown in Figure 6.6c is the product of the concentration and the discharge through the inlet. Due to the higher discharge, the sediment flux of the net exporting tides is generally larger than for net importing tides.

When looking at each individual tide, a correlation is made in Figure 6.7 between the trapping efficiency of Perkpolder and different hydrodynamic properties. The trapping efficiency is defined as the net sediment transport (import or export) divided by the total imported sediment in a tidal cycle. The same characteristics are found as Figure 6.6, namely that higher discharges (ebb or flood) and thus a higher tidal range (spring tides) lead more

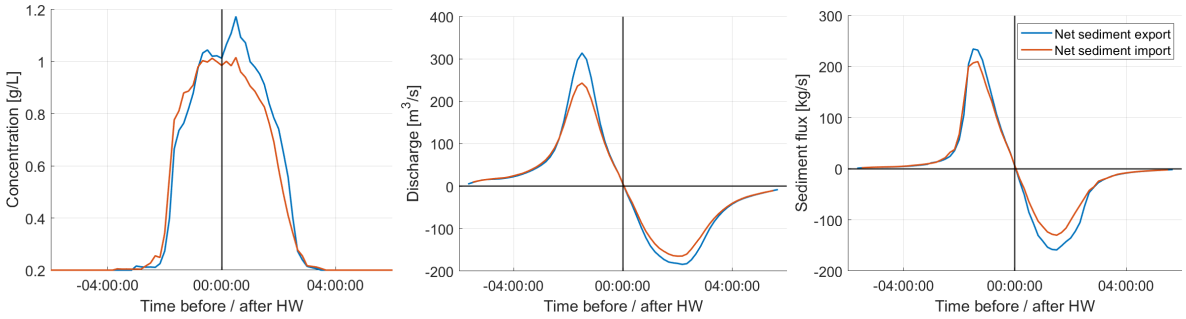

(a) Concentration **(b)** Discharge **(c)** Sediment flux

Figure 6.6: Distinction between net exporting tides and net importing tides. All tides that are net exporting and all tides that are net importing are centred around HW and averaged to create a profile of suspended sediment concentration, discharge and sediment flux.

often to negative trapping efficiencies. However, not all spring tides lead to negative trapping efficiencies. A difference in trapping efficiency from spring to neap tide or neap to spring tide could not be substantiated. The correlation of trapping efficiency with tidal range (-0.490) is higher than for high water (-0.381). High waters are also generated by setup due to wind, this effect seems not to be driving over the difference in water level during ebb and flood (tidal range). This is summarised in Figure 6.7c where the setup is correlated with the trapping efficiency which lead to a correlation coefficient of -0.244.

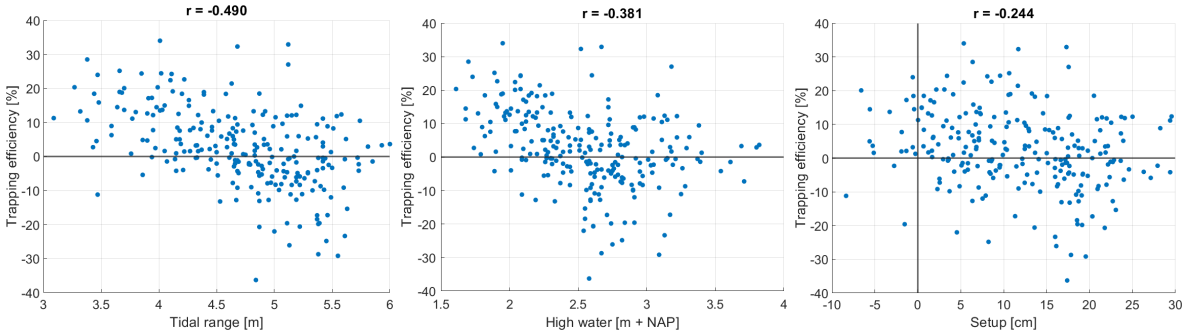

(a) Tidal range **(b)** High water **(c)** Setup

Figure 6.7: Trapping efficiency correlated with mean concentration during import of water over mean concentration during export of water, tidal range and flood discharge.

Wind, which generates waves and setup at Perkpolder is analysed, as sediment transport is very depended on wind influence as established in de Vet et al. (2018) and Colosimo et al. (2020). Winds from the West generally lead to a setup of water level near Perkpolder and winds from the east generally create set-down of water level near Perkpolder as shown in Appendix F. The response of the suspended sediment concentration and the sediment transport in Perkpolder on changing wind conditions is shown in Figure 6.8. This shows that there is not a direct interaction between wind magnitude and wind direction with net sediment import or export, since every wind quadrant shows net importing and net exporting tides. Wind speed and average concentration have a positive correlation, higher wind velocities create higher suspended sediment concentrations ($r = 0.38$). This is explained by wind generated waves stirring up local sediment. However, a higher wind speed does generally not lead to larger net import or export, since the correlation of wind speed and net sediment transport is very low ($r = 0.16$). Overall, wind seems to have a contribution to the suspended sediment concentration, however wind has no influence on the net import and export of sediment in Perkpolder.

6.4. Sediment balance Perkpolder

To connect the morphological development and net sediment import from the OBS measurements, a sediment balance is constructed. The volumes that are eroded or accreted are shown for each year in Figure 6.9a. In order to compare these volume changes with the net sediment import from the OBS measurements, the volume changes should be converted to mass changes. This is to compensate for the porosity in the bed, since the concentration from the OBS measurements is the sediment without porosity. Therefore the dry bed density from the measured sediment samples as shown in Figure 6.10 is used to calculate the mass change. For 2021 there are no bed samples available, therefore the 2020 data set is also used for 2021. These dry bed densities

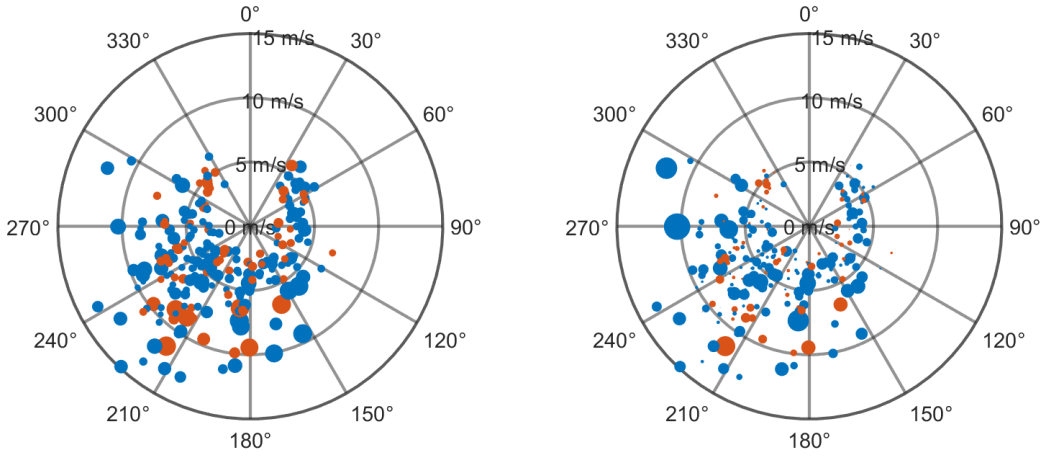

(a) Mean concentration

(b) Net sediment import/export

Figure 6.8: Polar plot for tide averaged wind direction (North is 0°) and wind speed. Blue dots show net importing tides, orange dots show net exporting tides. The size of the dot indicates qualitatively the mean concentration (a) and the absolute value of net sediment import or export (b).

are correct for the intertidal area, however for the pond and especially the frontal entrance area these dry bed densities are probably too small. This lead to an underestimation of the imported mass of the frontal entrance area.

The mass change is shown in Figure 6.9b, the marker shows the 'best estimate' while the error bars show the range mass changes. The best estimate of the mass change is determined by multiplying the volume change times the median bulk density. The upper limit is the volume change times the 75 percentile of the bulk density and the lower limit is determined as the volume change times the 25 percentile of the bulk density. The sediment flux of the OBS measurements as shown in Figure 6.5 has been converted to net mass import in Appendix E.

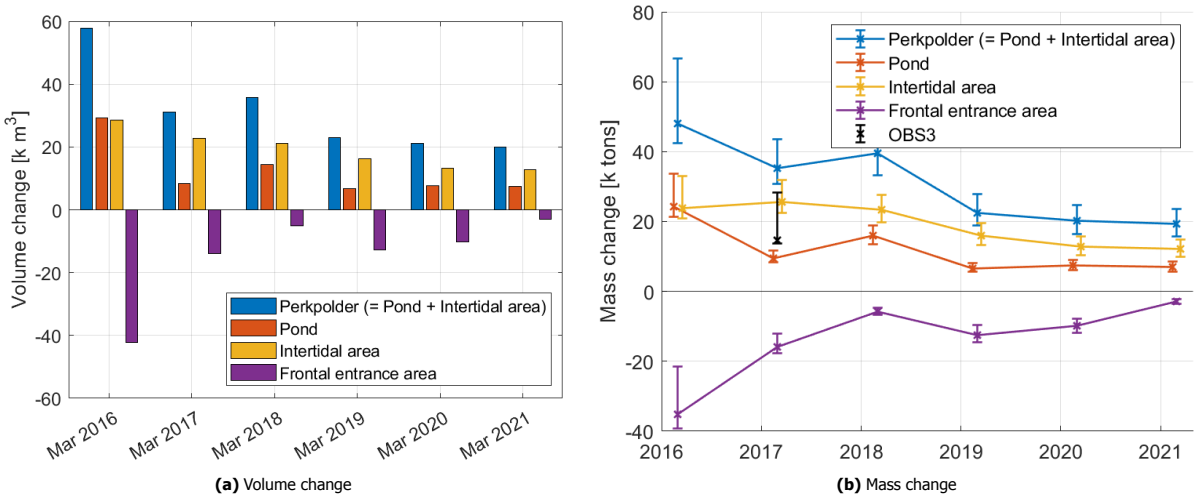

(a) Volume change

(b) Mass change

Figure 6.9: Volume changes and mass changes for the years 2016 to 2021. The volume and mass changes are yearly changes, except for March 2016. The observed change was in this case from the period June 2015 (opening of Perkpolder) to March 2016. Figure 6.9b shows the sediment mass import calculated from the OBS measurement in black.

The mass estimate of the OBS measurements is very sensitive to the combination of the calibration procedure and background concentration. Not a closed sediment balance could be made based on the OBS measurements and the volume changes of Perkpolder, however the suspended sediment concentration largely contributes to the measured morphological changes. The mass change of the frontal entrance area corresponds roughly to the mass change of the pond, which could indicate that the frontal entrance is the main sediment source for the pond.

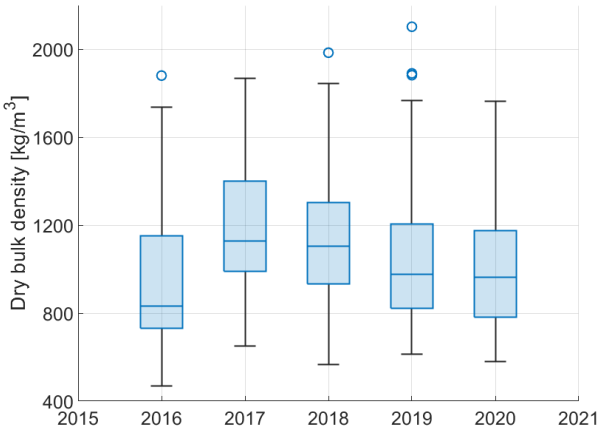

Figure 6.10: Box plot of bulk density between 2016 and 2020.

6.5. Key points

- Perkpolder is generally flood dominant. Moreover, decreasing velocities in landward direction are found which results in landward transport of fine sediment by settling lag.
- The average concentration profile at the inlet of Perkpolder indicates that the net sediment transport is determined by the response of Perkpolder and not the concentration during rising water levels.
- In the inlet, higher concentrations are found during autumn 2016 than winter 2017 which is opposing to suspended sediment concentrations in the Western Scheldt. Moreover, the change in trend of OBS measurements between autumn 2016 and winter 2017 corresponds with a change in trend of bed levels of the frontal entrance area between autumn 2016 and winter 2017. This indicates that the frontal entrance area is a source of sediment for Perkpolder.
- Only during a high tidal range and thus high velocities, high concentrations are observed. This stresses the contribution of locally stirred up sediment on top of suspended sediment of the Western Scheldt.
- In general tides create net import in Perkpolder, however there is a large temporal variability and even net exporting tides are found. The tidal range has the largest negative correlation with trapping efficiency ($r = -0.490$), which indicates that in general a higher tidal range leads to smaller trapping efficiencies and even negative trapping efficiencies.
- Wind effects increase suspended sediment concentrations ($r = 0.38$), however wind does not correlate with net sediment transport to Perkpolder.

7

Morphodynamic scenario modelling

This chapter presents the scenario modelling for the bathtub model of Perkpolder. The scenario modelling is performed for two main purposes: (1) enhanced understand of Perkpolder by process identification and (2) generalising the results from Perkpolder for other realignment projects. Section 7.1 shows the calibrated model and the validation of the model. Section 7.2 continues with a sensitivity study for Perkpolder, this gives confidence in the response of the acquired model. Lastly the results of the different scenarios is discussed in Section 7.3. The implications of the sensitivity study and the scenario modelling on the two purposes will be separately discussed in each section.

7.1. Results calibrated model

The hydrodynamic results of the bathtub model are presented and validated in Appendix C. The water levels of station Walsoorden are imposed at the entrance of Perkpolder. For calibration, the manning coefficient and viscosity are adapted such that the water levels, spatial velocity field and discharge through the entrance match the Western Scheldt model. The main morphological results of the calibrated model are shown in this section, starting with the sediment transport through the entrance.

As established in Chapter 3, three types of sediment (sand and two types of mud) are used to simulate the morphological development of Perkpolder. The two types of mud are used to include consolidation effects in the model. The main driver of sediment import and export within Perkpolder is the mud imposed at the entrance, defined via the boundary condition (Figure 7.1b). Mud base is only responsible for export as shown in Figure 7.1c, which is logical because the depth efficiency was set to zero such that the mud base could only erode. The assumption that the total eroding volume of mud-base is small compared to the total transport of mud-entrance is valid. Also a small amount of sand is imported to Perkpolder (Figure 7.1a), this is because the observation cross section is some grid cells removed from the boundary condition. So in the entrance region there is a limited amount of transport of sand.

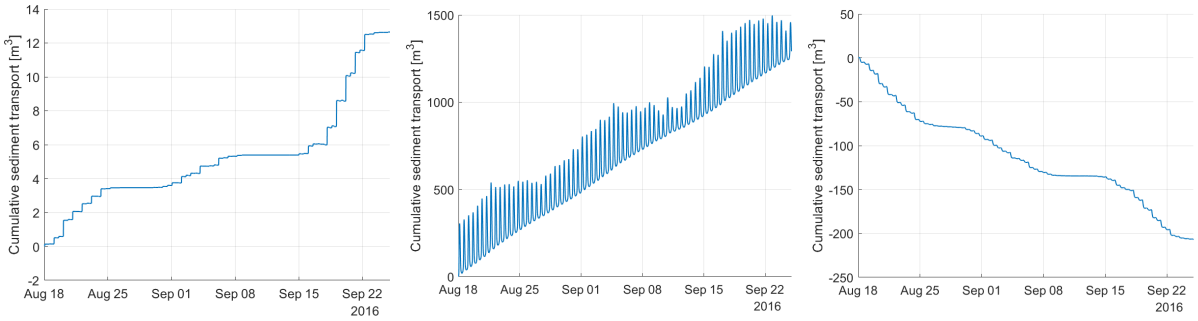

(a) Sand **(b)** Mud entrance **(c)** Mud base

Figure 7.1: Cumulative sediment transport of one month for different types of sediment through the entrance.

Figure 7.2 gives information how the sediment is transported through the entrance. The main transportation mode of sediment is via suspended load, which is expected for fine sediments. Bed load transport is negligible with respect to suspended load transport. Moreover, sediment is mainly transported via advection, however a non-negligible contribution is made by dispersive transport. In the sensitivity analysis, the effect of changing the

eddy diffusivity and thereby changing the amount of dispersive transport is discussed.

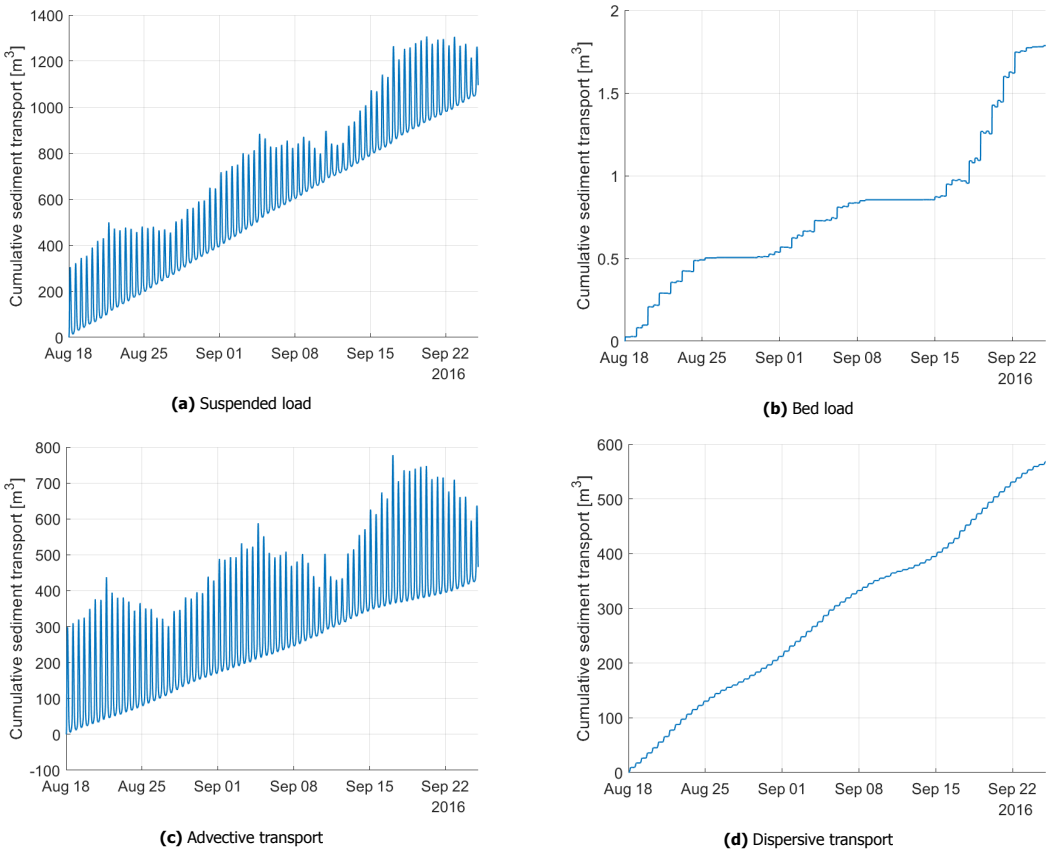

(a) Suspended load

(b) Bed load

(c) Advective transport

(d) Dispersive transport

Figure 7.2: Cumulative sediment transport of one month for different types of transport through the entrance.

The calibrated model will be validated using the bed level change measured from a combination of LIDAR, multibeam and vaklodingen. The trend at each grid point is determined in order to exclude yearly variations. Figure 7.3a shows the measured bed level changes and Figure 7.3b the calibrated model results. The model reproduces the main morphological developments: (1) erosion near the entrance and the beginning of the creeks; (2) infilling of the creeks landward of the first bifurcation; (3) sedimentation on the intertidal area with a smaller magnitude than sedimentation of the pond region.

Differences between the model and the measurements are found, for example the magnitude of the sedimentation on the intertidal area is higher than observed by measurements. Furthermore, the model simulates correctly that the creeks are accreting more than the intertidal area, but in reality the difference between accretion of the creeks and intertidal area is larger. Lastly, erosion near the entrance is only found in the main channel for the morphodynamic model, while the measurements show that the entire entrance region is eroding. The total eroded volume, accreted volume and net volume are shown in Table 7.1 for the yearly LIDAR measurements and the scaled model results. This is probably due to the water levels that are imposed at the entrance, that lead to different hydrodynamics near the entrance and thus a different sedimentation/erosion pattern (see Section 3.3.2). The sensitivity analysis in section 7.2 will shed more light on which processes could explain the differences. However, it is important to realise that this bathtub model is able to capture the main morphological developments of Perkpolder. Therefore the model is very useful in a scenario study where the differences with this calibrated model are analysed.

Table 7.1: Volumes of base model compared with measurements

Volume [m^3]	**Measurements**	**Base model**
Total eroded volume	$5.20 \cdot 10^3$	$4.41 \cdot 10^3$
Total accreted volume	$1.06 \cdot 10^5$	$9.45 \cdot 10^4$
Net volume	$1.00 \cdot 10^5$	$9.01 \cdot 10^4$

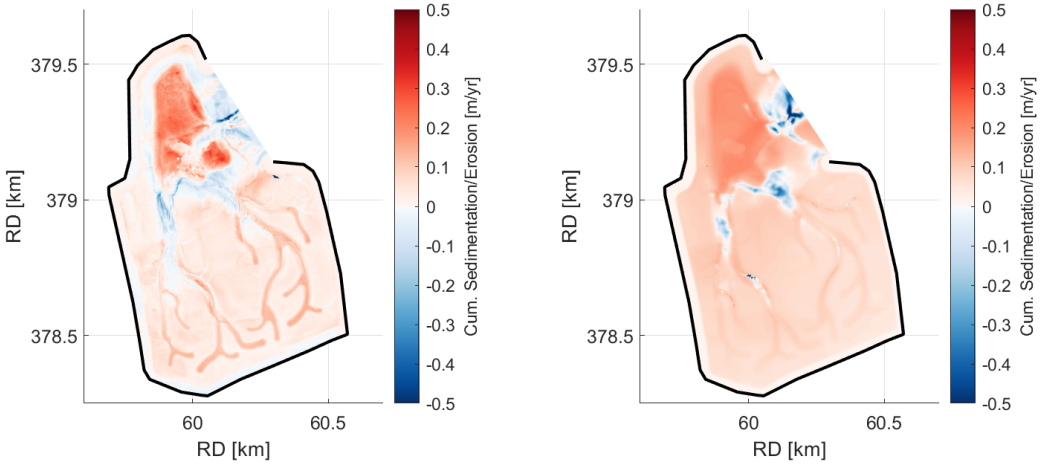

(a) Trend of yearly bed level changes between 2016 to 2021.

(b) Bathtub model results scaled to a year.

Figure 7.3: Comparison of the trend of yearly bed level changes measured by LIDAR, multibeam and vaklodingen and the bathtub model results. The bathtub model results are scaled to a year for comparison with yearly bed level changes.

To understand how the different sediments are interacting, the initial (after spin-up) and final sediment fraction of the three different types of sediment in the top layer is shown in Figure 7.4. The initial bed composition consists of sand (fraction: 0.3) and mud base (fraction 0.7). After the simulation both the sediment fraction of sand and mud base decreased and the sediment fraction of mud entrance increased. This corresponds with the sedimentary trend of Perkpolder caused by the mud applied at the entrance.

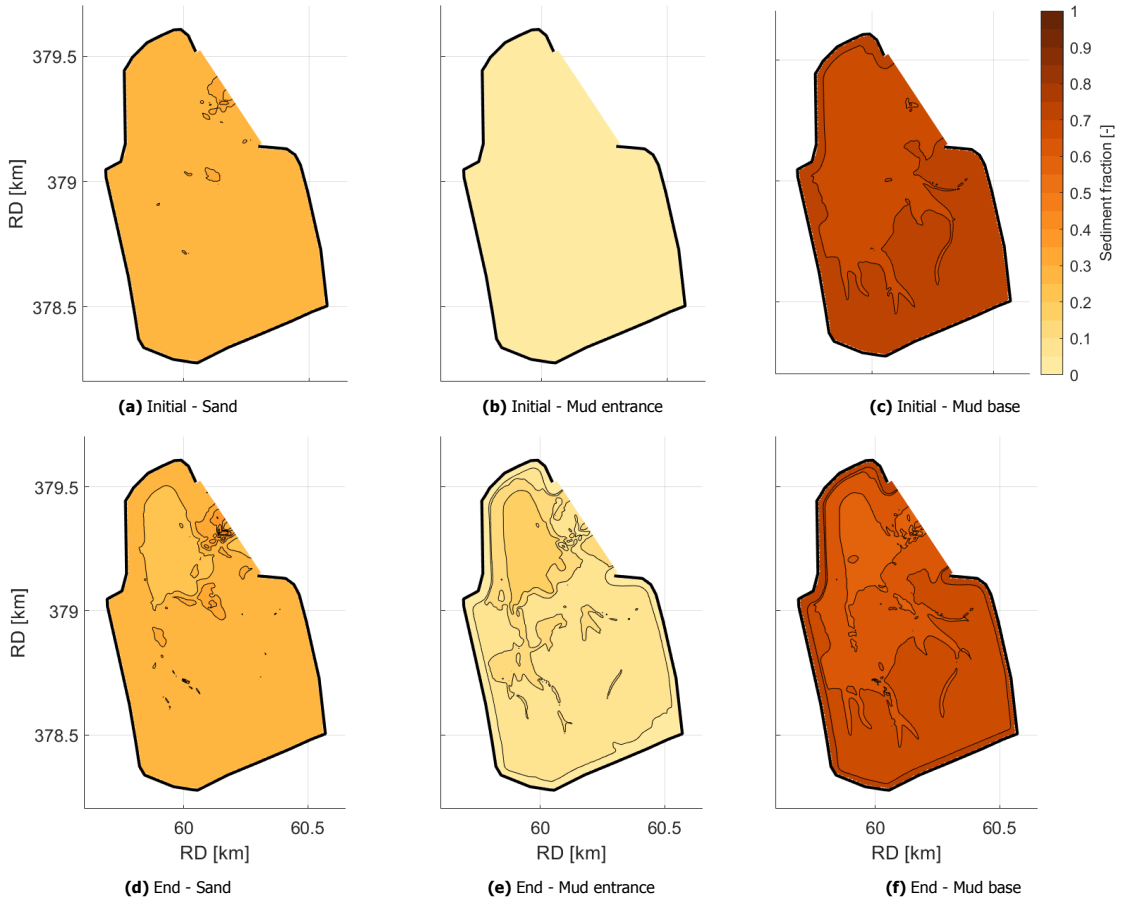

(a) Initial - Sand

(b) Initial - Mud entrance

(c) Initial - Mud base

(d) End - Sand

(e) End - Mud entrance

(f) End - Mud base

Figure 7.4: Initial (after spin-up) and final sediment fraction of the different types of sediment of the base run. The black contour lines shows the transition between different colours, which take place every 0.05 fraction.

7.2. Sensitivity analysis

A sensitivity analysis has been performed for the main parameters influencing the morphological response of the bathtub model. There are three main reasons to perform this sensitivity analysis as shown hereunder.

1. Understand how parameters influence the morphological results of the model and determine the robustness of the model.
2. Enhanced understanding of Perkpolder by understanding how certain parameters and processes influence Perkpolder.
3. Generalising the results of Perkpolder for other managed realignment projects.

Table 7.2 shows the alteration of each sensitivity run and the run number, this number is used in the results. Figure 7.5 presents the net import of sediment through the entrance of Perkpolder and the entrance of the intertidal area of Perkpolder for the different sensitivity runs (see Figure 3.6 for definition of these cross sections).

Table 7.2: Sensitivity runs and alteration. When *diffusivity: 10%* is stated, it means that 0.1 times the original diffusivity is used in the sensitivity run.

Run name	Alteration w.r.t. base
RUN-BASE	*n.a.*
RUN-A	Diffusivity: 10%
RUN-B	Median grain size: 150%
RUN-C	Settling velocity of mud entrance: 200%
RUN-D	Critical shear stress erosion of mud base: 200%
RUN-E	Critical shear stress erosion of mud entrance: 200%
RUN-F	Erosion parameter of mud base: 200%
RUN-G	Erosion parameter of mud entrance: 200%
RUN-H	Manning coefficient: 150%
RUN-I	Magnitude factor mud entrance: $\frac{1}{2}$
RUN-J	Magnitude factor mud entrance: 1
RUN-K	No depth efficiency mud base
RUN-L	Constant concentration mud entrance at boundary condition ($c = 0.33\ g/L$)
RUN-M	Wind and waves added

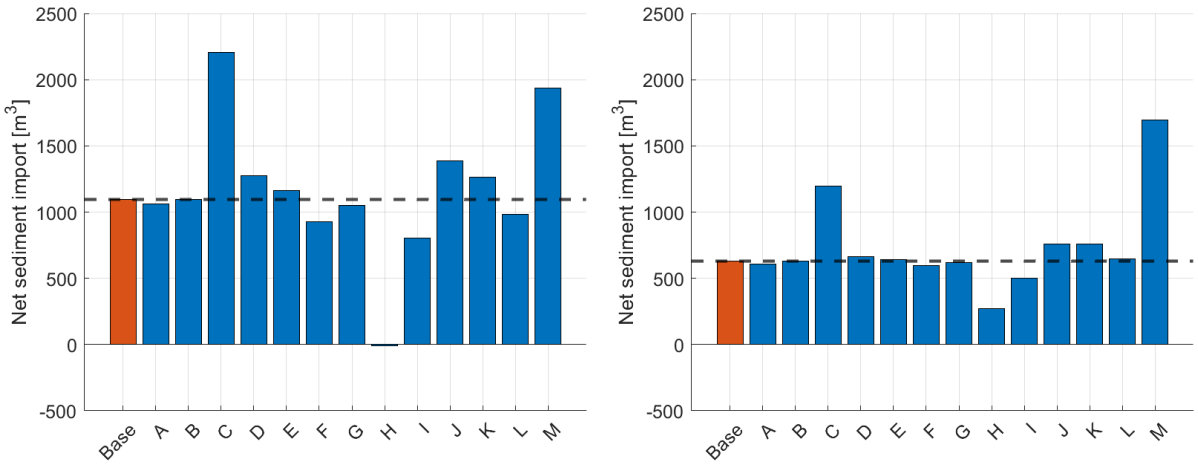

(a) Entrance **(b)** Intertidal area

Figure 7.5: Results of sensitivity analysis for the net import of one month for the entrance and intertidal area. The base run is shown in orange, the black line is added for readability of the graph and represents the net import of the base run.

7.2.1. Robustness of bathtub model

By changing the diffusivity with a factor 10, the net import with respect to the base run stays almost the same for the entrance and intertidal area. In Appendix G the dispersive and advective transport are plotted for the entrance (Figure G.1), which shows that the dispersive transport decreases with a factor 10 although the total net sediment import does not change. Thus the type of transport does not affect the morphodynamic results of the model.

To obtain the mud concentration at the boundary a linear relationship is established between the water levels and measured suspended sediment concentration at the inlet (Figure 3.8). In order to test how sensitive this relationship is for the net import of sediment a separate model run with a constant concentration of $0.33\,g/L$ has been setup (RUN-L). The concentration is the mean of the concentration applied at the base run. The net import of sediment through the entrance and on the intertidal area is almost the same for both simulations. This gives certainty that the relationship between water level and mud concentration near the inlet does not determine the net sediment transport of Perkpolder.

The grain size of sand has a negligible contribution to the net transport (RUN-B). Moreover, increasing the critical erosion rates (RUN-D and RUN-E) show less erosion near the inlet and the beginning of the creeks (see Appendix G for cum. sedimentation/erosion). By increasing the erosion parameter (RUN-F and RUN-G), the erosion is increased near the inlet and beginning of creeks. However this does not have a large influence on the total net transport. When the depth efficiency is set to 1 for the base mud (RUN-K), it is expected that the eroded sediment near the entrance and beginning of the creeks is deposited on the intertidal area, creating difficult to erode locations and a higher net import.

The main factors determining the net sediment transport in Perkpolder are the settling velocity (RUN-B), the Manning coefficient (RUN-H), the mud concentration at the boundary condition (RUN-I and RUN-J) and the influence of wind and waves (RUN-M). The mud concentration at the boundary directly influences the amount of available sediment and the main parameter influencing the settling of fine sediment is the settling velocity, so a large dependency on the net transport was expected. The Manning coefficient determines the amount of friction near the bed and when increased, bed shear stresses are much higher (see Figure G.2) and therefore sediment is more easily stirred up. This generates a lot of erosion at the start of the creeks and entrance area (see Appendix G), eventually leading to net export.

When wind and waves are included the net transport on the intertidal area is much higher. This is because small waves in the pond region keep sediment in suspension, which can then be transported to the intertidal area. As shown in Figure G.2 the bed shear stress in the pond is higher. Moreover Figure 7.6 shows that especially at the start of the intertidal area and the first part of the creeks, more erosion takes place due to breaking of waves. The settling velocity in the base run was set to a relatively low value (0.01 mm/s) while measurements in the Western Scheldt indicate settling velocities of 0.1 to $0.2\,mm/s$ (Temmerman et al., 2003a; Winterwerp et al., 1993). This is because wind and waves are not included in the base run and therefore a higher settling velocity is needed to achieve the same sedimentation at the intertidal area.

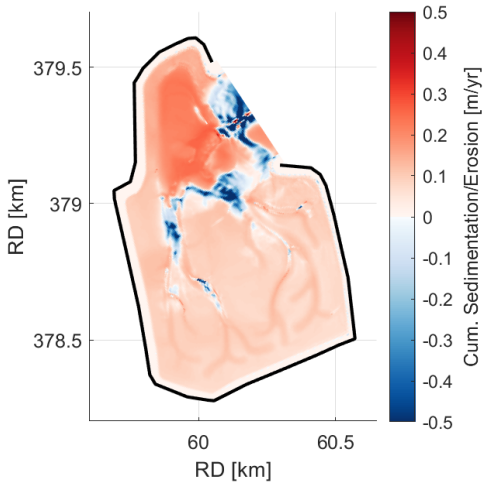

Figure 7.6: Cumulative sedimentation/erosion of Perkpolder of model run including wind and wave effects.

7.2.2. Enhanced understanding of Perkpolder

Section 6.3 shows that the tidal range has a negative correlation with trapping efficiency ($r = -0.49$). Thus the tidal range has a significant effect on the trapping of sediment. When comparing this with the model results, only net importing tides are discovered (see e.g. Figure 7.2a). Moreover the temporal variation is almost not visible. Figure 7.7a shows the correlation between the trapping efficiency and tidal range for the base model, which shows clearly a negative trend without net exporting tides. Figure 7.1b shows that the net import for every tide (large or small tidal range) is almost the same. However, tides with a large tidal range have large gross transports and

therefore the trapping efficiency is smaller for a large tidal range.

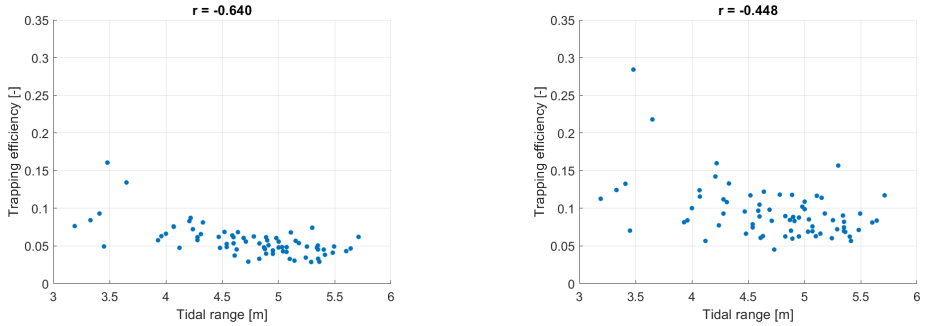

(a) RUN-BASE **(b)** RUN-M

Figure 7.7: Correlation between trapping efficiency and tidal range for two models: the base case and the run with wind and wave effects included.

The temporal variability is more clearly visible in Figure 7.7b, where the influence of wind and waves is included in the model simulation. Therefore it seems that the temporal variability is mainly caused by the effects of wind and small amplitude waves in Perkpolder. However even with wind and wave included, no net exporting (and thus negative trapping efficiencies) are found.

Moreover from the two types of mud it is deducted that consolidation processes play an important role within Perkpolder. In order to create the same sedimentation/erosion patterns, the critical shear stress for erosion should be enlarged for the base layer, or else erosion rates would be too high near the entrance and creeks. This contributes also to the low settling velocity. Over a year, consolidation of the settled fine sediment would create lower bed levels. Consolidation is implicitly included in the bathymetry measurements, however the model does not take consolidation into account. Therefore sedimentation rates using a realistic settling velocity generate sedimentation rates that are too high, this will then be taken into account by decreasing the settling velocity.

7.2.3. Generalisation for other realignment projects

One aspect from this sensitivity analysis that is considered for this goal is the mud applied at the boundary condition. Lowering of the supply of mud by means of the boundary condition leads to significant lower accretion rates within Perkpolder. The linear trend between the increase of the mean concentration at the boundary and the resulting net import on Perkpolder has a gradient of 1.253 with 95% confidence bounds of 1.245 and 1.262. This means that increasing the mean concentration by a factor 2, the net import becomes a factor 2.5 of the base case of Perkpolder. The Western Scheldt is a relatively turbid estuary (Van Der Wal et al., 2010). Therefore lower suspended sediment concentrations in other estuaries will lead to less net import and thus less sedimentation of the realignment site.

7.3. Scenario modelling

Scenario studies have been performed to understand how the response of Perkpolder differs under different circumstances and to make a generalisation for other realignment projects. The results of the different scenario runs are shown per goal of the scenario modelling. The different type of scenario runs is shown in Table 7.2.

Table 7.3: Description of scenario run.

Run name	Scenario description
RUN-BASE	*n.a.*
RUN-S1	No pond
RUN-S2	Constant creeks
RUN-S3	Converging creeks
RUN-S4	Bed level $+0.5\,m$
RUN-S5	Bed level $+1.0\,m$
RUN-S6	Bed level $+1.5\,m$
RUN-S7	Decreased tidal range (factor 1.5)
RUN-S8	Constant creeks (small)
RUN-S9	Converging creeks (small)

7.3.1. Enhanced understanding of Perkpolder

To assess the influence of the pond on the sedimentation of the intertidal area, a scenario run has been made in which the pond is filled up. The initial bathymetry of the scenario run is shown in Figure 7.8a. Figure 7.8b shows the cumulative sedimentation/erosion of Perkpolder with the new scenario. When comparing this with the sedimentation/erosion of the base run (Figure 7.8c), a decrease in sedimentation is seen near the pond. This is expected, since the water depth in the pond decreased. Moreover, no differences are observed in the sedimentation of the intertidal area and creeks. This means that the sedimentation of Perkpolder is depended on the hydrodynamic forcing (inundation time, flow velocities) only and that the pond does not act as a buffer of sediment. When the pond is fully filled, it is therefore not expected that the intertidal area will accrete more.

In the sensitivity study, when applying wind and wave processes, the net import on the intertidal area increased. This is explained by wind generated waves that keep sediment in suspension in the pond area of Perkpolder and therefore more sediment is transported to the intertidal area. When the pond is filled, the waves will be smaller and therefore more sediment could be trapped in the pond region. The effects of wind and waves is not included in this scenario run. Moreover the boundary conditions consists only of mud and not sand, it is expected that sand will settle in the pond and when the pond is filled up, sand will probably move to the intertidal area.

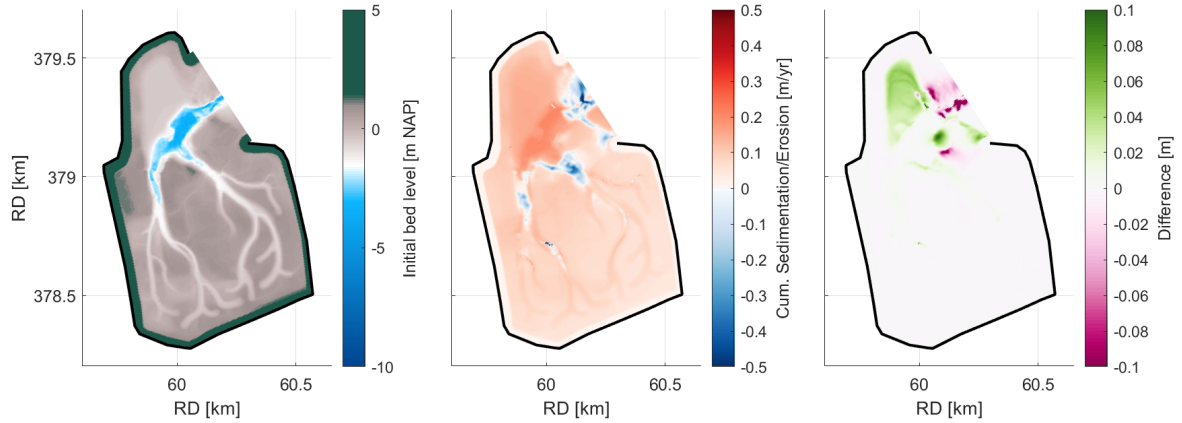

(a) Initial bathymetry **(b)** Sedimentation/erosion **(c)** Difference with base run

Figure 7.8: Results of scenario run with pond filled. The sedimentation/erosion is scaled to represent a whole year. Figure 7.8c shows the difference of sedimentation/erosion of the scenario run with respect to the base run. Green means that less sedimentation or more erosion took place w.r.t. the base run. Purple means that more sedimentation or less erosion took place w.r.t. the base run.

To understand how Perkpolder will evolve in time, three scenario runs have been created, in which the bed level of the entire area of Perkpolder has been increased with respectively 0.5, 1.0 and $1.5\,m$. This includes the entrance and creeks, therefore higher erosion rates are expected near these areas. The results for the three runs are shown in Figure 7.9. Even with an increase of $1.5\,m$, the area of Perkpolder is accreting. The accretion rate decreases with higher bed levels, which correspond with literature. Kirwan et al. (2016) shows that intertidal areas have higher accretion rates with higher inundation times. When the bed level in Perkpolder increase, without changing the hydrodynamic forcing, the inundation time decreases and thus the accretion decreases.

When the bed level of Perkpolder increases, the tidal prism of Perkpolder decreases (less water is transported in and out of Perkpolder). Therefore the creeks will become smaller, since the conveying capacity will be less. This is clearly seen in Figure 7.9, in Figure 7.9c the erosion of the creeks is less than Figure 7.9a, although the bed level of the creek has increased more.

Based on the accretion rates of the intertidal area of Perkpolder, an estimate is made about the development of the intertidal area. From Figure 7.9, the average bed level increase of the intertidal area of Perkpolder is deducted. The average bed level increase per year is shown in Table 7.4. The base run has too much sedimentation in the intertidal area over a year, therefore the accretion rate of the base run is decreased with a factor of 1.9 in order to match the average bed level increase from 2016 to 2021 for which the base run was calibrated.

Figure 7.10a shows the current estimate of the development of the intertidal area of Perkpolder, based on measurements and predictions from the model run. This should be seen as an indication, since only one representative month has been modelled, which does not represent all the variations over seasons and years. Moreover, sea level rise, which plays an important role on this time scale is not included. Furthermore, when the bed levels increase and the inundation times becomes smaller, vegetation will become important for sediment trapping (e.g.

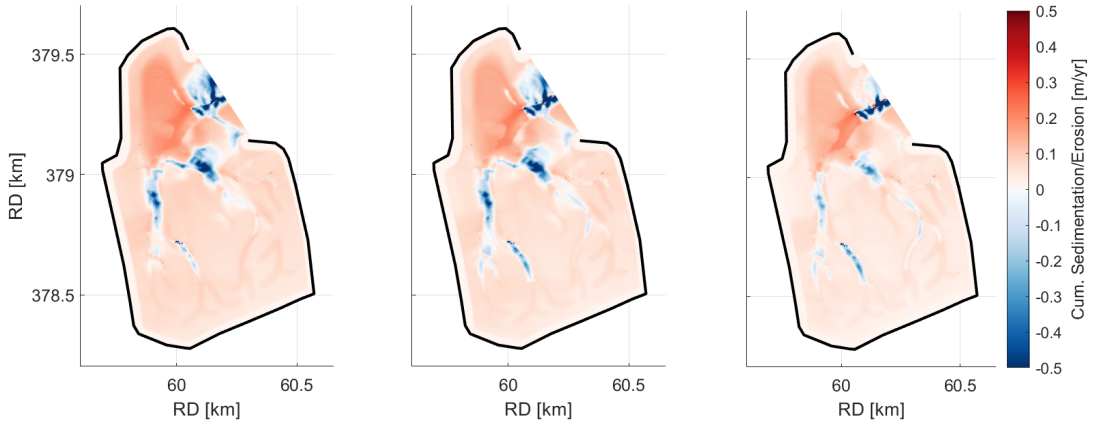

(a) Bed level $+0.5\ m$ **(b)** Bed level $+1.0\ m$ **(c)** Bed level $+1.5\ m$

Figure 7.9: Cumulative sedimentation/erosion for increased bed levels of Perkpolder scaled to represent a whole year.

Table 7.4: Average bed level increase of intertidal area for different scenarios.

Run number	Avg. accr. rate [cm/yr]	Scaled accr. rate [cm/yr]
RUN-BASE	6.0	3.2
RUN-S4	4.1	2.2
RUN-S5	3.1	1.7
RUN-S6	2.9	1.5

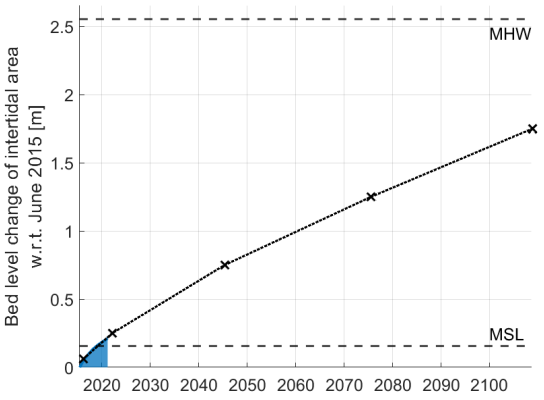

(a) Estimate of development of intertidal area of Perkpolder. The blue enclosed area represents the measurements at the intertidal area. The prognoses are based on the scaled bed level increase of the scenario models. The tidal datums are converted from NAP to elevation above mean bed level of the intertidal area in 2015.

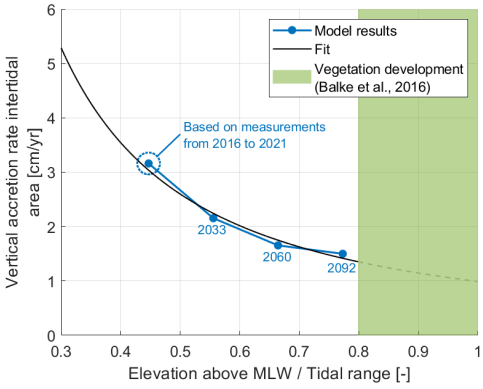

(b) Fit of function $y = A \cdot x^B$ to estimate the vertical accretion rate of the intertidal area. The results are model results from the base RUN and scenario S4, S5 and S6. The blue text states the year when the intertidal is expected to reach the respective elevation (from Figure 7.10a). The green shaded area represents the average height after which vegetation will develop.

Figure 7.10: Prognosis of the development of the intertidal area.

Morris et al. (2002)). This has not been included in the model and will result in significant changes near higher bed levels. However, this prediction shows an estimate of the time scale of the accretion of the intertidal area within Perkpolder.

7.3.2. Generalisation for other realignment projects

From Temmerman et al. (2003b), Morris (2012) and Belzen et al. (2021), it is known that sedimentation rates level off as inundation times become smaller until vegetation develops. This is endorsed by the research in this thesis. For the period that vegetation is not yet developing, the vertical accretion rate can be determined based on a power-relation of the inundation period. The inundation period can be expressed as the elevation of the intertidal area above MLW (z) divided by the tidal range (H). From Figure 7.10a, a power-relation will be fitted to the base run and scenario S4, S5 and S6 as shown in Equation 7.1.

$$\delta\left(\frac{z}{H}\right) = A \cdot \left(\frac{z}{H}\right)^{-B} \tag{7.1}$$

For Perkpolder, A is equal to 1.0 and the power B is equal to 1.4. This shows that on the long term, inundation period is an important driver for sediment trapping. It should be noted that the $3.2\ cm$ accretion from the measurements includes a period in which the frontal entrance area was a source and differs significantly spatially (e.g. in the creeks). Therefore the full morphological development is not captured in a single relation as Equation 7.1, but Figure 7.10b shows the importance of the inundation period for the trapping efficiency of the realigned area.

In Chapter 5, the development of the creeks has been thoroughly described. The conveying capacity of the creeks decreased throughout the intertidal area and this resulted in erosion at the beginning of the creeks and sedimentation at the end of the creeks. Using scenario RUN-S2, RUN-S3, RUN-S8 and RUN-S9 the effect of converging and/or smaller creeks is evaluated.

The initial bathymetry of the runs is shown in Figure 7.11. The bends are removed to clearly see the difference in morphological development between constant and converging creeks. Furthermore, the bends could create local scour effects (bend scour) which may affect the validity of the results for generalisation. These scenarios can therefore not be compared with the base run. RUN-S2 and RUN-S3 are a combination of scenarios in which constant and converging creeks with a minimum bed level of $-2.5\ m$ *NAP* and a bottom width of $20\ m$ is applied. The converging creeks start also with a bottom width of $20\ m$ which decreases linearly in landward direction. The other set of creeks (RUN-S8 and RUN-S9) consists of constant and converging creeks that are smaller, namely a bottom elevation of $-1.5\ m$ *NAP* and a bottom width of $10\ m$.

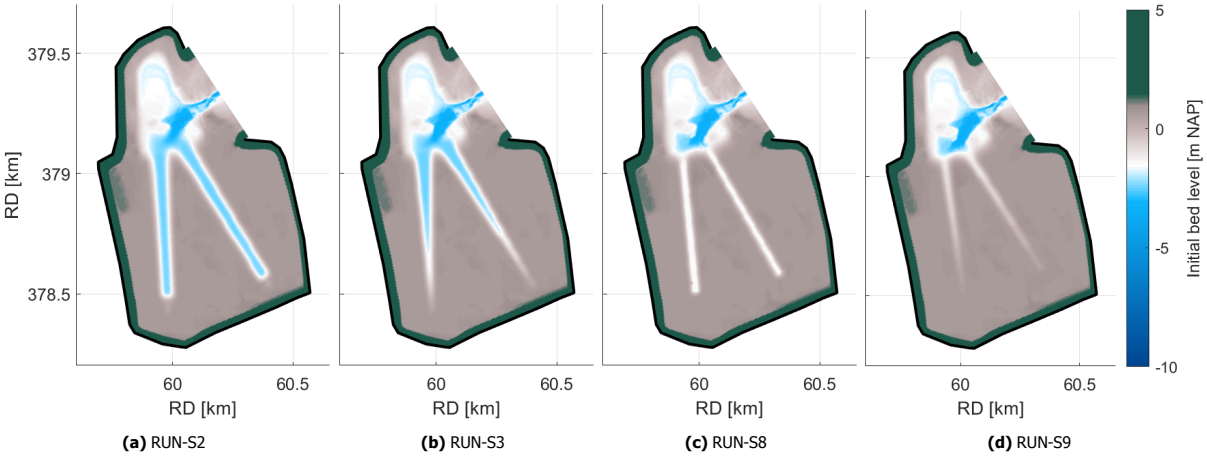

(a) RUN-S2 **(b)** RUN-S3 **(c)** RUN-S8 **(d)** RUN-S9

Figure 7.11: Initial bed levels for runs with new type of creeks.

The cumulative sedimentation and erosion for scenario RUN-S2 and RUN-S3 and the difference between the two scenarios is shown in Figure 7.12. It is observed that both creeks are filling up with sediment. This indicates that the creeks are designed too large for the intertidal area. Thus flow velocities are too small within the creeks which lead to sedimentation within the creeks. It is observed that the constant creeks have more accretion, especially near the end of the creeks. Moreover, it is striking that sedimentation in the intertidal area is not affected by the creek geometry. Therefore it seems that the creeks convey the water to the intertidal area, however the impact on settling and trapping of sediment in the intertidal area is limited.

To assess the effect of smaller creeks, Figure 7.13 shows the results of two extra scenarios in which the creeks are smaller. The differences between the two types of creeks are much more pronounced. These creeks are set up too small, a lot of erosion takes place in the creeks. For the constant creeks, this takes only place in the beginning. This is the same behaviour as seen in the current developed creeks of Perkpolder (RUN-BASE). Moreover, since the conveying capacity of the creeks is too small, the intertidal area near the pond is eroding, because water is conveyed not only via the creeks, but also via the intertidal area. Moreover, accretion rates at the intertidal area are smaller than in Figure 7.12 which shows that creeks that are setup too small creeks do affect the accretion rate of the intertidal area.

Figure 7.12 and 7.13 show qualitatively that there is a certain optimal creek cross sectional area which depends mostly on the conveying capacity and thus the tidal prism of the intertidal area. However, this optimal creek cross sectional area changes longitudinally along the creek, since the tidal prism decreases throughout the intertidal area. A relation could be made between the tidal prism of the creek and the cross sectional area. However when there is a complex creek system consisting of multiple creeks with multiple bifurcations, the tidal prism and thus

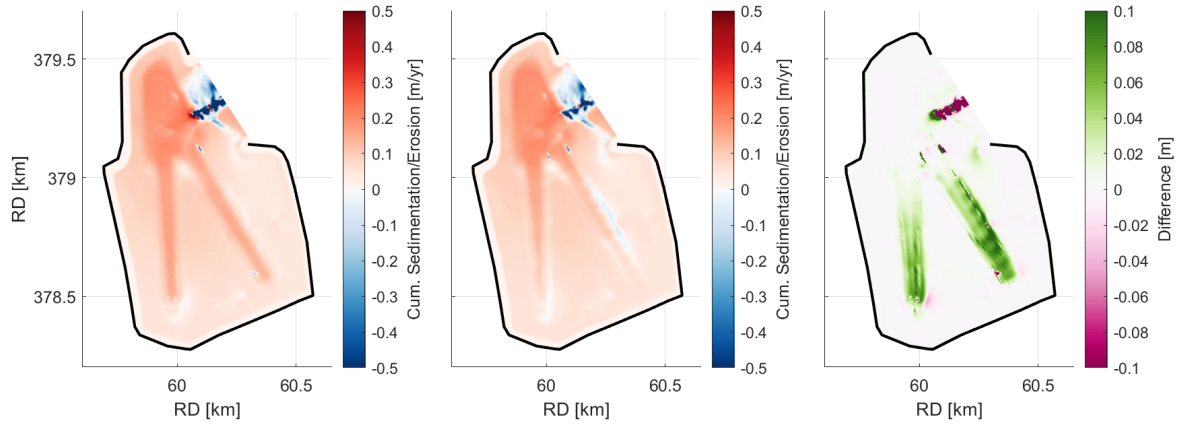

(a) Constant creeks **(b)** Converging creeks **(c)** Difference

Figure 7.12: Cumulative sedimentation/erosion results scaled for one year of scenario run with constant and converging creeks. Moreover the difference between the converging and constant creeks is shown. Green means that less sedimentation or more erosion took place w.r.t. the constant creeks. Purple means that more sedimentation or less erosion took place w.r.t. the constant creeks.

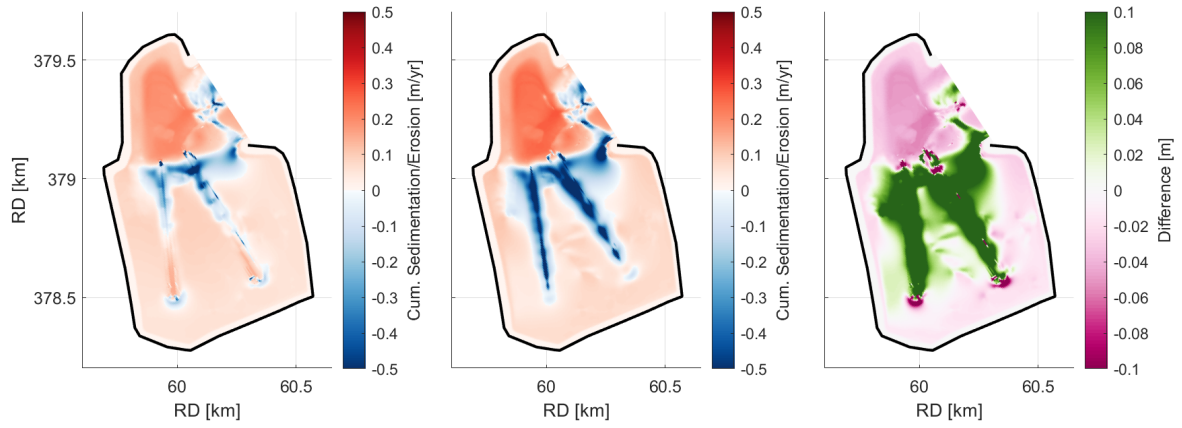

(a) Constant creeks **(b)** Converging creeks **(c)** Difference

Figure 7.13: Cumulative sedimentation/erosion results scaled for one year of scenario run with constant and converging small creeks. Moreover the difference between the converging and constant creeks is shown. Green means that less sedimentation or more erosion took place w.r.t. the constant creeks. Purple means that more sedimentation or less erosion took place w.r.t. the constant creeks.

conveying capacity is very hard to estimate. Therefore hydrodynamic model simulations are an easier way to indicate if the creek layout is large enough and able to convey the water to the intertidal area. As shown in Figure 7.14, bed shear stresses give an indication if the conveying capacity of the creeks is enough. When the bed shear stresses exceed $1\ N/m^2$ erosion takes definitively place at the seaward side of the intertidal area.

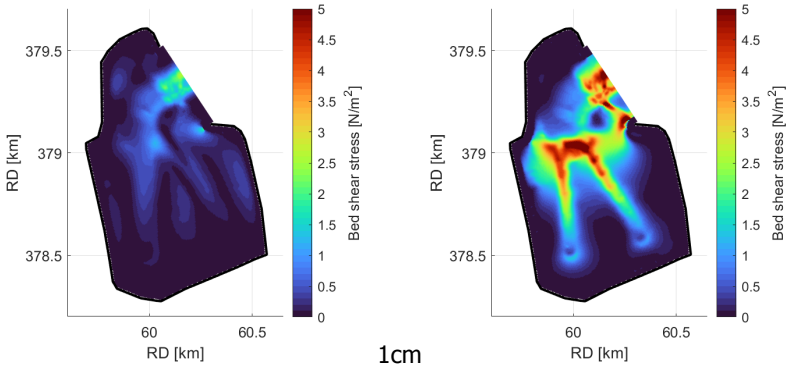

(a) Run with constant large creeks (RUN-S2). **(b)** Run with constant small creeks (RUN-S8).

Figure 7.14: Bed shear stresses at Perkpolder

Furthermore, the impact of the tidal range is investigated to compare Perkpolder with different estuaries. In RUN-S7, the tidal range has been decreased with a factor 1.5 as shown in Figure 7.15a. This is done by subtracting MSL from the water level signal, then dividing the water level signal by 1.5 and lastly add MSL again. This ensures that MSL did not change due to the decrease of the tidal range.

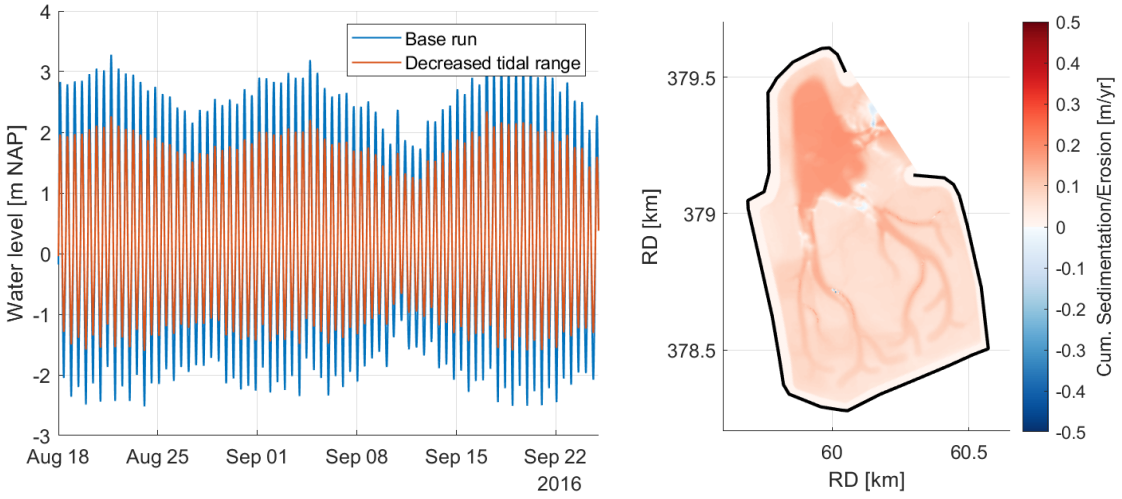

(a) Water levels of base run and run with tidal range decreased with a factor 1.5.

(b) Cumulative sedimentation/erosion of Perkpolder scaled for one year of model run with a decreased tidal range.

Figure 7.15: Results of RUN-S7: scenario study with a decreased tidal range.

As shown in Figure 7.15b, the erosion near the entrance and the start of the creeks has decreased and the accretion rate of the pond and intertidal area decreased. This is explained by two effects of decreasing the tidal range. If the tidal range is decreased, the change in water levels is less and therefore flow velocities are lower. The erosion observed near the entrance and start of the creeks was because of high flow velocities, therefore the erosion is less for a smaller tidal range. Furthermore, a lower tidal range leads to smaller inundation times of the intertidal areas. This, in turn, leads to less sedimentation of the intertidal area. When the tidal range is decreased by a factor 1.5, the resulting mean accretion of the intertidal area decreased with a factor 1.8.

7.4. Key points

- The bathtub model is able to reproduce the relevant morphological developments, namely (1) erosion near the entrance and the beginning of the creeks; (2) infilling of the creeks landward of the first bifurcation; (3) sedimentation on the intertidal area with a smaller magnitude than sedimentation of the pond region.
- Model simulation show a negative correlation between trapping efficiencies and tidal range, which correspond with measurements. However the temporal variability is small and there are no negative trapping efficiencies. With waves and wind added the trapping efficiencies show more temporal variability, however no negative trapping efficiencies.
- After filling up the pond, no differences are observed in the sedimentation of the intertidal area and creeks. This shows that the pond does not influence the accretion rate of the intertidal area.
- A higher elevation of the bed level leads to smaller inundation times and therefore decreases the accretion rate of the intertidal area. A trend line in the form of $y = A \cdot x^B$ has been fitted between the elevation of the intertidal above mean low water divided by the mean tidal range and the vertical accretion rate of the intertidal area. For Perkpolder, A is equal to 1.0 and the power B is equal to 1.4. This indicates that, on the long term, inundation times are important for the trapping efficiency of the intertidal area. This will be the case until vegetation develops, which alters again the trapping efficiency.
- Converging creeks fit better with the decreasing conveying capacity of the creeks (Chapter 5), from model simulations it is concluded that converging creeks lead to less sedimentation within the creeks with respect to constant creeks without affecting the intertidal area. However, when the creeks are setup too small, erosion takes place at the seaward side of the intertidal area. Bed shear stresses are a good indicator to determine if creeks are able to convey the water to the intertidal area.
- When the tidal range is decreased, the flow velocities are lower and thus the erosion near the entrance and beginning of creeks is smaller. Moreover, the inundation time is smaller for the intertidal area and thus the accretion rate of the intertidal area decreases.

8

Discussion

This chapter starts with discussing the validity of the data sets and model results in Section 8.1. Section 8.2 connects the results from the previous chapters to a system-broad understanding of Perkpolder. Lastly, the results are generalised for realignment projects in Section 8.3.

8.1. Validity of data analysis and models

The foundations of the data analyses in Chapter 4 to Chapter 6 are the bathymetry data and OBS measurements. Limitations for the bathymetric data are due to inaccuracies in the measurements and interpolation of the data (see Chapter 5) and because the exact measurement date is not known. Therefore, yearly erosion rates can differ, however, since multiple measurements are taken, the trend over years is robust.

The OBS measurements have multiple error sources (described in detail in Appendix D), these follow for example from the calibration procedure or algae present in the water column. Moreover, the concentration is measured $10\,cm$ above the bed and therefore not equal to the depth average concentration. Lastly, the measurement device has been removed from the water to replace the batteries and remove debris. These are all sources that create a different bias for the measurements. However, since there are two measurement devices deployed at the same time, these can be used to validate the general tendencies in the data. Therefore, if both devices shows the same trend, these trends are likely to be caused by physical drivers of the suspended sediment and not by one of the errors.

The Delft3D FM model is a fully calibrated and validated model for the hydrodynamics of Perkpolder. It is a 2D model, which does not consider wave forcing, moreover the grid size of $15\,m$ is relatively coarse for a detailed area as Perkpolder, especially for creeks which have a minimum width $10\,m$. The water levels and flow velocities near the entrance of Perkpolder are accurately reproduced by the model (see Appendix A). Therefore this model is used as indication for the (peak) velocities at Perkpolder. The conclusions in this thesis are based on the general flow field and tendencies in flow velocities for which the Western Scheldt model is proven to be a good instrument.

The Delft3D 4 bathtub model is a 2D morphodynamic model that builds on the Western Scheldt model. This model reproduces the flow velocities found in the Western Scheldt model quite well, except near the boundary condition. Moreover, it shows the same sedimentation/erosion pattern as seen with measurements, although not accurate reproducing every detail. The morphological response is modelled using one sand and two mud fractions. The two mud fractions are used to include consolidation effects. After entrainment, the consolidated mud should have the same properties (critical shear stress for erosion) as the non-consolidated mud. This cannot be modelled in Delft3D, so when the consolidated mud settles, this creates locations that are more resistant to erosion, therefore the consolidated mud is altered such that it can only erode and not settle. Since the total volume of eroded material is small compared to the total volume of settled material, this assumption can be made. The boundary conditions consists only of mud sediment and no sand, which could alter the morphological response of Perkpolder (see e.g. Weisscher et al. (2022)). Moreover the contribution of wind and waves, which is important as established in Chapter 7, is not included in the scenario runs. This leads to less sedimentation on the intertidal area and less erosion in the beginning of the creeks, therefore the settling velocity and critical shear stress for erosion have been altered to create the same morphological response. This model will thus have less temporal variability, however this will not alter the conclusions in this thesis.

8.2. Understanding the system Perkpolder

Figure 8.1 shows the main steps for an accreting system, which is used here to unravel the mechanisms driving the evolution of Perkpolder. Sediment is entrained from a certain source and transported to the area of interest where it is deposited. In order to get net accretion, the sediment should stay at the bed and not be re-entrained (trapped).

Figure 8.1: Flow diagram of main processes for an accreting system as Perkpolder.

Sediment source
Suspended sediment from the Western scheldt originates from marine and fluvial mud from respectively the North Sea and the river Scheldt (Verlaan, 1998). Moreover, sediment is entrained from the channels and intertidal areas of the system. However, the concentrations and temporal variability in the Western Scheldt do not fully clarify the concentrations measured in the inlet of Perkpolder. As determined from concentration and bed level measurements, the frontal entrance area had a significant contribution to the suspended sediment supply of Perkpolder. It is characterised as a finite source which eroded quickly in the first years and increased sedimentation within Perkpolder during these years. Measurements from other managed realignments with a former intertidal area or salt marsh in front of it, show similar insights (Rotman et al., 2008).

Entrainment
The suspended sediment concentration measured near the inlet of Perkpolder consists of suspended sediment from the Western Scheldt and the frontal entrance area. Sediment from the Western Scheldt is already in suspension when entering Perkpolder. Sediment in the frontal entrance area is stirred up by high bed shear stresses. High bed shear stresses can occur due to a high tidal range, wind generated waves, ship generated waves or a combination of these events. Chapter 6 shows that only during high velocities high suspended sediment concentrations are found. These high velocities are mainly generated by a high tidal range (tidal range higher than $4.5\ m$). Furthermore, high wind velocities contribute to high suspended sediment concentrations ($r = 0.38$). The effect of wind generated waves is larger with a high tidal range, since this increases the fetch length and water depth near Perkpolder (Gatto et al., 2017).

The contribution of ship generated waves for tidal flats in the Western Scheldt has been investigated by Huisman et al. (2010) and Aldershof (2020). In both cases ship generated waves had a large influence on the bed shear stresses and thus also on stirring up of sediment. Since the main channel of the Western Scheldt is adjacent to the frontal entrance channel, the contribution of ship generated waves can be significant.

Sediment transport
Chapter 2 shows that the main barotropic sediment transport processes are due to the asymmetry of the tide and lag effects. Perkpolder is generally flood dominant as established in Chapter 6. The peak flood velocity is higher than the peak ebb velocity, which creates a net import of relatively coarse sediment (Bosboom et al., 2022). Moreover, the intertidal area is inundated during flood slack waters and runs dry during ebb slack waters, creating a net landward transport of fine sediment as established by Friedrichs (2011).

In general, decreasing velocities in landward direction are observed as shown in Chapter 5, this leads to a net landward transport of relatively fine sediment by settling lag (Gatto et al., 2017). Moreover, the bathtub model and sediment cores demonstrate that the clay from Perkpolder is subjected to consolidation, leading to a higher critical velocity threshold for erosion than the critical threshold for deposition. This process (scour lag) enhances the net landward transport of fine sediment by settling lag (Gatto et al., 2017).

Deposition
Sediment samples reveal that coarse sediment settles in relatively higher hydrodynamic energetic conditions (e.g. the creeks). The fine sediment is transported as suspended sediment to the tidal flats (Chapter 4). At these flats, the dominant grain size is smaller than in the creeks. As the tide rises and spills over the creek banks, the expansion of the flow decreases its speed, the heaviest particles will quickly settle inside the creek. The fines pass the creeks but do not settle due to high energetic conditions. These are transported in suspension across the flat and settle in the upper part when slack tide occurs (Brunetta et al., 2019).

Moreover, in the first year (2015), the deepest part of the inlet was far above MLW. Therefore, during part of the tidal cycle no inflow occurred. This lead to two important effects, when the water level was below the minimum

depth of the inlet, the water was blocked and flow velocities inside Perkpolder were very low. Therefore, during this time, sediment could settle in the pond, the intertidal area had already run dry. Secondly, after blocking of the flow the water levels inside Perkpolder need to catch up with the water levels outside of Perkpolder, which results in a higher peak discharge and thus higher peak velocities. More sediment could then be transported to Perkpolder. Both these effects corresponds with relatively high accretion rates found in the first year of the pond. Since 2016, the inlet was deep enough to convey water during an entire tidal cycle and accretion rates decreased.

Sediment trapping
In large parts of the pond and intertidal area, peak flow velocities are small enough for sediment to be trapped at Perkpolder and not resuspended (threshold lag) as shown in Chapter 5. Suspended sediment measurements show trapping efficiencies up to 40%. The main influencing parameter is the tidal range ($r = -0.49$). A high tidal range leads in general to smaller or even negative (net export) trapping efficiencies. When looking at the model results, the same correlation is found, namely that trapping efficiencies decrease with increasing tidal range. However, the tidal range does not create the temporal variability as shown by the measurements and no negative trapping efficiencies are observed (see Chapter 7). When including wind and waves to the model, the model showed more temporal variability. Although Perkpolder is a relatively small tidal basin ($70\,ha$), wind and waves may significantly affect the trapping efficiencies of Perkpolder. Net export due to internally generated wind waves has been found to play a large role in other realignment projects (Williams et al., 2002). Propagating waves create turbulence in the water column that prevent deposition, and breaking waves create high bed shear stresses that resuspend deposited muds, allowing sediment to be exported on the ebb tide (Williams et al., 2002).

8.3. General insights for realignment projects

A direct comparison of managed realignment sites is difficult due to differences between project characteristics. In this thesis, it is discovered that initial bathymetry, suspended sediment concentration (from different sources), tidal forcing and wind and wave conditions have a significant effect on the development of the realigned area. All of the above conditions are necessary for a detailed comparison between two realignment sites, however still general characteristics for realignment sites can be exploited for understanding and designing of different sites.

First, Perkpolder is compared with other intertidal areas in the Western Scheldt to indicate potential differences between realignment sites and other intertidal areas. From de Vet et al. (2017) it is concluded that intertidal areas in the Western Scheldt increase on average almost $1\ cm$ per year. After the initial response, the intertidal area of Perkpolder accreted with a rate of about $3\ cm$ per year, which is significantly higher than other intertidal areas. This is likely caused by the larger disequilibrium of Perkpolder than tidal flats in the Western Scheldt. When increasing the bed level of Perkpolder with $1.5\ m$, the accretion rates are halved. Furthermore, Perkpolder is relatively sheltered and is less exposed to waves than the other intertidal areas in the Western Scheldt. As a first estimate for initial sedimentation of the intertidal area, the vertical accretion rate of the intertidal area of the realignment is a multiple times the average vertical accretion of other intertidal areas within the same estuary.

Scenario runs show that increasing bed levels (Chapter 7) and thus decreasing inundation times result in lower accretion rates of the intertidal area. Moreover, from measurements it has been established that lower lying areas accrete more than areas with higher elevations (Chapter 5). This confirms the general trend found at realignment sites where accretion rates decrease when inundation times decrease (Morris, 2012; Temmerman et al., 2003b). On the long term, until development of vegetation, the inundation period is an important driver for the trapping efficiency of sediment, these results match with Belzen et al. (2021). However, initially much more factors are at play, e.g. the influence of multiple sediment sources and the initial bathymetry. When vegetation develops, trapping efficiencies increase and therefore accretion rates become higher (Belzen et al., 2021; Friess et al., 2012).

Kirwan et al. (2016) used two main factors to estimate the adaptability of an intertidal area to sea level rise, namely the suspended sediment concentration and the tidal range. The availability of suspended sediment directly influences the accretion rate of realigned site, which corresponds with e.g. Friedrichs (2011). Moreover, a decrease in tidal range leads to two main effects, namely a decrease in flow velocities and secondly a decrease in inundation time of the intertidal area. When flow velocities are decreasing, erosion will decrease. Furthermore, due to the lower inundation times, the accretion rate of the intertidal area decreases. Hence, managed realignments in turbid basins with a relatively high tidal range, create substantial accretion rates of intertidal areas and thus a favourable adaptation capacity to sea level rise.

In this realignment site, creeks have been excavated to enhance the flow to the intertidal area (van Ginkel, 2019). Although three types of creeks have been used, the uniform layout was not efficient from a morphological point of view. The creeks eroded at the beginning and accreted for the remainder (Chapter 5). Also in other realignment sites significant higher accretion rates inside creeks have been measured (e.g. Eertman et al. (2002)). In order to reduce this effect, converging creeks are proposed. This matches the required, decreasing conveying capacity

of the creeks on the intertidal area (Chapter 5). Moreover, lower sedimentation rates have been found in the creeks with converging creeks. However, when the creeks are set-up too small accretion rates in the intertidal area will decrease. Chapter 7 shows that bed shear stresses can be used as indication for the size of creeks, thus a hydrodynamic model can solely be used to optimise the creek layout. This study focuses only on morphodynamic development of the creeks, when vegetation is developing, the function of the creeks may be different (e.g. drainage for vegetation (Crooks et al., 2002), control the distribution of vegetation (Sanderson et al., 2001; Zheng et al., 2016) or provide habitat for juvenile fish (Miller et al., 1997)). Hence, a priori it may be challenging to design the perfect creeks for a specific location.

The inlet characteristics of the realignment site steers the conveying capacity of the site (Chapter 5) and the sediment flux through the entrance (Weisscher et al., 2022). The original dikes in the entrance of Perkpolder were lowered substantially above MLW. Therefore, the depth of the entrance was restraining for the tidal flow. In combination with a deeper lying area below the threshold of the entrance (pond) created a sediment trap. On the other hand, restriction of the flow and therefore limited input of sediment could also lead to less sediment import (e.g. seen in Alkborough by Wheeler et al. (2008)).

9

Conclusions

The objective of this research was to determine the main processes and driving conditions that steer the hydrodynamics and morphodynamics of Perkpolder and use Perkpolder as case study to allow for optimisation of future realignment projects.

(1) What drives the temporal variability in suspended sediment import and export in the basin of Perkpolder?

The import is considered on two time scales. On a yearly time scale, two distinct periods in the morphological development of Perkpolder were present, namely the first year (June 2015 to March 2016) and the following years (March 2016 to March 2021). Three reasons were found to explain this difference:

1. Before the area of Perkpolder was opened as intertidal area, the polder has been redesigned and excavated (e.g. creeks and a pond) to create this new realignment area. The initial conditions were far from the conditions in the equilibrium position of intertidal areas. Therefore sedimentation rates for Perkpolder and erosion rates for the frontal entrance area were initially very high.
2. Initially the dykes have been lowered to create the inlet of Perkpolder. However, the minimum depth was above MLW, therefore the inlet blocked the flow during part of the tide. This created a slack time in the pond area and increased flow velocities during rising water levels. This increased sedimentation rates in the pond in the first year.
3. The frontal entrance area acted as a source of sediment in the first year(s). Especially in the first year, the frontal entrance area eroded significantly (average erosion: $-0.27\ m/yr$). The frontal entrance area is considered a finite source and erosion rates decreased to $0.04 m/yr$ in the next years. Using OBS measurements it has been proven that the suspended sediment entering Perkpolder consisted of sediment from the frontal entrance area.

In general, Perkpolder is net importing. However, there is a strong temporal variability on a tidal time scale and sometimes tides are net exporting. The concentration profile measured at the inlet of Perkpolder shows that the concentration after high water, thus the response of Perkpolder, leads to net import or net export. Moreover, a negative correlation is found ($r = -0.49$) between trapping efficiencies and the tidal range. Negative trapping efficiencies are only found for high tidal ranges. Modelling studies substantiate this negative correlation between trapping efficiencies and tidal range. When including wind and wave effects, more variability in trapping efficiencies is found.

(2) What is the contribution of the frontal entrance area and Western Scheldt to the sediment accretion at Perkpolder?

The concentrations and temporal variability in the Western Scheldt do not explain the concentrations measured in the inlet of Perkpolder. The bathymetry and OBS measurements show that the frontal entrance area is a finite source which eroded quickly in the first years and enhanced sedimentation within Perkpolder during these years:

1. The erosion rate of the frontal entrance area and the sedimentation rate of the pond show the same behaviour. In the first year, the sedimentation rate of the pond was a factor of 4.5 higher than the next year. Similarly, the erosion rate of the frontal entrance area, which is a factor 6.5 higher than the next years.
2. The results of the OBS measurements show the highest concentrations in September and October which is opposing to the trend of the suspended sediment concentrations in the Western Scheldt.

3. Between 2016 and 2017 a change in trend is found in the bed levels of the frontal entrance area. During 2016 the frontal entrance area is eroding in a much higher pace and stabilising in winter 2017. The same trend in decayed sediment movement is observed in suspended sediment concentrations where concentrations are higher in autumn 2016 than winter 2017.

(3) What is the accretion rate potential of Perkpolder and what processes dominate this?

The average accretion rate of Perkpolder in the first year is $0.13\ m/yr$, after that Perkpolder accretes with $0.04\ m/yr$ per year. The main differences between these time periods are explained in the response of research question 1. Moreover, the accretion rate is spatially very different, the pond faced higher accretion rates of $0.61\ m/yr$ in the first year and $0.14\ m/yr$ from 2016 and 2021. The intertidal area experienced less accretion, namely $0.07\ m/yr$ in the first year and $0.03\ m/yr$ thereafter. The accretion rates found in Perkpolder are higher than other intertidal areas in the Western Scheldt (de Vet et al., 2017). Compared to other managed realignment areas, these are average accretion rates, since rates of a few millimetres to tens of centimetres are found in other realignment areas (Morris, 2012; Temmerman et al., 2003b).

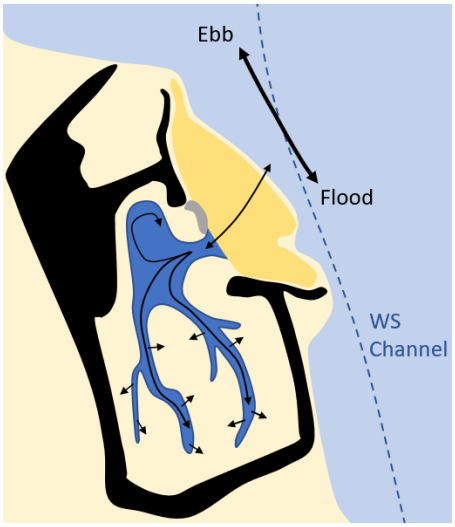

Figure 9.1: Overview of main currents at Perkpolder.

The main flow patterns in Perkpolder are shown in Figure 9.1, these currents lead to net landward transport due to lag effects and asymmetry of the tide. Modelling results show that inundation times are very important for the accretion rate of the intertidal area. Higher elevated areas will have smaller accretion rates, since the inundation time is smaller. When Perkpolder is elevated with $1.5\ m$, the accretion rate will roughly be halved. When vegetation is able to develop on the intertidal area, sedimentation rates will possibly increase due to higher trapping efficiencies by vegetation (Friess et al., 2012).

(4) What processes and (initial) conditions determine the growing capacity of intertidal areas after a managed realignment?

The morphological response and development after a managed realignment depends mostly on the forcing of the estuary and initial bathymetry and differs spatially and temporally. The forcing of the estuary is summarised in two main factors that influence the realignment area, namely the suspended sediment concentration and tidal range. When the suspended sediment concentration is higher, there is more deposition in the realigned area. Moreover, the tidal range determines the governing (peak) flow velocities and inundation period of the intertidal area. A higher tidal range, creates larger peak velocities and thus more erosion at already eroding areas (e.g. at the entrance or beginning of the creeks). At the same time the inundation time of the intertidal area increases and the accretion rate of the intertidal area increases.

The initial bathymetry of the realignment determines the response of the realigned area. The pond, a deeper lying area within the realigned area acts as a sink for the sediment. However, the accretion rates on the intertidal area did not change when the pond was filled up. The creeks convey water and sediment to the intertidal areas. When the creeks are set-up too small, accretion rates at the intertidal area will decrease. Moreover, converging creeks match better with the decreasing conveying capacity of the creeks.

Altogether, there is a lot of temporal and spatial variability in the morphodynamic development of managed realignments due to multiple processes simultaneously acting over different time scales. Therefore, predicting the morphodynamic development of a new managed realignment site cannot be performed without identifying the individual processes.

10

Recommendations

In this thesis, the research focused on the morphological development of the managed realignment Perkpolder and the implications for future realignment projects. In this chapter, suggestions are provided to enable better predictions of the morphological behaviour of such systems and more effective design standards of future realignment projects.

Further research on Perkpolder

The model developed in this thesis has a large advantage with respect to other morphodynamic models of realignment projects. Namely, it is calibrated based on measurements after the realignment, while models as Gourgue et al. (2022) consider a hypothetical response after the realignment. The morphological results of the bathtub model provide therefore valuable additions to studies considering models based on hypothetical morphological development. At the moment, this model can only indicate the time scale of the development of the realigned area until salt marsh formation, since vegetation is not included. It is expected from Belzen et al. (2021) that the sediment accretion is accelerated as soon as vegetation establishes.

Three types of sediment have been modelled in the bathtub model. Whereas this model includes sand-mud interaction, the boundary condition consists only of mud. In other modelling studies in the Western Scheldt, e.g. Weisscher et al. (2022), the impact of sand and mud on the development of the managed realignment has been evaluated. It is shown in Weisscher et al. (2022) that sand may have a significant contribution to the accretion of the managed realignments and could therefore impact the results. It is advisable to investigate how the ratio of mud and sand supplied by the estuary alters the morphological development of a managed realignment.

Chirol et al. (2018) parameterised channel length, creek mouth width and cross sectional area of the creeks based on catchment area, potential semi-diurnal tidal prism and total channel length. This has been done for natural salt marshes in the United Kingdom. It could be valuable to test how the creeks for managed realignment projects as Perkpolder fit in these projections and if these projections can be used as design guideline for future creek designs.

Future realignment projects

This report showed how the different processes and subsystems contribute to the morphological change at the managed realignment site of Perkpolder. This section contains recommendations for designing and setting up future realignment projects.

Short basin approximation. Based on flow velocity measurements, it has been concluded that the short basin approximation is a reliable method to determine the discharge and velocities through the inlet. However, two conditions should be met. First of all, the short basin approximation is only valid for 'short basins', so basins with a length shorter than $1/20$ of the forcing waves (tidal waves). Secondly, the entrance and/or frontal entrance area should not limit the flow. Therefore it should be validated if the minimum elevation of these areas is at least below MLLW.

Measurements. In the first years, various conditions and processes affect simultaneously the morphological development of Perkpolder. This includes the contribution of different sediment sources, the initial bathymetry and wind and wave effects. Each of them acts on a different time scale. Moreover, sedimentation rates differ spatially and cannot be fully modelled beforehand. Therefore, it is recommended to measure the bathymetry of new realignment sites for a sufficiently long period capturing all time scales (e.g. 10 years) in order to minimise

wrong predictions and preliminary conclusions. Furthermore, the measurements should have a frequency which is large enough to differentiate between the different processes. Therefore, in the first years, it is advised to measure bathymetry multiple times per year (e.g. 4 times), in later years the measurement frequency may decrease to e.g. once every year.

Accretion estimate. This thesis showed that the forcing characteristics of the estuary (tidal range and suspended sediment concentration) has a large effect on the sedimentation rate in Perkpolder. Moreover, accretion rates of intertidal areas in the same estuary can be indicative for the potential vertical accretion of the realignment project. As discovered in this research, Perkpolder had an initial accretion rate of 3 times the average accretion rate of other intertidal areas. This larger rate was explained by the larger disequilibrium (lower elevation w.r.t. MSL) and the more sheltered orientation compared to other intertidal areas. These conditions are typical for new realignment projects and therefore a first estimate of the accretion rate of the managed realignment is a number of times the accretion rate of other tidal flats within the estuary.

Initial bathymetry. The initial bathymetry influenced largely the response of Perkpolder. As determined in Chapter 7, creeks are important for conveying the water and sediment to the intertidal area. The optimal creek cross-sectional area depends on the conveying capacity of the creeks and therefore the tidal prism. The creeks should be large enough to convey the water to the intertidal area, or else erosion takes place at the seaward side of the intertidal area. In order to set-up the creeks in a different realignment project, it is recommended to make a hydrodynamic model including the initial bathymetry and proposed creek lay-out. Bed shear stresses of the model will illustrate whether the creeks are sufficiently able to convey the water to the intertidal area.

The combination of a pond and inlet excavated above MLW resulted in a large sediment sink at Perkpolder. Over time, natural processes shape the realignment area and fill up the pond (Figure 4.4). Therefore, when excavating a pond is practical (e.g. use the sediment for dike reinforcements), it can be performed and does not harm the realignment. Namely, model results indicate that the pond does not influence the sedimentation of the intertidal area. However, creating a pond on purpose (for e.g. pressure release of groundwater or creating a sub literal ecosystem) is not advisable, since it rapidly fills up. When the main purpose of the realignment project is to trap as much sediment as possible, e.g. in the Ems estuary to decrease the excess of sediment (Donner et al., 2012), a realignment project containing a pond and the inlet substantially above MLW is very helpful in trapping sediment.

References

Aldershof, M. (2020). *Impact of ship waves on sediment transport at two tidal flats in the western scheldt* (Master's thesis). University of Twente.

Allen, J. (2000). Morphodynamics of holocene salt marshes: A review sketch from the atlantic and southern north sea coasts of europe. *Quaternary Science Reviews*, *19*(12), 1155–1231. https://doi.org/https://doi.org/10.1016/S0277-3791(99)00034-7

Balke, T., Stock, M., Jensen, K., Bouma, T. J., & Kleyer, M. (2016). A global analysis of the seaward salt marsh extent: The importance of tidal range. *Water Resources Research*, *52*(5), 3775–3786.

Barbier, E. B., Hacker, S. D., Kennedy, C., Koch, E. W., Stier, A. C., & Silliman, B. R. (2011). The value of estuarine and coastal ecosystem services. *Ecological monographs*, *81*(2), 169–193.

Battjes, J. A., & Groenendijk, H. W. (2000). Wave height distributions on shallow foreshores. *Coastal engineering*, *40*(3), 161–182.

Beauchard, O., Jacobs, S., Cox, T. J. S., Maris, T., Vrebos, D., Van Braeckel, A., & Meire, P. (2011). A new technique for tidal habitat restoration: Evaluation of its hydrological potentials. *Ecological Engineering*, *37*(11), 1849–1858.

Belzen, J. V., Rienstra, G., & Bouma, T. (2021). Dubbele dijken als robuuste waterkerende landschappen voor een welvarende zuidwestelijke delta. https://doi.org/10.25850/nioz/7b.b.kb

Best, Ü. S. N., Van der Wegen, M., Dijkstra, J., Willemsen, P. W. J. M., Borsje, B. W., & Roelvink, D. J. A. (2018). Do salt marshes survive sea level rise? modelling wave action, morphodynamics and vegetation dynamics. *Environmental Modelling & Software*, *109*, 152–166. https://doi.org/https://doi.org/10.1016/j.envsoft.2018.08.004

Boersema, M. (2015). Projectplan monitoring en onderzoek perkpolder.

Bolle, A., Wang, Z. B., Amos, C., & De Ronde, J. (2010). The influence of changes in tidal asymmetry on residual sediment transport in the western scheldt [The Coastal Morphodynamics of Venice Lagoon and its Inlets]. *Continental Shelf Research*, *30*(8), 871–882. https://doi.org/https://doi.org/10.1016/j.csr.2010.03.001

Bosboom, J., & Stive, M. J. F. (2022). *Coastal dynamics*. TU Delft Open. https://doi.org/https://doi.org/10.5074/T.2021.001

Bridges, T., Simm, J., & King, J. (2021). International guidelines on natural and nature-based features. *FLOODrisk 2020-4th European Conference on Flood Risk Management*.

Brown, S. L., Pinder, A., Scott, L., Bass, J., Rispin, E., Brown, S., Garbutt, A., Thomson, A., Spencer, T., Moller, I., et al. (2007). Wash banks flood defence scheme. freiston environmental monitoring 2002-2006.

Brunetta, R., de Paiva, J. S., & Ciavola, P. (2019). Morphological evolution of an intertidal area following a setback scheme: A case study from the perkpolder basin (netherlands). *Frontiers in Earth Science*, *7*. https://doi.org/10.3389/feart.2019.00228

Chen, M. S., Wartel, S., Eck, B. V., & Maldegem, D. V. (2005). Suspended matter in the scheldt estuary. *Hydrobiologia*, *540*(1), 79–104.

Chen, Y., Dong, J., Xiao, X., Zhang, M., Tian, B., Zhou, Y., Li, B., & Ma, Z. (2016). Land claim and loss of tidal flats in the yangtze estuary. *Scientific Reports*, *6*(1), 1–10.

Chirol, C., Haigh, I., Pontee, N., Thompson, C., & Gallop, S. L. (2018). Parametrizing tidal creek morphology in mature saltmarshes using semi-automated extraction from lidar. *Remote Sensing of Environment*, *209*, 291–311.

Clapp, J. (2009). *Managed realignment in the humber estuary: Factors influencing sedimentation* (Doctoral dissertation). University of Hull.

Colosimo, I., de Vet, P. L. M., van Maren, D. S., Reniers, A. J. H. M., Winterwerp, J. C., & van Prooijen, B. C. (2020). The impact of wind on flow and sediment transport over intertidal flats. *Journal of Marine Science and Engineering*, *8*(11), 910.

Crooks, S., Schutten, J., Sheern, G. D., Pye, K., & Davy, A. J. (2002). Drainage and elevation as factors in the restoration of salt marsh in britain. *Restoration ecology*, *10*(3), 591–602.

Dam, G., Van der Wegen, M., Taal, M., Van der Spek, A., & Bliek, B. (2017). Reconstructing the sediment budget of the western scheldt 1860-1955.

De Jong, D. J., & de Jonge, V. N. (1995). Dynamics and distribution of microphytobenthic chlorophyll-a in the western scheldt estuary (sw netherlands). *Hydrobiologia*, *311*(1), 21–30.

De Mesel, I. G., Ysebaert, T., & Kamermans, P. (2013). *Klimaatbestendige dijken: Het concept wisselpolders* (tech. rep.). IMARES.

De Vriend, H. J., Wang, Z. B., Ysebaert, T., Herman, P. M. J., & Ding, P. (2011). Eco-morphological problems in the yangtze estuary and the western scheldt. *Wetlands*, *31*(6), 1033–1042.

de Kramer, D. (2008). *Ontwerpnota buitendijkse natuurontwikkeling* (tech. rep.). RWS Dienst Zeeland.

de Vet, P. L. M., & van der Werf, J. J. (2022). *Concept delft3d-fm modellering buitendijkse maatregelen baalhoek & knuitershoek, westerschelde*.

de Vet, P. L. M., van Prooijen, B. C., Schrijvershof, R. A., van der Werf, J. J., Ysebaert, T., Schrijver, M. C., & Wang, Z. B. (2018). The importance of combined tidal and meteorological forces for the flow and sediment transport on intertidal shoals. *Journal of Geophysical Research: Earth Surface*, *123*, 2464–2480. https://doi.org/10.1029/2018JF004605

de Vet, P. L. M., van Prooijen, B. C., & Wang, Z. B. (2017). The differences in morphological development between the intertidal flats of the eastern and western scheldt. *Geomorphology*, *281*, 31–42. https://doi.org/10.1016/j.geomorph.2016.12.031

de Vet, P. L. M., van Prooijen, B., Colosimo, I., Steiner, N., Ysebaert, T., Herman, P., & Wang, Z. B. (2020). Variations in storm-induced bed level dynamics across intertidal flats. *Scientific Reports*, *10*(1), 1–15.

Dix, M., Abd-Elrahman, A., Dewitt, B., & Nash Jr, L. (2012). Accuracy evaluation of terrestrial lidar and multibeam sonar systems mounted on a survey vessel. *Journal of Surveying Engineering*, *138*(4), 203–213.

Dixon, M., Morris, R. K. A., Scott, C., Birchenough, A., & Colclough, S. (2008). Managed realignment–lessons from wallasea, uk. *Proceedings of the Institution of Civil Engineers-Maritime Engineering*, *161*(2), 61–71.

Doeglas, D. (1968). Grain-size indices, classification and environment. *Sedimentology*, *10*(2), 83–100.

Donner, M., Ladage, F., & Stoschek, O. (2012). Impact and retention potential of tidal polders in an estuary with high suspended sediment concentrations. *Proceedings of 10th International Conference on Hydroscience & Engineering (ICHE), Orlando, Florida., University of Central Florida*.

Dronkers, J. (1986). Tidal asymmetry and estuarine morphology. *Netherlands Journal of Sea Research*, *20*(2), 117–131. https://doi.org/https://doi.org/10.1016/0077-7579(86)90036-0

Dyer, K. R. (1973). *Estuaries: A physical introduction*.

Dyer, K. (1997). Partially mixed and well-mixed estuaries. *Estuaries—-a physical introduction, 2nd edition, eds. John Wiley and Sons*, 136–164.

Eertman, R. H. M., Kornman, B. A., Stikvoort, E., & Verbeek, H. (2002). Restoration of the sieperda tidal marsh in the scheldt estuary, the netherlands. *Restoration Ecology*, *10*(3), 438–449.

Esteves, L. S. (2014). Methods of implementation. *Managed realignment: A viable long-term coastal management strategy?* (pp. 33–44). Springer.

Ettema, R. (2006). Hunter rouse—his work in retrospect. *Journal of Hydraulic Engineering*, *132*(12), 1248–1258.

European Commission. (2021). Communication from the commission to the european parliament, the council, the european economic and social committee and the committee of the regions forging a climate-resilient europe - the new eu strategy on adaptation to climate change.

Fettweis, M., Sas, M., & Monbaliu, J. (1998). Seasonal, neap-spring and tidal variation of cohesive sediment concentration in the scheldt estuary, belgium. *Estuarine, Coastal and Shelf Science*, *47*(1), 21–36.

Fondriest Environmental, Inc. (2019). Measuring turbidity, tss, and water clarity. https://www.fondriest.com/environmental-measurements/measurements/measuring-water-quality/turbidity-sensors-meters-and-methods/

French, P. W. (2006). Managed realignment–the developing story of a comparatively new approach to soft engineering. *Estuarine, Coastal and Shelf Science*, *67*(3), 409–423.

Friedrichs, C. T. (2011). *Tidal flat morphodynamics: A synthesis* (Vol. 3). Elsevier Inc. https://doi.org/10.1016/B978-0-12-374711-2.00307-7

Friedrichs, C. T. (1996). Uniform bottom shear stress and equilibrium hyposometry of intertidal flats.

Friess, D. A., Krauss, K. W., Horstman, E. M., Balke, T., Bouma, T. J., Galli, D., & Webb, E. L. (2012). Are all intertidal wetlands naturally created equal? bottlenecks, thresholds and knowledge gaps to mangrove and saltmarsh ecosystems. *Biological Reviews*, *87*(2), 346–366.

Garbutt, R. A., Reading, C. J., Wolters, M., Gray, A. J., & Rothery, P. (2006). Monitoring the development of intertidal habitats on former agricultural land after the managed realignment of coastal defences at tollesbury, essex, uk. *Marine pollution bulletin*, *53*(1-4), 155–164.

Gatto, V. M., van Prooijen, B. C., & Wang, Z. B. (2017). Net sediment transport in tidal basins: Quantifying the tidal barotropic mechanisms in a unified framework. *Ocean Dynamics*, *67*(11), 1385–1406.

Gourgue, O., van Belzen, J., Schwarz, C., Vandenbruwaene, W., Vanlede, J., Belliard, J.-P., Fagherazzi, S., Bouma, T. J., van de Koppel, J., & Temmerman, S. (2022). Biogeomorphic modeling to assess the resilience of tidal-marsh restoration to sea level rise and sediment supply. *Earth Surface Dynamics*, *10*(3), 531–553.

Grabemann, H. J., Grabemann, I., & Eppel, D. P. (2004). Climate change and hydrodynamic impact in the jade-weser area: A case study. *Coastline Reports*, *1*, 83–91.

Green, M. O., & Coco, G. (2007). Sediment transport on an estuarine intertidal flat: Measurements and conceptual model of waves, rainfall and exchanges with a tidal creek. *Estuarine, Coastal and Shelf Science*, *72*(4), 553–569.

Green, M. O. (2011). Very small waves and associated sediment resuspension on an estuarine intertidal flat. *Estuarine, coastal and shelf science*, *93*(4), 449–459.

Green, M. O., & Coco, G. (2014). Review of wave-driven sediment resuspension and transport in estuaries. *Reviews of Geophysics*, *52*(1), 77–117.

Groen, P. (1967). On the residual transport of suspended matter by an alternating tidal current. *Netherlands Journal of Sea Research*, *3*(4), 564–574.

Guo, C., He, Q., van Prooijen, B. C., Guo, L., Manning, A. J., & Bass, S. (2018). Investigation of flocculation dynamics under changing hydrodynamic forcing on an intertidal mudflat. *Marine Geology*, *395*, 120–132.

Herman, P. M., Middelburg, J. J., & Heip, C. H. (2001). Benthic community structure and sediment processes on an intertidal flat: Results from the ecoflat project [European Land-Ocean Interaction]. *Continental Shelf Research*, *21*(18), 2055–2071. https://doi.org/https://doi.org/10.1016/S0278-4343(01)00042-5

Hinkel, J., Lincke, D., Vafeidis, A. T., Perrette, M., Nicholls, R. J., Tol, R. S. J., Marzeion, B., Fettweis, X., Ionescu, C., & Levermann, A. (2014). Coastal flood damage and adaptation costs under 21st century sea-level rise. *Proceedings of the National Academy of Sciences*, *111*(9), 3292–3297.

Hu, Z., van der Wal, D., Cai, H., van Belzen, J., & Bouma, T. J. (2018). Dynamic equilibrium behaviour observed on two contrasting tidal flats from daily monitoring of bed-level changes. *Geomorphology*, *311*, 114–126. https://doi.org/https://doi.org/10.1016/j.geomorph.2018.03.025

Hu, Z., Wang, Z. B., Zitman, T. J., Stive, M. J. F., & Bouma, T. J. (2015). Predicting long-term and short-term tidal flat morphodynamics using a dynamic equilibrium theory. *Journal of Geophysical Research: Earth Surface*, *120*(9), 1803–1823.

Huisman, B., Schroevers, R., & van der Wal, M. (2010). *Erosie van het slik van bath* (tech. rep.). Deltares.

Jarrett, J. T. (1976). *Tidal prism-inlet area relationships* (Vol. 3). US Department of Defense, Department of the Army, Corps of Engineers …

Jeuken, M. C. J. L. (2000). On the morphological behaviour of tidal channels in the westerschelde estuary.

Jongepier, I., Wang, C., Missiaen, T., Soens, T., & Temmerman, S. (2015). Intertidal landscape response time to dike breaching and stepwise re-embankment: A combined historical and geomorphological study. *Geomorphology*, *236*, 64–78.

Kirby, R. (2000). Practical implications of tidal flat shape. *Continental Shelf Research*, *20*(10), 1061–1077. https://doi.org/https://doi.org/10.1016/S0278-4343(00)00012-1

Kirwan, M. L., Guntenspergen, G. R., d'Alpaos, A., Morris, J. T., Mudd, S. M., & Temmerman, S. (2010). Limits on the adaptability of coastal marshes to rising sea level. *Geophysical research letters*, *37*(23).

Kirwan, M. L., & Megonigal, J. P. (2013). Tidal wetland stability in the face of human impacts and sea-level rise. *Nature*, *504*(7478), 53–60.

Kirwan, M. L., Temmerman, S., Skeehan, E. E., Guntenspergen, G. R., & Fagherazzi, S. (2016). Overestimation of marsh vulnerability to sea level rise. *Nature Climate Change*, *6*(3), 253–260.

Kumbhakar, M., Ghoshal, K., & Singh, V. P. (2017). Derivation of rouse equation for sediment concentration using shannon entropy. *Physica A: Statistical Mechanics and its Applications*, *465*, 494–499.

Liu, Z., Fagherazzi, S., & Cui, B. (2021). Success of coastal wetlands restoration is driven by sediment availability. *Communications Earth & Environment*, *2*(1), 1–9.

Lotze, H. K., Lenihan, H. S., Bourque, B. J., Bradbury, R. H., Cooke, R. G., Kay, M. C., Kidwell, S. M., Kirby, M. X., Peterson, C. H., & Jackson, J. B. (2006). Depletion, degradation, and recovery potential of estuaries and coastal seas. *Science*, *312*(5781), 1806–1809.

Marijs, K., & Paree, E. (2004). Nauwkeurigheid vaklodingen westerschelde en -monding "de praktijk". *Technical report Meetinformatiediesnt Zeeland Vlissingen (in Dutch)*.

Mazik, K., Musk, W., Dawes, O., Solyanko, K., Brown, S., Mander, L., & Elliott, M. (2010). Managed realignment as compensation for the loss of intertidal mudflat: A short term solution to a long term problem? *Estuarine, Coastal and Shelf Science*, *90*(1), 11–20. https://doi.org/https://doi.org/10.1016/j.ecss.2010.07.009

Miller, J. A., & Simenstad, C. A. (1997). A comparative assessment of a natural and created estuarine slough as rearing habitat for juvenile chinook and coho salmon. *Estuaries*, *20*(4), 792–806.

Ministerie van V&W. (2008). *Natuurcompensatie porgramma westerschelde eindrapportage 1998-2008*.

Morris, J. T., Sundareshwar, P. V., Nietch, C. T., Kjerfve, B., & Cahoon, D. R. (2002). Responses of coastal wetlands to rising sea level. *Ecology*, *83*(10), 2869–2877.

Morris, R. K. A. (2012). Managed realignment: A sediment management perspective. *Ocean & coastal management*, *65*, 59–66.

Nederbragt, G. (2001). Seasonal variations of suspended sediment and diatoms in the western scheldt.

Neves, R. (1995). Three-dimensional model system for baroclinic estuarine dynamics and suspended sediment transport in a mesotidal estuary. *WIT Transactions on The Built Environment*.

Nicholls, R. J., Brown, S., Goodwin, P., Wahl, T., Lowe, J., Solan, M., Godbold, J. A., Haigh, I. D., Lincke, D., Hinkel, J., et al. (2018). Stabilization of global temperature at 1.5 c and 2.0 c: Implications for coastal areas. *Philosophical Transactions of the Royal Society A: Mathematical, Physical and Engineering Sciences*, *376*(2119), 20160448.

Nichols, M. M. (1986). Effects of fine sediment resuspension in estuaries. *Estuarine cohesive sediment dynamics* (pp. 5–42). Springer.

O'Brien, M. P. (1931). Estuary tidal prisms related to entrance areas. *Civil Engineering*.

O'Brien, M. P. (1969). Equilibrium flow areas of inlets on sandy coasts. *Journal of the Waterways and Harbors Division*, *95*(1), 43–52.

Oppenheimer, M., Glavovic, B., Hinkel, J., van de Wal, R., Magnan, A. K., Abd-Elgawad, A., Cai, R., Cifuentes-Jara, M., Deconto, R. M., Ghosh, T., et al. (2019). Sea level rise and implications for low lying islands, coasts and communities.

Paiva, J. N. S. D., de Vet, P. L. M., van der Werf, J. J., Louw, P. G. B. D., Visser, M., Rodriguez, S. G., Walles, B., Bouma, T. J., & Ysebaert, T. J. W. (2019). *Perkpolder tidal restoration*. Centre of expertise delta technology.

Pawlowicz, R., Beardsley, B., & Lentz, S. (2002). Classical tidal harmonic analysis including error estimates in matlab using t_tide. *Computers and Geosciences*, *28*, 929–937.

Postma, H. (1961). Transport and accumulation of suspended matter in the dutch wadden sea. *Netherlands Journal of Sea Research*, *1*(1-2), 148–190.

Pritchard, D., Hogg, A. J., & Roberts, W. (2002). Morphological modelling of intertidal mudflats: The role of cross-shore tidal currents. *Continental shelf research*, *22*(11-13), 1887–1895.

Pritchard, D. W. (1967). What is an estuary: Physical viewpoint.

Rasmussen, P. P., Gray, J. R., Glysson, G. D., & Ziegler, A. C. (2009). *Guidelines and procedures for computing timeseries suspended-sediment concentrations and loads from in-stream turbidity-sensor and streamflow data*. U.S. Geological Survey Techniques; Methods.

Rawson, J., Brown, S. L., Collins, M., & Hamer, B. (2004). *Freiston shore-lessons learnt for realignment design and habitat creation*.

Research, A. (1998). Review of coastal habitat creation, restoration and recharge schemes.

Ridderinkhof, H. (1988). Tidal and residual flows in the western dutch wadden sea i: Numerical model results. *Netherlands Journal of Sea Research*, *22*(1), 1–21.

Roberts, W., Le Hir, P., & Whitehouse, R. J. S. (2000). Investigation using simple mathematical models of the effect of tidal currents and waves on the profile shape of intertidal mudflats. *Continental Shelf Research*, *20*(10-11), 1079–1097.

Rotman, R., Naylor, L., McDonnell, R., & MacNiocaill, C. (2008). Sediment transport on the freiston shore managed realignment site: An investigation using environmental magnetism. *Geomorphology*, *100*(3-4), 241–255.

Sanderson, E. W., Foin, T. C., & Ustin, S. L. (2001). A simple empirical model of salt marsh plant spatial distributions with respect to a tidal channel network. *Ecological Modelling*, *139*(2-3), 293–307.

Scheldecommissie. (2019). Systeemanalyse natuur schelde-estuarium.

Schuerch, M., Spencer, T., Temmerman, S., Kirwan, M. L., Wolff, C., Lincke, D., McOwen, C. J., Pickering, M. D., Reef, R., Vafeidis, A. T., et al. (2018). Future response of global coastal wetlands to sea-level rise. *Nature*, *561*(7722), 231–234.

Shennan, I., & Horton, B. (2002). Holocene land-and sea-level changes in great britain. *Journal of Quaternary Science: Published for the Quaternary Research Association*, *17*(5-6), 511–526.

Sistermans, P., & Nieuwenhuis, O. (2004). Western scheldt estuary (the netherlands). *Amersfoort: DHV group*.

Syvitski, J. P. M., Kettner, A. J., Overeem, I., Hutton, E. W. H., Hannon, M. T., Brakenridge, G. R., Day, J., Vörösmarty, C., Saito, Y., Giosan, L., et al. (2009). Sinking deltas due to human activities. *Nature Geoscience*, *2*(10), 681–686.

Talke, S. A., & Stacey, M. T. (2008). Suspended sediment fluxes at an intertidal flat: The shifting influence of wave, wind, tidal, and freshwater forcing. *Continental Shelf Research*, *28*(6), 710–725.

Temmerman, S., Govers, G., Meire, P., & Wartel, S. (2003a). Modelling long-term tidal marsh growth under changing tidal conditions and suspended sediment concentrations, scheldt estuary, belgium. *Marine Geology*, *193*(1-2), 151–169.

Temmerman, S., Govers, G., Wartel, S., & Meire, P. (2003b). Spatial and temporal factors controlling short-term sedimentation in a salt and freshwater tidal marsh, scheldt estuary, belgium, sw netherlands. *Earth Surface Processes and Landforms: The Journal of the British Geomorphological Research Group*, *28*(7), 739–755.

Temmerman, S., Meire, P., Bouma, T. J., Herman, P. M. J., Ysebaert, T., & De Vriend, H. J. (2013). Ecosystem-based coastal defence in the face of global change. *Nature*, *504*(7478), 79–83.

Turner Designs Inc. (n.d.). *Turner c3 and c6* [Rev. Al].

Tuukkanen, T., Marttila, H., & Kløve, B. (2014). Effect of soil properties on peat erosion and suspended sediment delivery in drained peatlands. *Water Resources Research*, *50*(4), 3523–3535.

van den Hoven, K., Kroeze, C., & van Loon-Steensma, J. M. (2022). Characteristics of realigned dikes in coastal europe: Overview and opportunities for nature-based flood protection. *Ocean & Coastal Management*, *222*, 106116. https://doi.org/https://doi.org/10.1016/j.ocecoaman.2022.106116

Van Der Wal, D., Van Kessel, T., Eleveld, M. A., & Vanlede, J. (2010). Spatial heterogeneity in estuarine mud dynamics. *Ocean Dynamics*, *60*, 519–533. https://doi.org/10.1007/s10236-010-0271-9

Van der Wal, D., Wielemaker-Van den Dool, A., & Herman, P. M. (2008). Spatial patterns, rates and mechanisms of saltmarsh cycles (westerschelde, the netherlands). *Estuarine, Coastal and Shelf Science*, *76*(2), 357–368. https://doi.org/https://doi.org/10.1016/j.ecss.2007.07.017

van der Vegt, H., & van der Wegen, M. (2021). Invloed van erosieresistente lagen op morfologische verandering in de westerschelde.

Van Maren, D. S., & Winterwerp, J. C. (2013). The role of flow asymmetry and mud properties on tidal flat sedimentation. *Continental Shelf Research*, *60*, S71–S84.

Van Straaten, L. M. J. U., & Kuenen, P. H. (1957). *Accumulation of fine grained sediments in the dutch waddensea*.

Van Wijnen, H. J., & Bakker, J. P. (2001). Long-term surface elevation change in salt marshes: A prediction of marsh response to future sea-level rise. *Estuarine, Coastal and Shelf Science*, *52*(3), 381–390.

van Ginkel, M. (2019). *Projectplan aanpassing waterkering perkpolder* (tech. rep.). Royal Haskoning.

van Kessel, T., Vanlede, J., & de Kok, J. (2011). Development of a mud transport model for the scheldt estuary. *Continental Shelf Research*, *31*. https://doi.org/10.1016/j.csr.2010.12.006

van Wesenbeeck, B. K., Mulder, J. P. M., Marchand, M., Reed, D. J., de Vries, M. B., de Vriend, H. J., & Herman, P. M. J. (2014). Damming deltas: A practice of the past? towards nature-based flood defenses. *Estuarine, coastal and shelf science*, *140*, 1–6.

Verbeek, H. (2005). Ontwikkelingsschets 2010 schelde-estuarium, besluiten van de nederlandse en vlaamse regering.

Verlaan, P. A. J. (1998). Mixing of marine and fluvial particles in the scheldt estuary.

Vousdoukas, M. I., Mentaschi, L., Hinkel, J., Ward, P. J., Mongelli, I., Ciscar, J.-C., & Feyen, L. (2020). Economic motivation for raising coastal flood defenses in europe. *Nature communications*, *11*(1), 1–11.

Wang, Z. B., Jeuken, C., & De Vriend, H. J. (1999). Tidal asymmetry and residual sediment transport in estuaries. *Delft Hydraulics report Z2749*.

Wang, Z. B., Jeuken, M. C. J. L., Gerritsen, H., de Vriend, H. J., & Kornman, B. A. (2002). Morphology and asymmetry of the vertical tide in the westerschelde estuary. *Continental Shelf Research*, *22*(17), 2599–2609. https://doi.org/https://doi.org/10.1016/S0278-4343(02)00134-6

Wang, Z. B., Van Maren, D. S., Ding, P. X., Yang, S. L., Van Prooijen, B. C., De Vet, P. L. M., Winterwerp, J. C., De Vriend, H. J., Stive, M. J. F., & He, Q. (2015). Human impacts on morphodynamic thresholds in estuarine systems [Coastal Seas in a Changing World: Anthropogenic Impact and Environmental Responses]. *Continental Shelf Research*, *111*, 174–183. https://doi.org/https://doi.org/10.1016/j.csr.2015.08.009

Wang, Z. B., Vandenbruwaene, W., Taal, M., & Winterwerp, H. (2019). Amplification and deformation of tidal wave in the upper scheldt estuary. *Ocean Dynamics*, *69*(7), 829–839.

Warner, J. F., van Staveren, M. F., & van Tatenhove, J. (2018). Cutting dikes, cutting ties? reintroducing flood dynamics in coastal polders in bangladesh and the netherlands [Advancing Ecosystems and Disaster Risk Reduction in Policy, Planning, Implementation, and Management]. *International Journal of Disaster Risk Reduction*, *32*, 106–112. https://doi.org/https://doi.org/10.1016/j.ijdrr.2018.03.020

Watt, D. A. (1905). Notes on the improvement of river and harbor outlets in the united states. *Transactions of the American Society of Civil Engineers*, *55*(2), 288–305.

Weisscher, S. A. H., Baar, A. W., van Belzen, J., Bouma, T. J., & Kleinhans, M. G. (2022). Transitional polders along estuaries: Driving land-level rise and reducing flood propagation. *Nature-Based Solutions*, 100022.

Wheeler, D., Tan, S., Pontee, N., & Pygott, J. (2008). Alkborough scheme reduces extreme water levels in the humber estuary and creates new habitat.

Widdows, J., Blauw, A., Heip, C. H. R., Herman, P. M. J., Lucas, C. H., Middelburg, J. J., Schmidt, S., Brinsley, M. D., Twisk, F., & Verbeek, H. (2004). Role of physical and biological processes in sediment dynamics of a tidal flat in westerschelde estuary, sw netherlands. *Marine Ecology Progress Series*, *274*, 41–56.

Wiegmann, E. B., Perluka, R., Oude Elberink, S., & Vogelzang, J. (2005). Vaklodingen: De inwintechnieken en hun combinaties. *Report AGI-2005*.

Willemsen, P. W. J. M., Smits, B. P., Borsje, B. W., Herman, P. M. J., Dijkstra, J. T., Bouma, T. J., & Hulscher, S. J. M. H. (2022). Modelling decadal salt marsh development: Variability of the salt marsh edge under influence of waves and sediment availability. *Water Resources Research*, e2020WR028962.

Willemsen, P. W. J. M., Borsje, B. W., Vuik, V., Bouma, T. J., & Hulscher, S. J. (2020). Field-based decadal wave attenuating capacity of combined tidal flats and salt marshes. *Coastal Engineering*, *156*, 103628. https://doi.org/https://doi.org/10.1016/j.coastaleng.2019.103628

Williams, P. B., & Orr, M. K. (2002). Physical evolution of restored breached levee salt marshes in the san francisco bay estuary. *Restoration Ecology*, *10*(3), 527–542.

Winterwerp, J. C., Cornelisse, J. M., & Kuijper, C. (1993). A laboratory study on the behavior of mud from the western scheldt under tidal conditions. *Coastal and estuarine studies*, 295–295.

Yamashita, H. (2021). Case study c information for chapters 7, 8 and 9: Ago bay tidal flat restoration projects, shima city, mie prefecture, japanhiromi yamashita, naoyuki mikami, hideto uranaka, and hideki kokubu. *Coastal wetlands restoration* (pp. 87–92). Routledge.

Zheng, Z., Zhou, Y., Tian, B., & Ding, X. (2016). The spatial relationship between salt marsh vegetation patterns, soil elevation and tidal channels using remote sensing at chongming dongtan nature reserve, china. *Acta Oceanologica Sinica*, *35*(4), 26–34.

Zhu, Q., van Prooijen, B. C., Maan, D. C., Wang, Z. B., Yao, P., Daggers, T., & Yang, S. L. (2019). The heterogeneity of mudflat erodibility. *Geomorphology*, *345*, 106834. https://doi.org/https://doi.org/10.1016/j.geomorph.2019.106834

Zhu, Z., Vuik, V., Visser, P. J., Soens, T., van Wesenbeeck, B., van de Koppel, J., Jonkman, S. N., Temmerman, S., & Bouma, T. J. (2020). Historic storms and the hidden value of coastal wetlands for nature-based flood defence. *Nature Sustainability*, *3*(10), 853–862.

Zijl, F., Sumihar, J., & Verlaan, M. (2015). Application of data assimilation for improved operational water level forecasting on the northwest european shelf and north sea. *Ocean Dynamics*, *65*(12), 1699–1716.

Zijl, F., Verlaan, M., & Gerritsen, H. (2013). Improved water-level forecasting for the northwest european shelf and north sea through direct modelling of tide, surge and non-linear interaction. *Ocean Dynamics*, *63*(7), 823–847.

A

Delft3D FM validation

This appendix presents the results of the validation of the Delft3D FM model 'Buitendijkse Maatregelen'. First a limitation of the Delft3D model is shown in Section A.1. After that the validation procedure is shown, starting with the modelled water levels that will be compared with the measured water levels at station Walsoorden in Section A.2. Furthermore, the discharge at the inlet will be compared with the discharge determined from the ADCP measurements and the tidal storage approach in section A.3. Lastly the velocity of the model will be checked with the velocity measured from the aquadopp measurements in Section A.4.

A.1. Grid refinement error

Before the start of the validation of the Delft3D FM model, first a limitation of the model is shown near the transitions of grid refinements. Figure A.1 shows the average peak flood velocity of a part of the Western Scheldt including Perkpolder. When comparing this with Figure 3.4, it is concluded that at the boundaries of the grid refinements (areas circled in red) the average peak velocity is not continuous. In this appendix the water levels, velocities and discharge between the model and measurements will be compared. After the validation it can be concluded if the grid refinement leads to significant errors to the flow near and in Perkpolder.

However, a first conclusion can already be made. The model is currently not calibrated for morphodynamics, however the discontinuous peak velocity should be solved before a morphodynamic analysis is performed. Since these difference in peak velocities will lead to unrealistic sedimentation and erosion patterns outside Perkpolder. This is a reason not to use the Delft3D FM model as morphodynamic model.

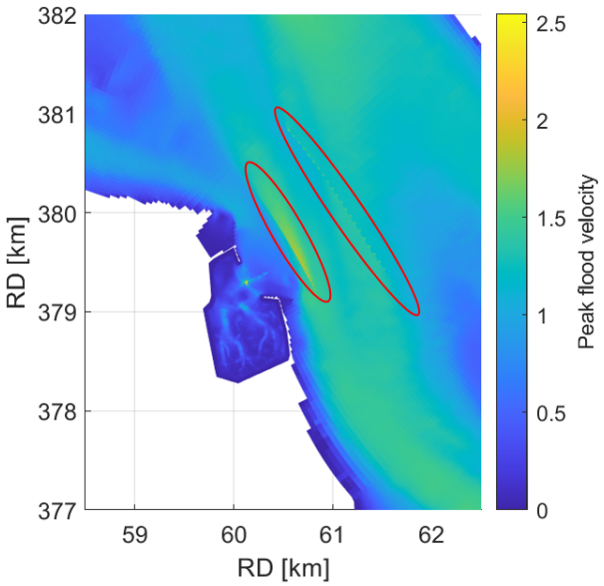

Figure A.1: Peak flow velocity of Western Scheldt and Perkpolder. Clearly visible are the numerical artefacts at the boundaries of the grid refinements (circled in red).

A.2. Water levels

The water levels of station Walsoorden and the model results are shown in Figure A.2. The bias for the water levels is equal to $-0.0058\,m$, the RMSE and uRMSE are equal to $0.067\,m$. The tidal range is in the order of $4.6\,m$, the bias and variance are both very small compared to the tidal range and this shows that the water levels are very accurate reproduced by the model.

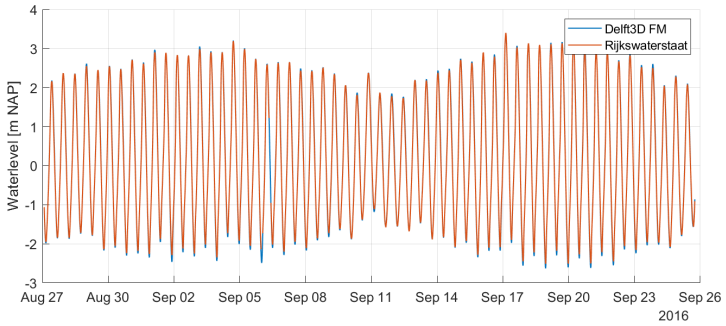

Figure A.2: Comparison of waterlevels of station Walsoorden and the model results.

A.3. Discharge at inlet

Figure A.3 shows the discharge at the inlet of Perkpolder for the model results, the tidal storage approach and the discharge based on velocities measured by aquadopp sensors. The discharge based on the aquadopp velocities is calculated by multiplying part of the cross section with the velocity from the aquadopp sensor, this procedure has been explained in Paiva et al., 2019. The model results are performed using the bathymetry of the Western Scheldt of respectively 2016 and 2018 and the bathymetry of Perkpolder for 2015 to 2021. The combinations of bathymetry of the Western Scheldt and Perkpolder are shown in Table 3.3. The water levels of 25-08-2016 to 25-09-2016 are used for the run, since this has been determined to be a representative month (de Vet et al., 2022).

The aquadopp measurements were measured in December 2015, therefore direct comparison for the water levels is not possible with the model runs, because the models are run for the water levels of 25-08-2016 to 25-09-2016. Therefore the aquadopp measurements and model results will be compared based on the closest tidal range to each other. Moreover the tidal storage results are plotted for both the tide of the aquadopp measurement and the compared tide of the model run.

A second limitation of the comparison of aquadopp measurements and model runs is that the aquadopp velocities are measured in December 2015. The bathymetry of Perkpolder closest to December 2015 is from March 2016. Moreover it is known that in the first year, Perkpolder is morphologically very active (see e.g. Figure 5.1). Especially the entrance is changing a lot in the first year (see Figure 5.8 and Figure 5.9b), which alters the discharge and velocities measured at the inlet. A thorough analysis of the effect of a changing inlet on the modelled discharges and velocities is performed in Appendix B. Therefore the discharges are visually compared to see if they show the same pattern.

Although the entrance of Perkpolder changed considerably according to chapter 5, the discharge of the ADCP measurements, the tidal storage approach and the model results show many similarities. However, Figure A.3c to Figure A.3g show that for tides with a high tidal range (spring tides) the peak discharge is underestimated by the tidal storage approach. This difference in peak discharge will be addressed in Appendix B. Lastly the ADCP measurements are very sensitive and show much more temporal changes than the tidal storage and model results.

A.4. Velocities at inlet

Figure A.4 and Figure A.5 compares respectively the angle and magnitude of the model results with the flow measurements of ADCP sensor MP0102. The location of this sensor is shown in Figure 3.3. This sensor has been chosen since the bed level difference in 2015 and 2016 was smallest as seen in Figure 5.8, therefore a different velocity signal due to bed level changes is limited as much as possible. Also these figures are very similar, except for the incoming peak magnitude, which has a large correlation with the incoming peak discharge. Overall the incoming peak magnitude (before HW) seems to be overestimated by the ADCP measurements. Since the local velocity is very sensitive to bathymetry changes, this could explain the difference. However the matching water levels and discharge gives enough confidence that the model results accurately reflect reality.

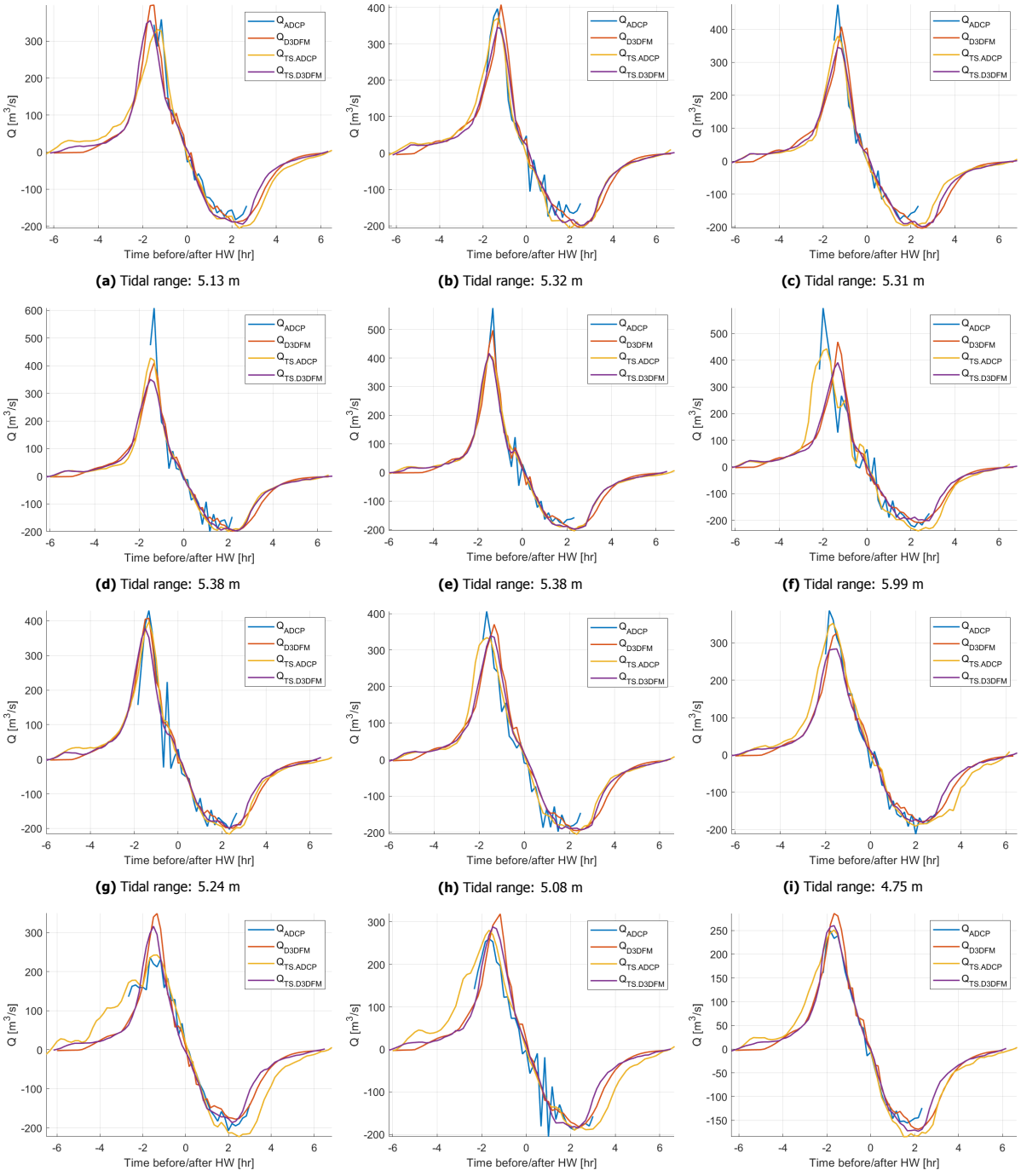

(a) Tidal range: 5.13 m **(b)** Tidal range: 5.32 m **(c)** Tidal range: 5.31 m

(d) Tidal range: 5.38 m **(e)** Tidal range: 5.38 m **(f)** Tidal range: 5.99 m

(g) Tidal range: 5.24 m **(h)** Tidal range: 5.08 m **(i)** Tidal range: 4.75 m

(j) Tidal range: 4.93 m **(k)** Tidal range: 4.85 m **(l)** Tidal range: 4.48 m

Figure A.3: Comparison of discharge using ADCP measurements (ADCP), tidal storage approach (TS) and model results (D3DFM). The tidal storage is used for the 2015 bed levels to correspond with the ADCP measurements (TS.ADCP) and the 2016 bed levels to correspond with the modelling period (TS.D3DFM).

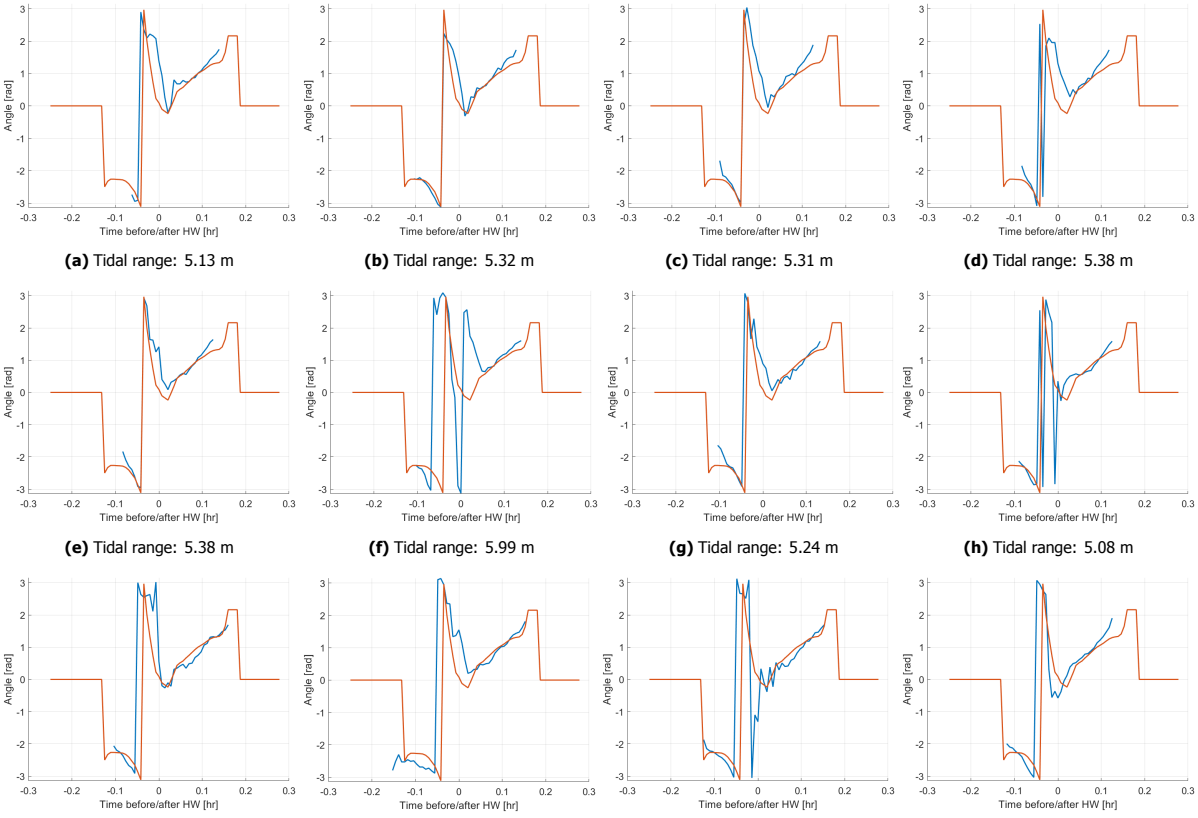

(a) Tidal range: 5.13 m **(b)** Tidal range: 5.32 m **(c)** Tidal range: 5.31 m **(d)** Tidal range: 5.38 m

(e) Tidal range: 5.38 m **(f)** Tidal range: 5.99 m **(g)** Tidal range: 5.24 m **(h)** Tidal range: 5.08 m

(i) Tidal range: 4.75 m **(j)** Tidal range: 4.93 m **(k)** Tidal range: 4.85 m **(l)** Tidal range: 4.48 m

Figure A.4: Comparison of angles using ADCP measurements and model results. The ADCP measurements are only measured during part of the tide. The tides of the ADCP measurements and model results are compared based on the closest tidal range.

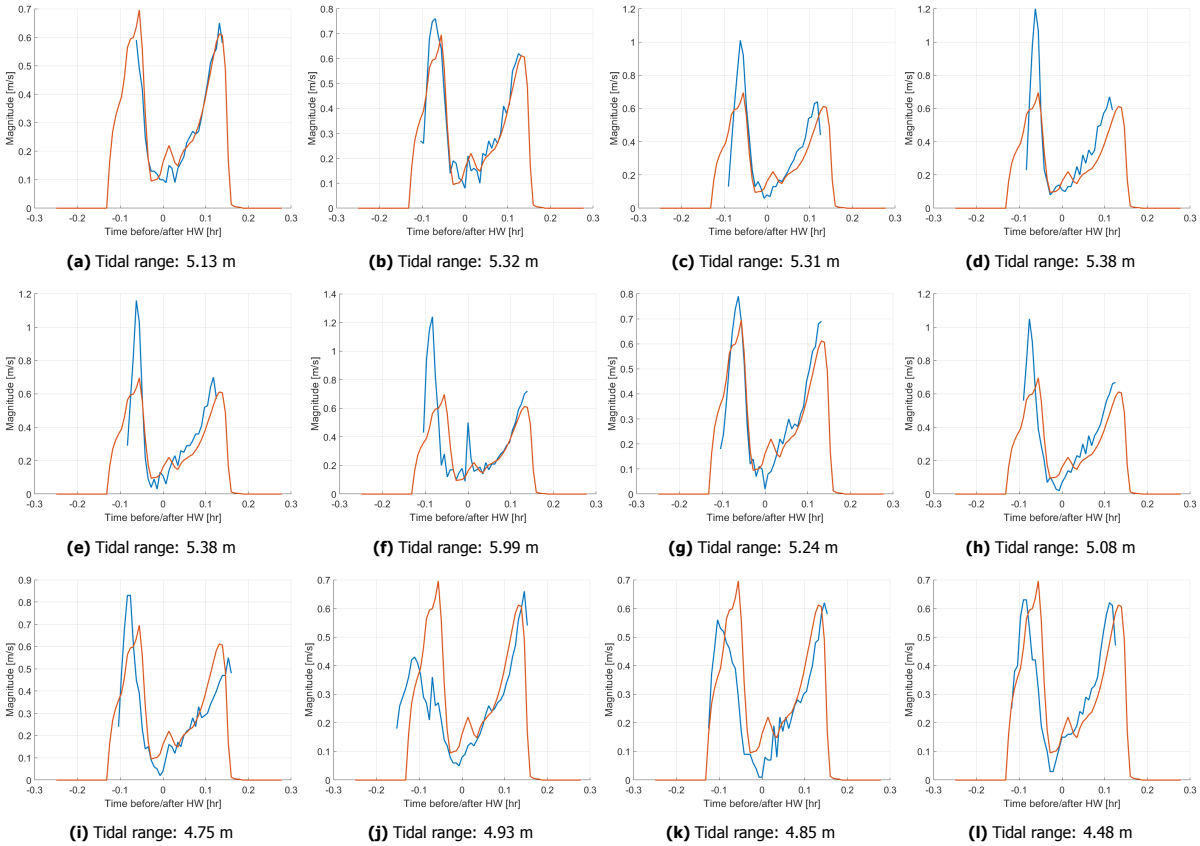

(a) Tidal range: 5.13 m **(b)** Tidal range: 5.32 m **(c)** Tidal range: 5.31 m **(d)** Tidal range: 5.38 m

(e) Tidal range: 5.38 m **(f)** Tidal range: 5.99 m **(g)** Tidal range: 5.24 m **(h)** Tidal range: 5.08 m

(i) Tidal range: 4.75 m **(j)** Tidal range: 4.93 m **(k)** Tidal range: 4.85 m **(l)** Tidal range: 4.48 m

Figure A.5: Comparison of velocity magnitude using ADCP measurements and model results. The ADCP measurements are only measured during part of the tide. The tides of the ADCP measurements and model results are compared based on the closest tidal range.

B

Entrance as threshold

This appendix presents a thorough analysis of the entrance of Perkpolder as addition on Chapter 5. As established in Figure 5.9b the minimum bed level of the entrance of Perkpolder is in 2015 above the low water datum, this means that during part of the tide there is no discharge in or out of Perkpolder. This effect is not captured by the tidal storage approach, since it assumes an instantaneous inflow of water based on the rate of change of water levels. The consequences of the entrance blocking the flow is examined in three sections. First, in Section B.1 the discharge modifications from the tidal storage approach are shown and explained, thereafter the change in water levels is discussed (Section B.2) and lastly in Section B.3 the effect on velocities within Perkpolder is considered.

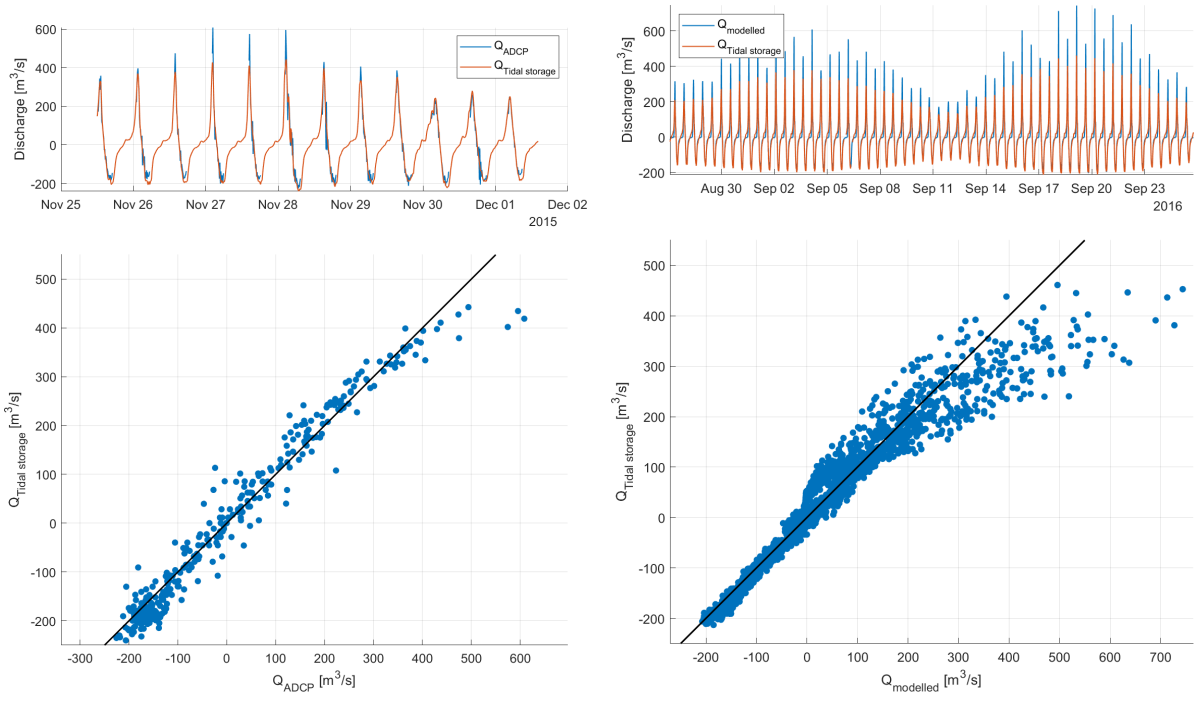

(a) ADCP and Tidal Storage

(b) Delft3D FM and Tidal Storage

Figure B.1: Comparison of tidal storage approach with respectively discharge calculated from ADCP measurements and discharge obtained from the Delft3D FM model. The top figure shows the time series of discharge and the bottom figure shows the similarities between both methods. Scattered data closer to the 1:1 line has a larger correlation.

B.1. Discharge modifications

As already established in Appendix A the discharge between the aquadopp measurements, tidal storage and model results show great similarities. However there are some interesting phenomena observed when closely examining the discharge distribution. The tidal storage approach underestimates the incoming peak discharge. This is both for the discharge computed from aquadopp measurements in december 2015 and the modelled discharge from Delft3D FM as shown in Figure B.1. It seems that the underestimation is larger during spring tides, than during neap tides. Moreover the model results show no incoming discharge for the first period of time. This phenomenon

cannot be backed up by the aquadopp measurements, since the sensors are above water during this period of the tide.

When connecting both observations, the flow is blocked for very low water levels in 2015, see also Figure B.2a. After blocking of the flow, the discharge will 'catch up' and more water will flow into Perkpolder during the remainder of the incoming tide, this creates the observed high incoming peak discharges. During spring tides the tidal range is larger and this lead to a lower LW and a higher HW than neap tides. Since the LW is lower, more water is blocked near the entrance creating a larger 'catch-up' effect and thus higher peak discharges.

Figure B.2b shows that the tidal prism is increasing from 2015 to 2016, this is because the entrance partially blocked the flow in the first year. After that a general decline in tidal prism is observed. Perkpolder acts as a sediment sink and therefore the bed levels are generally increasing (see e.g. Figure 5.1). Due to the accretion less water is entering Perkpolder each year and the tidal prism is subsequently decreased.

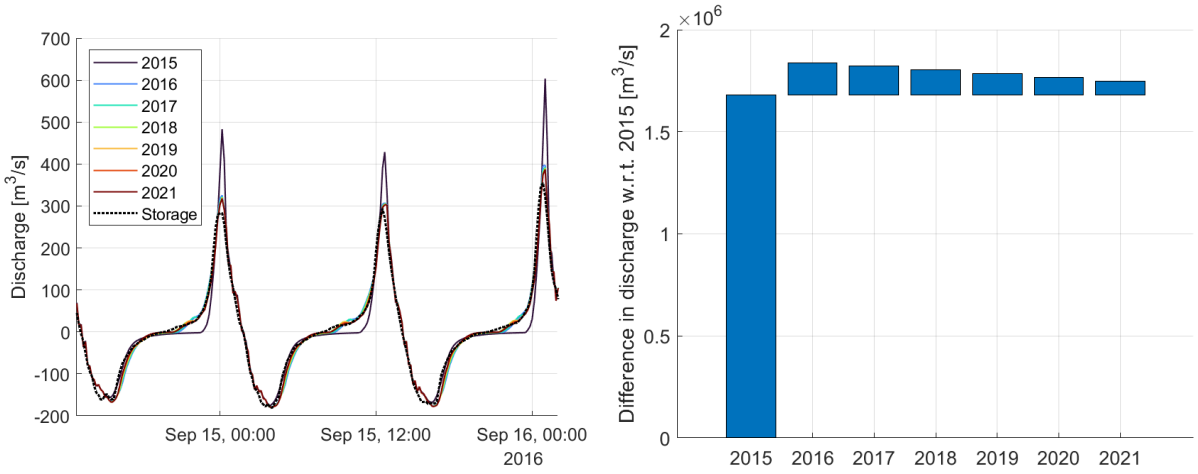

(a) Temporal evolution of discharge through entrance using bathymetry of 2015 to 2021 in Delft3D FM model. The black line shows the tidal storage approach using the bathymetry of 2018 as comparison.

(b) Average tidal prism of Perkpolder from the Western Scheldt model using the bathymetry from 2015 to 2021. The first bar shows the average of 2015, the other bars the difference with respect to 2015.

Figure B.2: Discharge through entrance of Perkpolder.

B.2. Changing water levels at the entrance of Perkpolder

Figure B.3 shows the water levels in the deepest part of the entrance for 2015 to 2020 and at measurement station Walsoorden. This shows the effect of the frontal entrance area and the entrance on the water levels near Perkpolder. The blocking of the flow in 2015 as described in Section B.1 is clearly seen.

Moreover, the water levels from 2016 to 2020 are not the same as station Walsoorden. During low water, the water levels are higher than the water level at station Walsoorden. The water depth in the frontal entrance area is very low during low water, therefore friction effects may have a significant influence on the flow. To test this hypothesis a control run has been performed in which the bed levels of the frontal entrance area and the entrance of Perkpolder are decreased to $-3\ m$ *NAP*. In this run, the water levels measured near the inlet are exactly the same as the water levels of station Walsoorden. This proves that frictional effects in the frontal entrance area change the water levels near the entrance. The water levels influence the discharge in Perkpolder, since this is directly coupled to the change in water levels.

B.3. Velocities in Perkpolder

The last effect that is discussed in this appendix is the effect of the entrance on the velocities within Perkpolder. The pond is a part that is initially excavated to a depth of $-3\ m$ *NAP* (van Ginkel, 2019). This pond is thus much deeper than the initial layout of the entrance (see e.g. Figure 5.8). Since the flow is blocked for part of the tide, the water within Perkpolder has low flow velocities for this period of time, which increases the slack time in which sediment can settle.

Figure B.4 shows the water levels and velocities in the pond of Perkpolder. In 2015 low velocities are lasting significantly longer than in 2018 when the entrance is not blocking the flow. Therefore sediment has more time to settle in the pond, the intertidal area already run dry. Moreover the peak velocity is increased, therefore more sediment could be transported into Perkpolder. This is a possible reason why the sedimentation rates in the pond

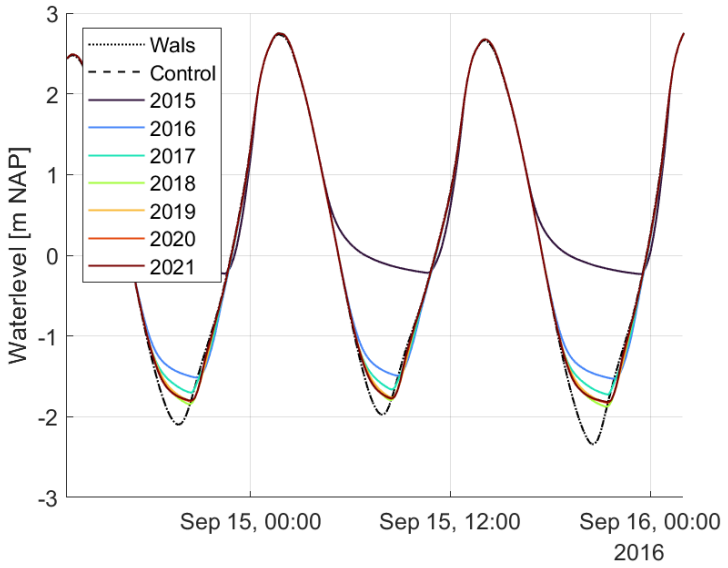

Figure B.3: Water levels in deepest point of the entrance at Perkpolder. In black the water levels of Walsoorden are plotted as reference.

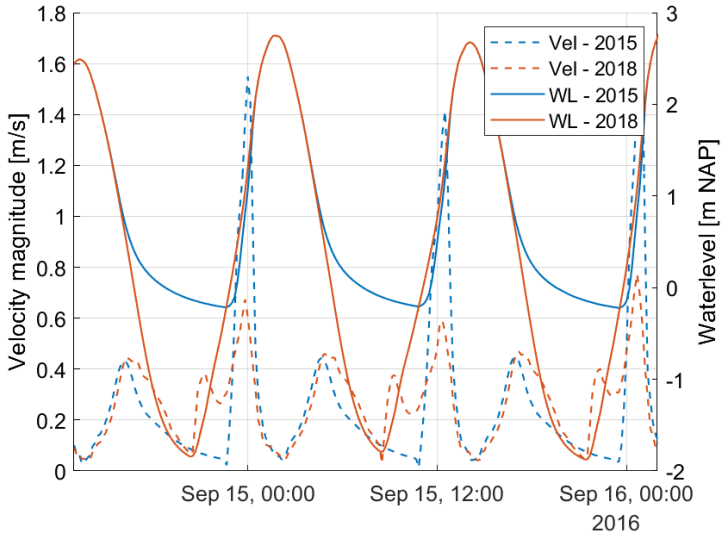

Figure B.4: Water levels and velocities in the middle of the pond of Perkpolder in 2015 and 2018.

of Perkpolder are significantly higher in the first year, than the next years.

C

Hydrodynamic validation Bathtub model

This chapter describes in detail the hydrodynamic calibration and validation of the bathtub model with respect to the Western Scheldt model. The Western Scheldt model takes the interaction of Perkpolder with the Western Scheldt into account. Furthermore the water levels, discharge and velocities are correctly reproduced near Perkpolder (see Appendix A). Therefore the velocity field of the Western Scheldt model is assumed to accurately represent reality and the bathtub model will be matched to this model.

There are a few parameters that are calibrated in order to match the hydrodynamics of Perkpolder, this includes the imposed boundary condition, the friction coefficient and horizontal viscosity. As base the friction coefficient and horizontal viscosity are taken close to the Western Scheldt model which means that a Manning friction coefficient of 0.022 is used and a horizontal viscosity of $1\ Ns/m^2$. The viscosity depends on the grid size of the model, since the bathtub model has a smaller grid size than the Western Scheldt model, the viscosity will not be enlarged and therefore set at $1\ Ns/m^2$.

To validate the bathtub model, the discharge near the entrance will be compared with the Western Scheldt model and the tidal storage approach in section C.1. Moreover section C.3 and C.2 shows a comparison of respectively the water levels and velocities over a tide.

C.1. Discharge at entrance

As boundary condition the water levels of station Walsoorden are imposed on the entrance of Perkpolder. In order to investigate if the water levels result in the correct flow of water, the discharge at the entrance will be compared as shown in Figure C.1. The Western Scheldt model and the bathtub model are in good alignment with each other. The tidal storage approach shows sometimes a higher deviation, however the general outline is the same. These deviations are merely caused by wiggles in the discharge profile of both the model simulations. The wiggles are also found in the ADCP measurements as shown in Figure A.3, therefore this gives confidence that these wiggles are not fully attributed to model artefacts, but occur in reality.

C.2. Water levels in Perkpolder

In this section the water levels over the entire realigned area will be compared with the Western Scheldt model in order to conclude if the water levels are accurately reproduced over the entire domain. Figure C.2 shows the averaged water level during a single tide for the bathtub model and Western Scheldt model. During low waters the water levels between the bathtub model and Delft3D model deviate. However the difference is still very small with respect to the tidal range. Therefore, the water levels are accurately reproduced over the entire domain.

C.3. Velocity field in Perkpolder

In order to examine the flow field within Perkpolder, the velocity field at eight instances within a single tide (tide of August 26, 2016 07:00 - 19:00) are compared. From the comparison in Figure C.3 the most important differences are discovered together with the implications these differences have on the outcome of the bathtub model. The deviations and possible effects on the morphodynamics are discussed hereunder.

The bathtub model has one boundary condition in which water levels are imposed. Due to this boundary condition the flow can only enter the domain perpendicular of the boundary condition. However due to the location of Perkpolder and the current direction of the Western Scheldt the flow is not coming perpendicular through the entrance into Perkpolder. This is seen especially at higher water levels, when the flow is not only entering Perkpolder via the deep entrance channel (see e.g. Figure C.3d), but through the entire entrance. During low water levels

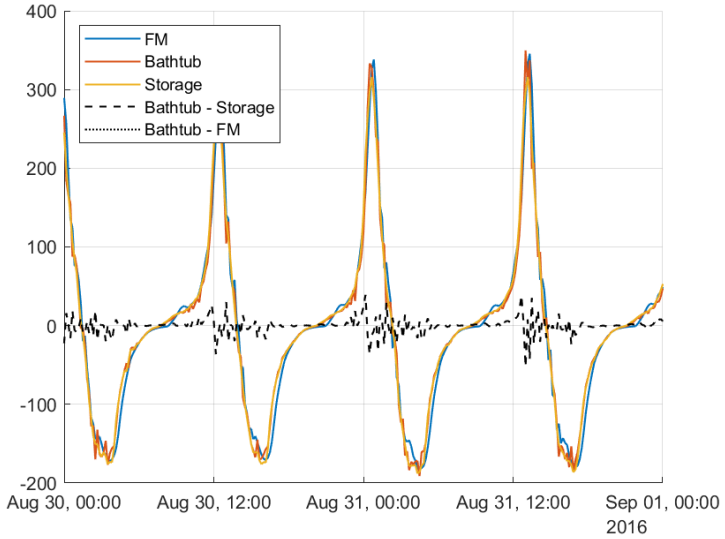

Figure C.1: Comparison of discharge at the entrance between bathtub model; Western Scheldt model and tidal storage approach. The differences are shown in the black lines.

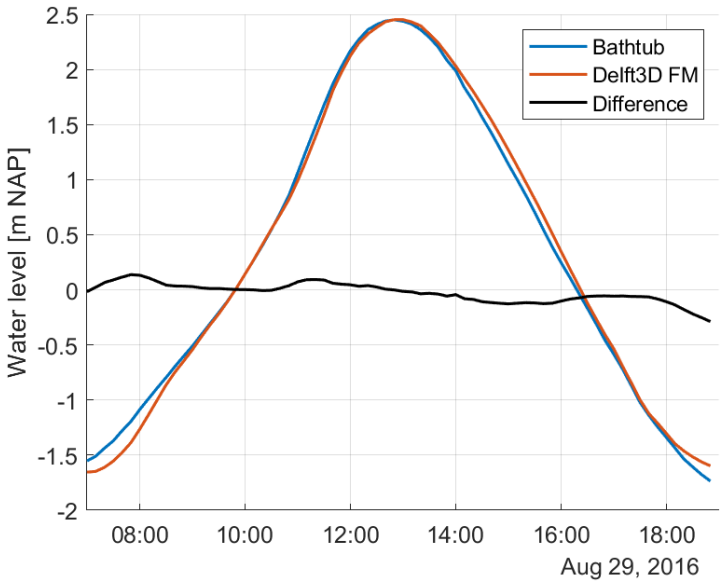

Figure C.2: Comparison of water levels averaged over the entire domain. The difference between the Western Scheldt and bathtub model is calculated by interpolating the Western Scheldt model on the bathtub grid and then averaging the difference of each cell.

the flow is entering and leaving via the deep channel of the entrance and the flow is modelled correctly. However, this difference in incoming flow has multiple effects on the spatial velocity pattern within Perkpolder and therefore on the morphological development.

In order to align the flow correctly with the direction of the flow in the Western Scheldt a solution was proposed with an artificial basin in front of Perkpolder which guides the flows with the correct angle through the entrance. However, for this solution, the boundary condition for sediments should also be applied in front of the frontal entrance area. In Chapter 6 has been established that the frontal entrance area has an important contribution to the suspended sediment concentration, therefore it is very hard to come up with a physically correct boundary condition for sediment which is located before the frontal entrance area.

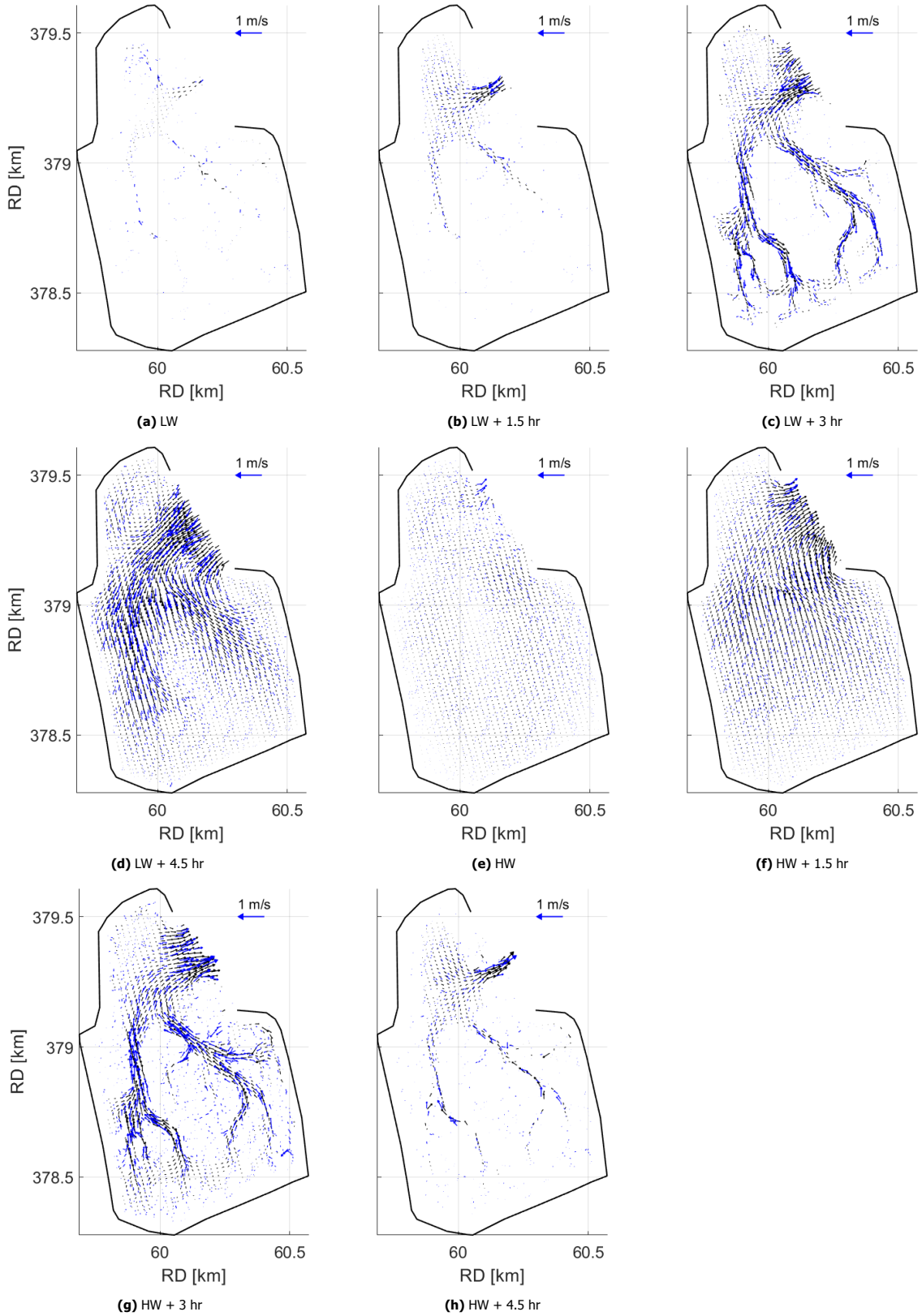

(a) LW **(b)** LW + 1.5 hr **(c)** LW + 3 hr

(d) LW + 4.5 hr **(e)** HW **(f)** HW + 1.5 hr

(g) HW + 3 hr **(h)** HW + 4.5 hr

Figure C.3: Comparison of spatial velocity field within Perkpolder between Western Scheldt model (blue) and bathtub model (black).

D

Calibration of OBS sensors

This Appendix shows the calibration procedure of the OBS data. First, in Section D.1 the available turbidity measurements will be converted to concentration data using calibration measurements. After that post processing of the generated concentration data will be performed in Section D.2. To show if the measured concentration can be used as depth average concentration, the Rouse number will be calculated in Section D.3. Lastly the limitations of this calibration procedure will be exclaimed in section D.4.

D.1. Turbidity measurements

The turbidity measurements are performed with a Turner C3. This device is a fluorometer which has optical sensors to measure turbidity (Turner Designs Inc., n.d.). Two sensors have been deployed from the period September 2016 to March 2017. In order to change the batteries and to remove left debris, the fluorometer is regularly removed from the water, the measurement intervals are shown in Table D.1.

Table D.1: Measurement intervals of OBS sensors. OBS1 is the sensor is the North-East corner and OBS3 is the sensor in the entrance.

Location	Method	ID	Date in	Date out	Period [days]
Entrance Breach	OBS	PA3-O	16-9-2016	20-10-2016	34
North-East corner	OBS	PA1-O	16-9-2016	20-10-2016	34
Entrance Breach	OBS	PA3-O	20-10-2016	20-12-2016	61
North-East corner	OBS	PA1-O	20-10-2016	20-12-2016	61
Entrance Breach	OBS	PA3-O	21-12-2016	17-1-2017	27
North-East corner	OBS	PA1-O	21-12-2016	17-1-2017	27
Entrance Breach	OBS	PA3-O	19-1-2017	19-4-2017	90
North-East corner	OBS	PA1-O	19-1-2017	19-4-2017	90

The turbidity of the flow is correlated to the suspended sediment concentration, since suspended particles reflect the emitted waves. However this relation is different per location (type of sediment) and differs due to differences in circumstances (Rasmussen et al., 2009). A linear regression model in the form of Equation D.1 is used to calibrate the turbidity measures with the suspended sediment concentration. In this thesis a linear or quadratic calibration curve will be fitted, therefore the exponent (A) is equal to 1 or 2. The calibration measurements have been performed in a lab using bed sediment of Perkpolder to calibrate both OBS sensors. It should be noted that the OBS sensors measure suspended sediment which is generally finer than bed material, therefore results between the calibration and reality will differ.

$$log_{10}(SSC) = a \cdot log_{10}(Turb) + b \rightarrow SSC = Turb^A + B \tag{D.1}$$

The results of the calibration are shown in Figure D.1 for OBS1 and in Figure D.2 for OBS3. The choice for the calibration curve depends on the regression coefficient and if the subset of measurements that occurs most frequent is calibrated correctly. Therefore some calibration curves do not go through all the calibration measurements, but only through the calibration measurements that are close to the most common measurements. Both sensors have a lot of turbidity measurements up to 80 *RFUB*, these correspond to the time where the sensor is above the water. Therefore these measurements will be filtered out when processed. Furthermore both measurements start measuring turbidity's from around 150 *RFUB*, inbetween 80 *RFUB* and 150 *RFUB* no measurements are recorded. This could indicate that there is a background turbidity of around 150 *RFUB*. This background turbidity is caused by sediment that is always in suspension and other particles that will never settle.

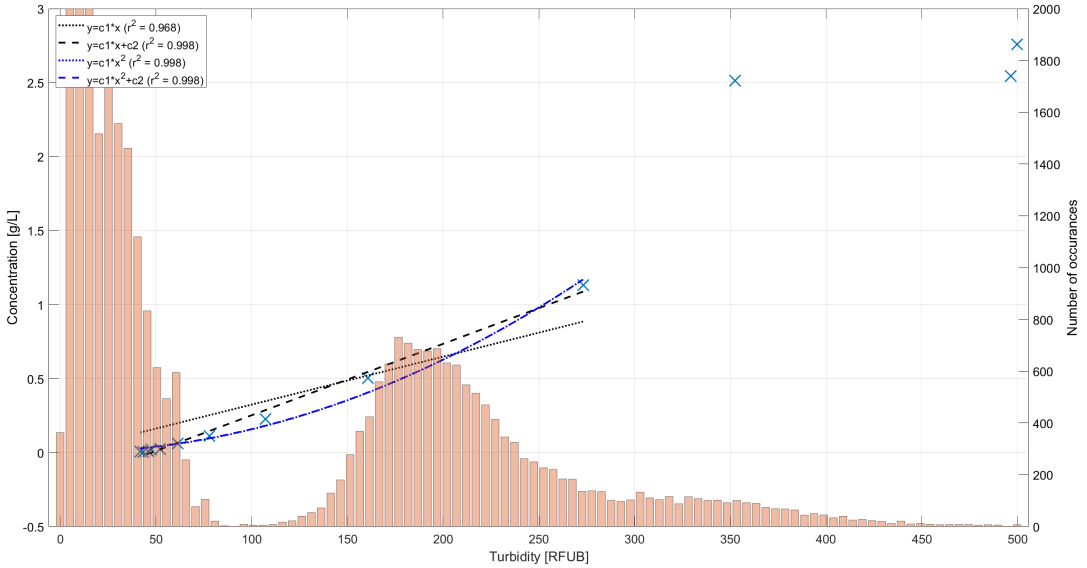

Figure D.1: Four different calibration curves with regression coefficient for OBS sensor 1 that are fitted to the lab measurements shown as a blue X. In orange the occurrence of each turbidity value is shown.

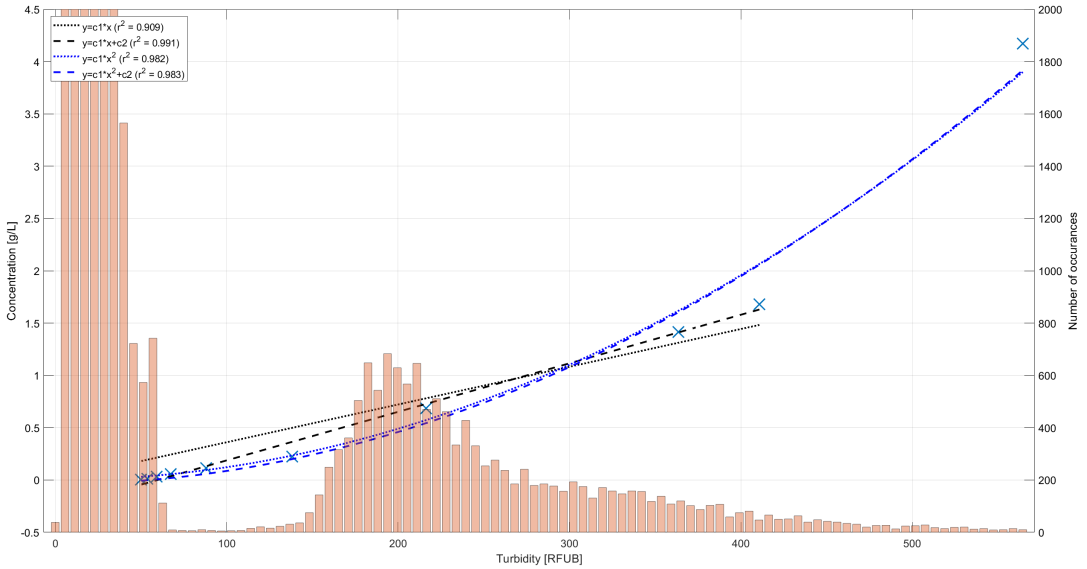

Figure D.2: Four different calibration curves with regression coefficient for OBS sensor 3 that are fitted to the lab measurements shown as a blue X. In orange the occurrence of each turbidity value is shown.

For both the sensors the linear regression line with a negative value for B has been chosen as the best fit. This fit has the highest correlation coefficient of 0.998 for OBS1 and 0.992 for OBS3. Moreover, this line represents the most frequent turbidity measurements very well, however very high turbidity values are typically underestimated. This fit has a negative value for B, which means that turbidity values below 60*RFUB* are negative which is not possible in reality. However turbidity's in this range are not included, since these are measurements when the sensor was above water. As benefit over the quadratic regression lines, the linear quadratic line can easily be scaled if necessary for modelling purposes. In order to ensure that the calibrated results accurately model the lab experiments, both measurements are plotted against each other to investigate a potential bias in Figure D.3. The linear regression line fits through all the calibration points for OBS1, however the error with the calibration results are larger for higher concentrations. For OBS3 the linear regression line seems to underpredict the very high turbidities, but shows a good fit for the rest of the measurements.

D.2. Concentration measurements

The OBS data of the two locations will be compared in order to see if the OBS sensors measure very local fluctuations or if the suspended sediment concentration is spatially in the same order. Before comparing the OBS

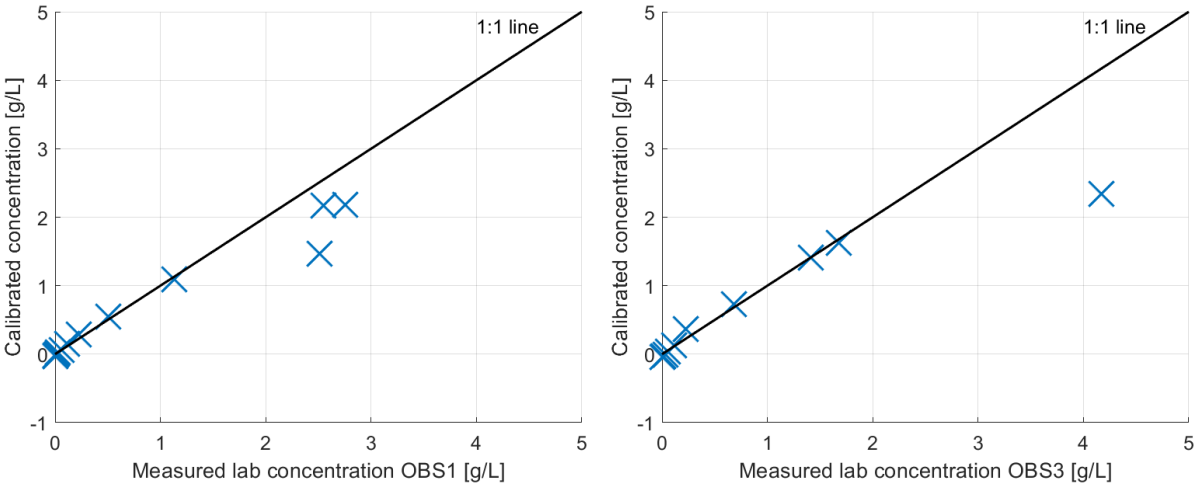

(a) OBS1 **(b)** OBS3

Figure D.3: Calibrated OBS measurements plotted against the measured lab concentration.

sensors, outliers are removed based on a threshold of 10 g/L. If the concentration is above the threshold value it will be seen as outlier and the value is interpolated between the value before and after the outlier. Furthermore it is known that OBS sensor 1 is located at $0.64\,m$ *NAP* and OBS sensor 3 at $1.04\,m$ *NAP*. When the water level is below the sensor height, the OBS measurement is removed.

When correlating the raw data as shown in Figure D.4 there is a reasonable correlation between the two sensors ($r = 0.74$), this means that the sensors are not picking up local extremes, but capture the suspended sediment concentration throughout Perkpolder quite well. In general OBS sensor 3 has larger concentration than OBS sensor 1, which is logical since OBS sensor 3 is located near the entrance of Perkpolder, while OBS sensor 1 is more located in a sheltered part of the polder. In September and October 2016 the sediment concentration is for both OBS sensor 1 and 3 significantly higher than during the rest of the period.

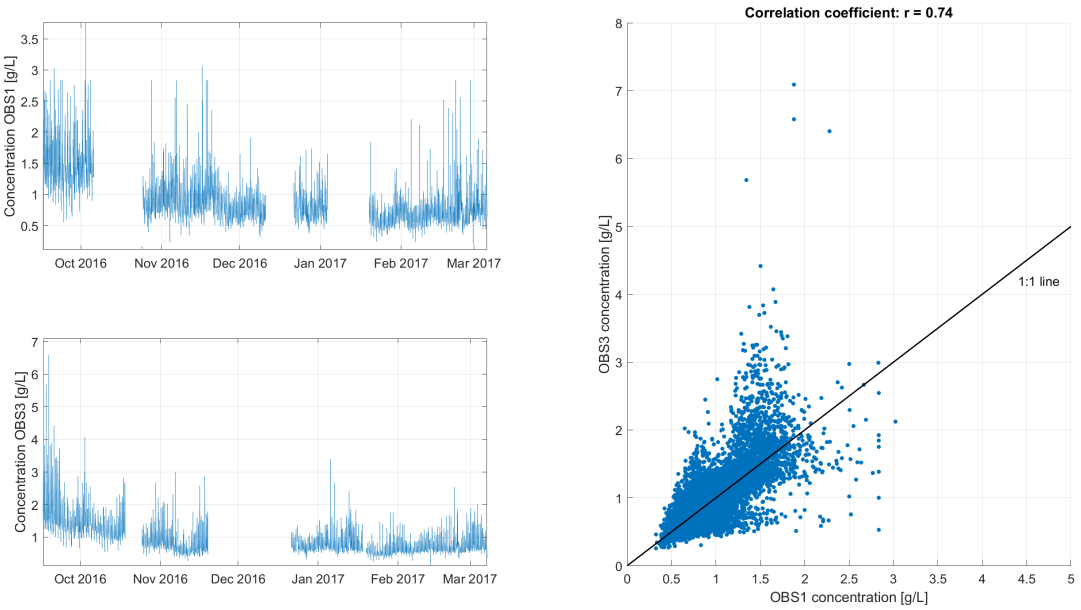

Figure D.4: Right: time series of OBS1 and OBS3 after processing of raw data. Left: correlation between OBS1 and OBS3.

D.3. Rouse number at measurement locations

Until now, it is implicitly assumed that the concentration measured by the OBS sensor is the depth averaged concentration. To validate this assumption, the Rouse number will be calculated. Assuming a steady, uniform

flow, Rouse derived an equation for the vertical distribution (along the water depth) of the suspended sediment concentration, shown in Equation D.2. In this equation, R_0 is the Rouse number, which can determined using Equation D.3 (Kumbhakar et al., 2017).

$$\frac{c}{c_a} = \left(\frac{y_0 - y}{y} \frac{a}{y_0 - a} \right)^{R_0} \tag{D.2}$$

$$R_0 = \frac{w_s}{\kappa u_*} = \frac{w_s}{\kappa \sqrt{\tau_0 / \rho}} \tag{D.3}$$

The Rouse number determines the shape of the sediment concentration profile as shown in Figure D.5. Therefore this is a good indication if the measured concentrations can be considered depth-averaged.

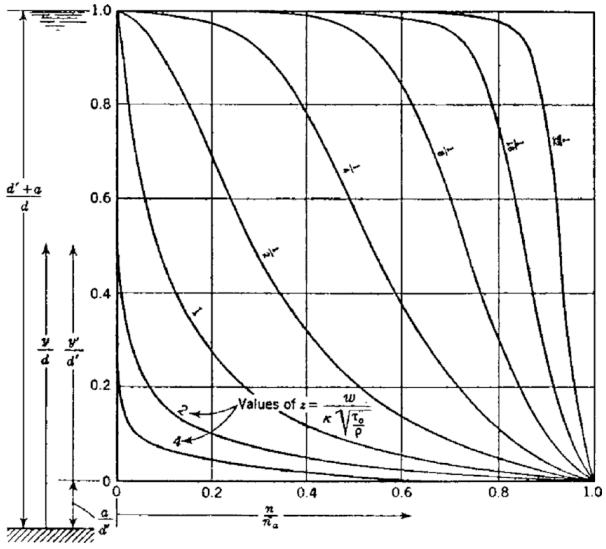

Figure D.5: Concentration profiles for different Rouse numbers ($1/32$ to 4) (Ettema, 2006).

To calculate the Rouse number for both measurement stations, an average bed shear stress will be determined for when the sensor is submerged in the water as shown in Figure D.6. This leads to an average bed shear stress of $0.02\,N/m^2$ for OBS1 and $0.23\,N/m^2$ for OBS3. Using a settling velocity of 0.2 mm/s which has been used more for the Western Scheldt (e.g. Temmerman et al. (2003a) and Winterwerp et al. (1993)). This leads to a Rouse number of 0.10 and 0.03 for respectively OBS1 and OBS3. So OBS1 is close to the line $1/8$ and OBS3 to $1/32$, the concentration is measured roughly $10\,cm$ above the bed, therefore OBS3 is likely to measure the depth averaged concentration while OBS1 will slightly overestimate the depth averaged concentration.

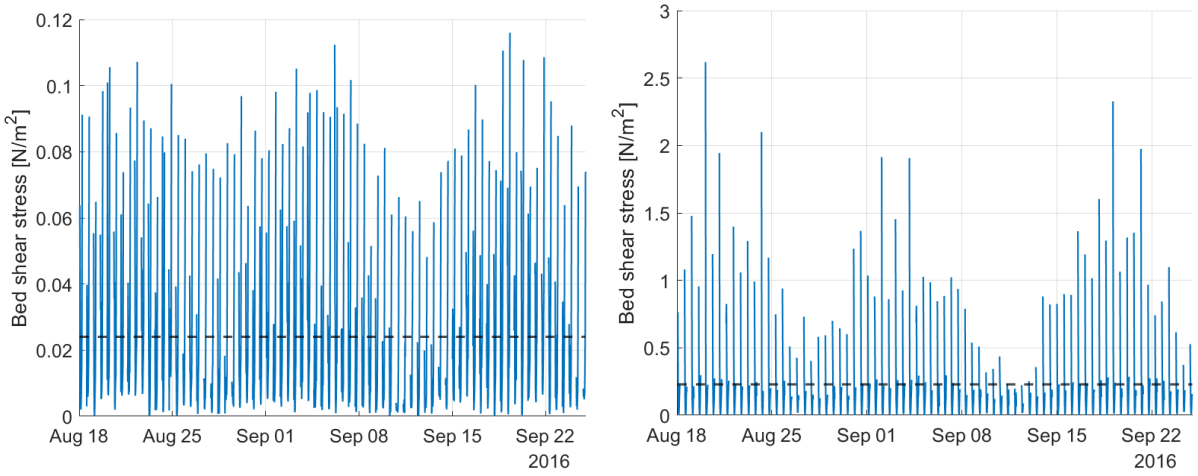

(a) OBS1

(b) OBS3

Figure D.6: Calibrated OBS measurements plotted against the measured lab concentration.

D.4. Calibration restrictions

It is important to understand the restrictions of the calibration procedure, in order to weight the conclusions from this data set. Four sources for errors in the calibration procedure are discussed.

- The first error source is the type of material used for calibration. For the calibration procedure material from the bed has been used, however suspended sediment that is measured is typically finer than the bed material for the calibration curve. This can cause an overestimation of the suspended sediment concentration, since larger particles reflect more light.
- As shown in Table D.1 the OBS sensors have been removed from the water for multiple times. The reason for removal is not given, however it is possible that debris is removed from the device. This debris can also give an overestimation of the measured suspended sediment concentration. It is striking that the high turbidity values of September and October are mainly found during the first measurement interval from 16-9-2016 to 20-10-2016.
- The third error source in the measurement of suspended sediment is the algae concentration. Since algae will also reflect the emitted waves, the algae season could be a factor of influence on the measurements. De Jong et al., 1995 and Nederbragt, 2001 show that algae concentration is highest in the early summer (May to July) and decreases to a minimum in the winter months. The concentration difference in algae between the different months is significant, however the concentration of algae is in the Western Scheldt in the order of $\mu g/L$ while the suspended sediment concentration is in the order of mg/L (Nederbragt, 2001).
- OBS1 has an average Rouse number of 0.10, therefore the measured concentrations near the bed will be higher than the depth averaged concentration (see Figure D.5). OBS3 has a Rouse number of 0.03 corresponding with an almost equal concentration profile over the vertical, therefore OBS3 is a good estimate for the depth averaged profile. This could explain why OBS1 and OBS3 have almost the same magnitude, although OBS1 is located in calmer conditions.

E

Mass estimate of OBS measurement

This appendix shows how the mass import is determined from the imported sediment based on the OBS data. Moreover the methodology and calculations behind the error range of the mass import are shown. The range of imported mass based on the OBS data can come from two sources, namely different calibration curves (linear or quadratic) and different background concentrations. In total there are six combinations that can lead to a different mass import, the total imported sediment (excluding pores) is shown in Figure E.1.

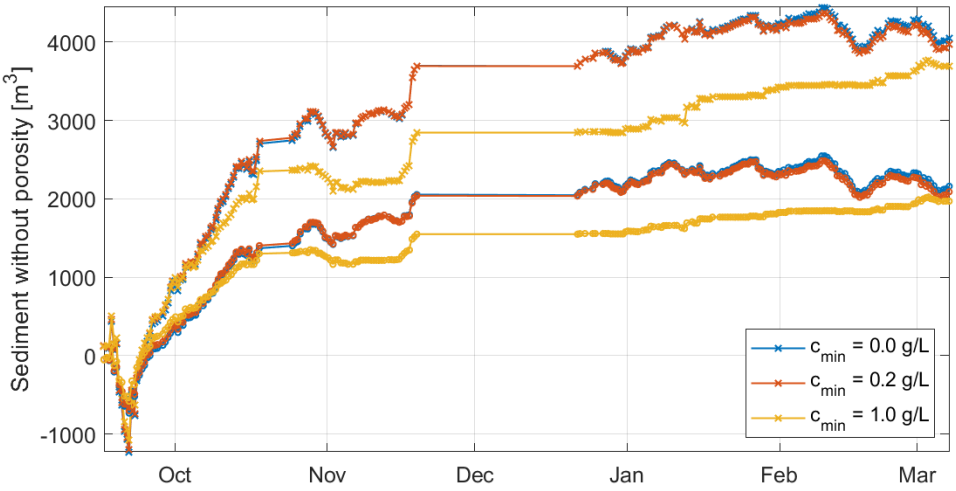

Figure E.1: Total sediment import (excluding pores) for different calibration curves: quadratic (X) and linear (O). Moreover different background concentrations are assumed when the sensor is above water.

The range in total imported sediment of the measurement period will result in the range of total yearly mass import. The turbidity sensor measures the concentration of suspended sediment in the water, therefore the total sediment volume is without pores. Equation E.1 is used to convert the concentration to total sediment mass per year. To compensate for the fact that the OBS measurements are from 16-9-2016 to 19-4-2017 (with a lack of data from 19 Nov to 21 Dec), the data are corrected to resemble a whole year. The result of this calculation is shown in Table E.1.

$$m_s = V_s \cdot \rho_s \cdot \frac{t_{year}}{t_{measurement}} \tag{E.1}$$

Concluding from Appendix D the linear calibration curve was favoured above the quadratic calibration curve. Furthermore, it was found that the background concentration for the turbidity measurements lies around 150 *RFUB* which after calibration corresponds with the $0.2 g/L$. Therefore the best estimate is determined to be the linear calibration curve with a background concentration of $0.2\, g/L$. The error bars show the margin between the quadratic calibration curve with a background concentration of $0\ g/L$ to the linear calibration curve with a background concentration of $1.0\, g/L$.

Table E.1: Mass range for different calibration curves and background concentrations.

Calibration curve	Background concentration [g/L]	Total sediment import (without porosity) [m^3]	Total yearly mass import [k ton]
Quadratic ($y = a \cdot x^2$)	0.0	4053	28.21
	0.2	3966	27.60
	1.0	3691	25.68
Linear ($y = a \cdot x + b$)	0.0	2160	15.03
	0.2	2089	14.54
	1.0	1970	13.71

F

Hydrodynamic properties of Perkpolder

This appendix shows the hydrodynamic properties of Perkpolder, this includes the presentation of the water levels at measurement station Walsoorden in Section F.1. Moreover, the water level change which is an indication of the flow velocities within Perkpolder is correlated to the tidal range in Section F.2. Section F.3 analyses the set up generated by wind. Lastly, in Section F.4 the trapping efficiency and net sediment transport are correlated to different hydrodynamic properties to indicate which processes may be leading for net sediment transport.

F.1. Water levels

Water levels of measurement station Walsoorden, close to Perkpolder, are shown in Figure F.1 from the 25th of August to the 25th of September. This time period has been used as representative month in de Vet et al. (2022) and will also be used as representative month for the models in this thesis. Missing data is shown in Figure F.1 as a discontinuity of the water level, this data is interpolated in order to correct for missing data. Since the missing data does not exceed more than 2 hours, this will not have a large effect on the results.

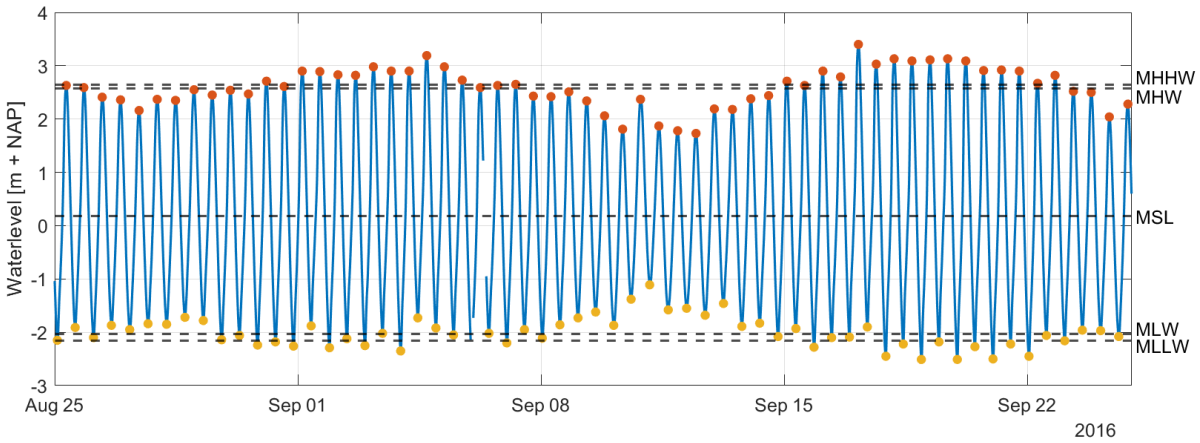

Figure F.1: Water level measurements at station Walsoorden for 25-8-2016 to 25-9-2016. The red and yellow dots show respectively the maximum and minimum water level during a tidal cycle. The black lines show the calculated tidal levels (Mean Higher High Water (MHHW); Mean High Water (MHW); Mean Sea Level (MSL); Mean Low Water (MLW); Mean Lower Low Water (MLLW))

F.2. Water level change and tidal range

Figure F.2 shows the correlation between the water level change and the tidal range for falling ($r = -0.95$) and rising ($r = 0.98$) water levels, so during inflow and outflow of Perkpolder. The water levels of 2016 and 2017 (the same period as the OBS measurements) have been used for this analysis. Concluding from Figure F.2, a large tidal range leads to higher changes in water level and thus subsequently to higher velocities within Perkpolder.

F.3. Set up due to wind

This section assesses the influence of wind on the water levels measured at Walsoorden. The residual of the water level between the measured water level at Walsoorden and the geometric water level based on the tidal constituents at Walsoorden is calculated. The amplitude and phase of the different constituents has been determined using the

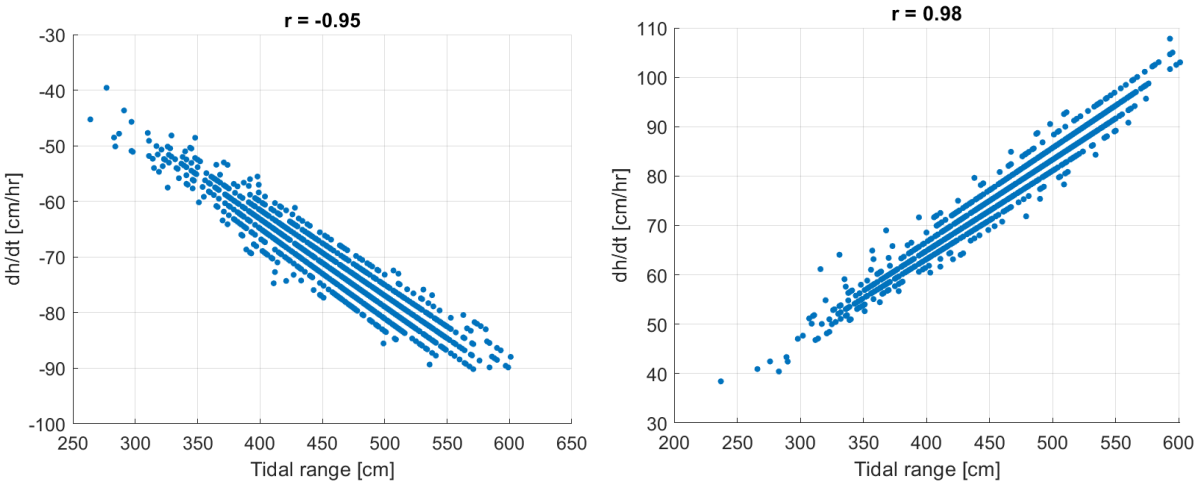

(a) Falling water levels

(b) Rising water levels

Figure F.2: Correlation between rising and falling water levels and tidal range using water levels of 2016 and 2017.

package T_TIDE of Matlab (Pawlowicz et al., 2002). By subtracting the geometric tide from the measured water levels an indication of the setup by wind is acquired. The residual water level is correlated with the wind speed of each wind quadrant, to indicate if setup or set-down is generated. Figure F.3 shows the correlation for each wind quadrant. In general winds coming from the east create set-down and winds coming from the West create setup near Perkpolder.

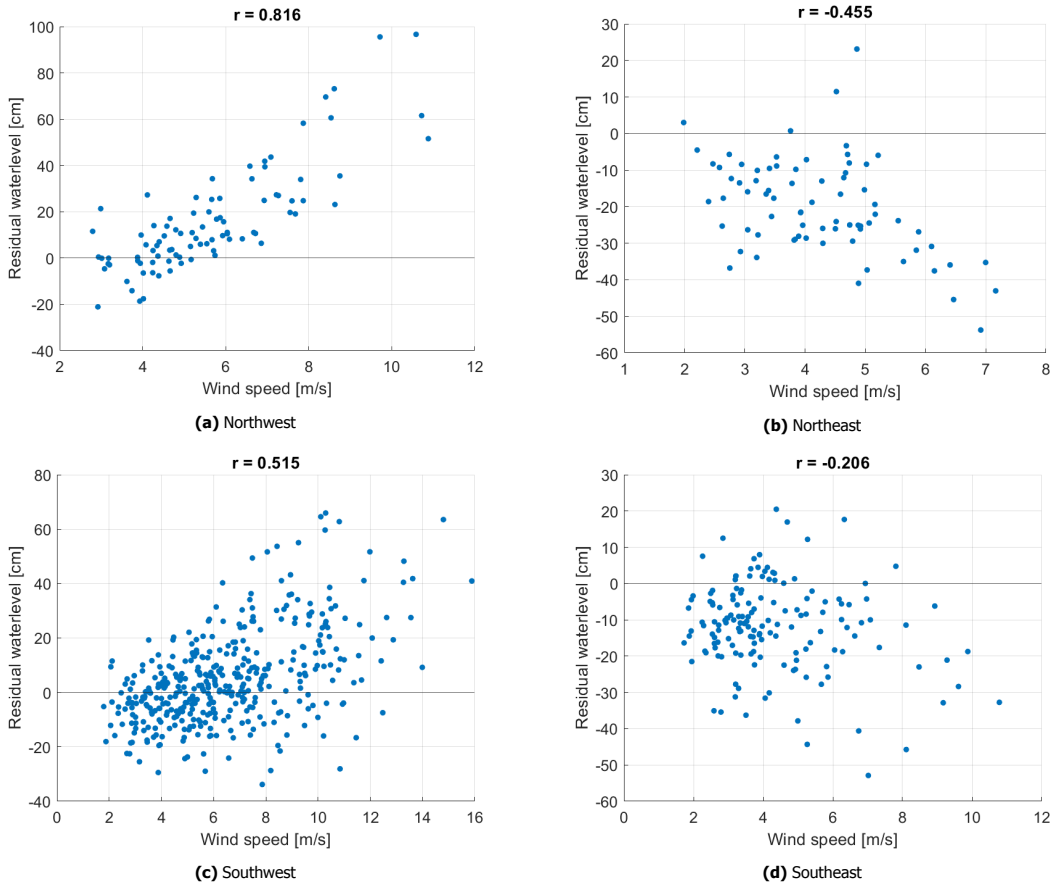

(a) Northwest

(b) Northeast

(c) Southwest

(d) Southeast

Figure F.3: Correlation between wind speed and residual water level for each wind quadrant. The residual water level is calculated by subtracting the geometric water level from the measured water level.

F.4. Correlation of hydrodynamic properties with trapping efficiencies and net sediment transport

Figure F.4 shows the correlation of different hydrodynamic and meteorological properties of Perkpolder with the net sediment transport and/or trapping efficiency. The trapping efficiency is defined as the net import/export divided by the total imported sediment. Figure F.4 and 6.7 show that the tidal range has the largest negative correlation with the trapping efficiency ($r = -0.49$). The correlation of flood discharge (Figure F.4d) and maximum velocity (Figure F.4e) with trapping efficiency is smaller than the correlation of tidal range with trapping (Figure 6.7a) efficiency. Moreover, a high flood discharge and therefore high maximum velocity are mainly caused by a high tidal range.

Secondly, although the correlation with trapping efficiency and tidal range is significant, the correlation with net sediment transport is much smaller, namely $r = -0.31$ (Figure F.4a). However the same phenomena is visible, namely that almost all net exporting tides have a tidal range larger than $4.5\ m$. The contribution of wind on net sediment transport (Figure F.4i) or trapping efficiency (Figure F.4f) seems to be limited, since no correlation could be found.

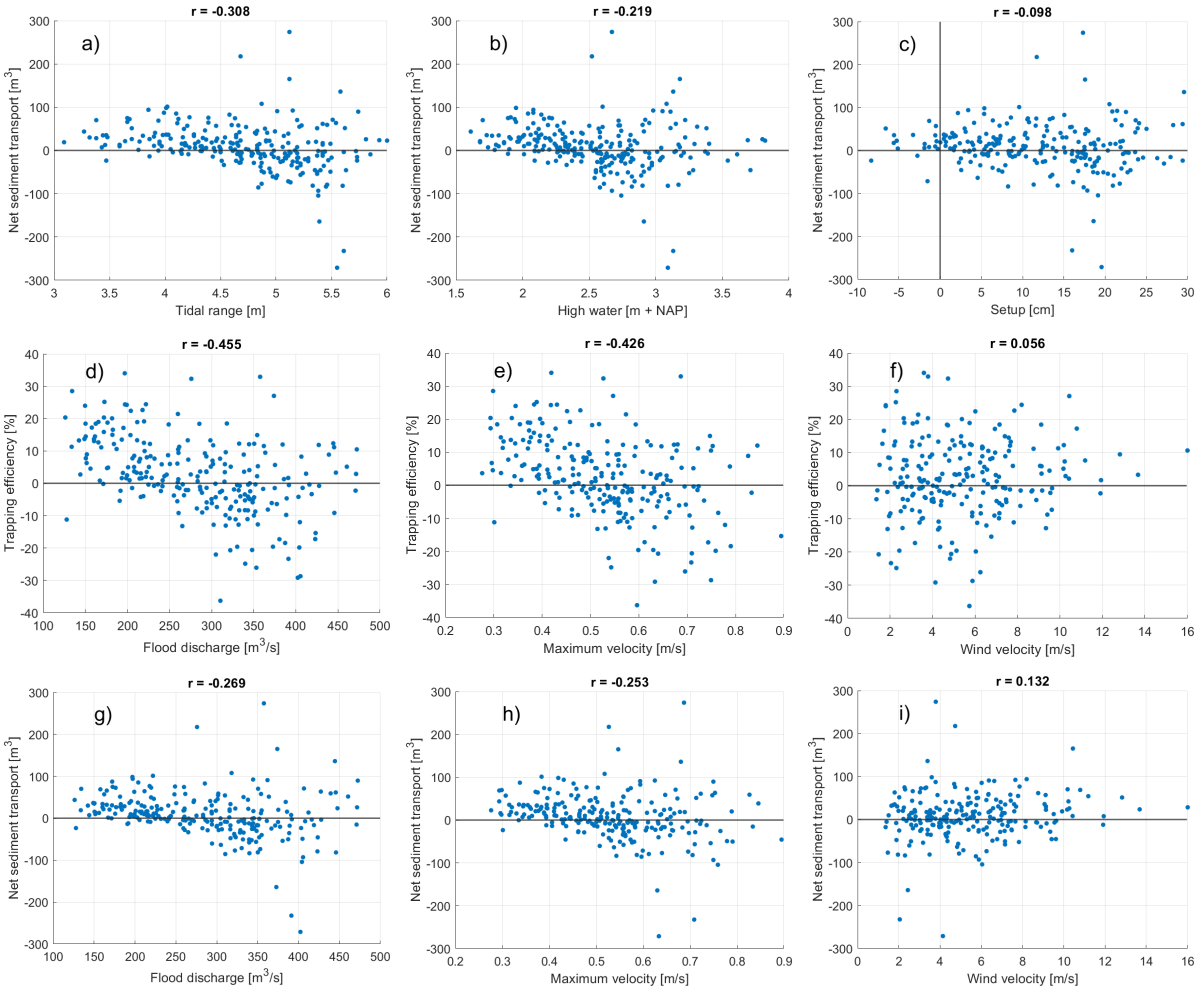

Figure F.4: Correlation of different hydrodynamic properties with net sediment transport and trapping efficiency.

G

Modelling results

This appendix shows the results of the sensitivity and scenario runs for the bathtub model. Section G.1 presents the cumulative advective and dispersive transport for RUN-A, in which the diffusivity was decreased with a factor 10. Section G.2 shows the differences in bed shear stresses in the pond for the different scenario runs. Section G.3 presents the relevant parameters to setup the wave and wind module in Delft3D. Lastly, Section G.4 shows the cumulative erosion/sedimentation results for all of the sensitivity and scenario runs.

G.1. Sediment transport when decreasing diffusivity

Figure G.1 shows the cumulative dispersive and advective transport through the entrance of Perkpolder for the model RUN-A, in which the diffusivity is decreased with a factor 10. When comparing Figure G.1 with Figure 7.2, the dispersive transport decreases almost with a factor of 10, however the total net import at the end of the simulation stays almost the same. Therefore the mode of transport will not have a large influence on the net sediment transport within Perkpolder.

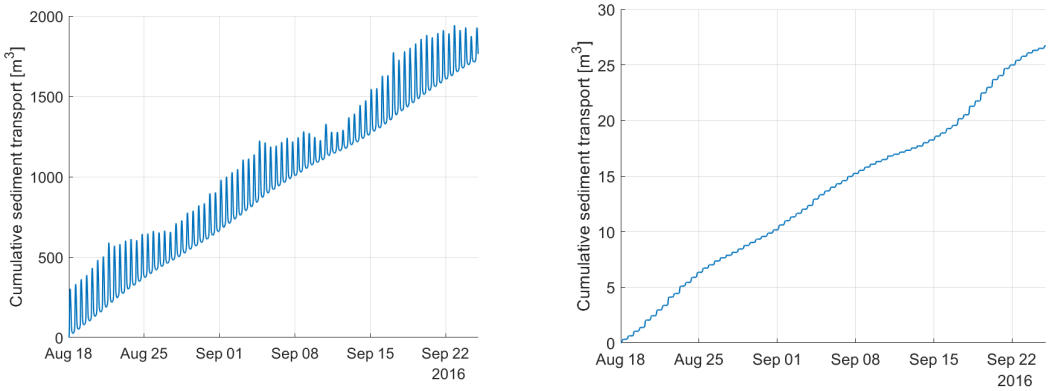

(a) Advective transport

(b) Dispersive transport

Figure G.1: Cumulative dispersive and advective sediment transport of mud-entrance in RUN-A.

G.2. Bed shear stresses in pond

The bed shear stresses in location *Pond-III* (see Figure 3.6) is presented in Figure G.2 to show how the different sensitivity simulations alter the bed shear stresses in the pond. The manning coefficient (friction coefficient) has a large influence on the magnitude of the bed shear stresses. A higher friction coefficient leads to higher bed shear stresses under the same hydrodynamic conditions. Moreover, wind and wave effects show a higher mean bed shear stress and a larger spreading. So, wind and wave effects create in general higher bed shear stresses with more temporal differences.

G.3. Parameters for simulation with wave and wind forcing

Table G.1 shows the processes and main parameters of the wave module that are used in RUN-M. These parameters have been based on de Vet et al. (2018) and have been adapted to Perkpolder if necessary (e.g. the boundary condition).

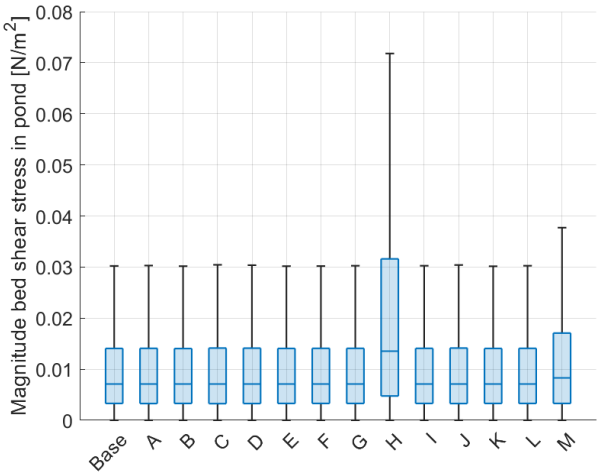

Figure G.2: Box plot of bed shear stress in the pond for different scenario runs. For visibility, outliers are not shown.

Table G.1: Parameters of wave and wind module for RUN-M.

Module	Parameter	Value	Unit
Communication	Coupling interval	30	min
Boundary	Orientation	NorthEast	–
	Significant wave height	0.2	m
	Peak period	10	s
	Direction	180	°
	Directional spreading	4	°
Processes	Spectrum	JONSWAP	–
	Peak enhancement factor of Jonswap spectrum	3.3	–
	Generation mode of physics	3	–
	Alpha coefficient for wave breaking	1	–
	Gamma coefficient for wave breaking	0.55	–
	Bottom friction type	Madsen et al.	–
	Bottom friction coefficient	0.05	–
	Include wind growth	True	–
	Formulation of whitecapping	Komen et al.	–
	Include diffraction	False	–
	Include triads	False	–
	Include quadruplets	True	–
	Include refraction	True	–
	Include frequency shifting in frequency space	True	–

G.4. Cumulative sedimentation/erosion

This section presents the cumulative sedimentation/erosion in Figure G.3 and G.4 for all the sensitivity runs (RUN-A to RUN-M) and the scenario runs (RUN-S1 to RUN-S9). These figures can be used as background to investigate how the sensitivity and scenario runs altered the morphology of Perkpolder. Moreover the erosion, accretion and net volume of each of the runs together with the mean bed level change of the intertidal area is shown in Table G.2.

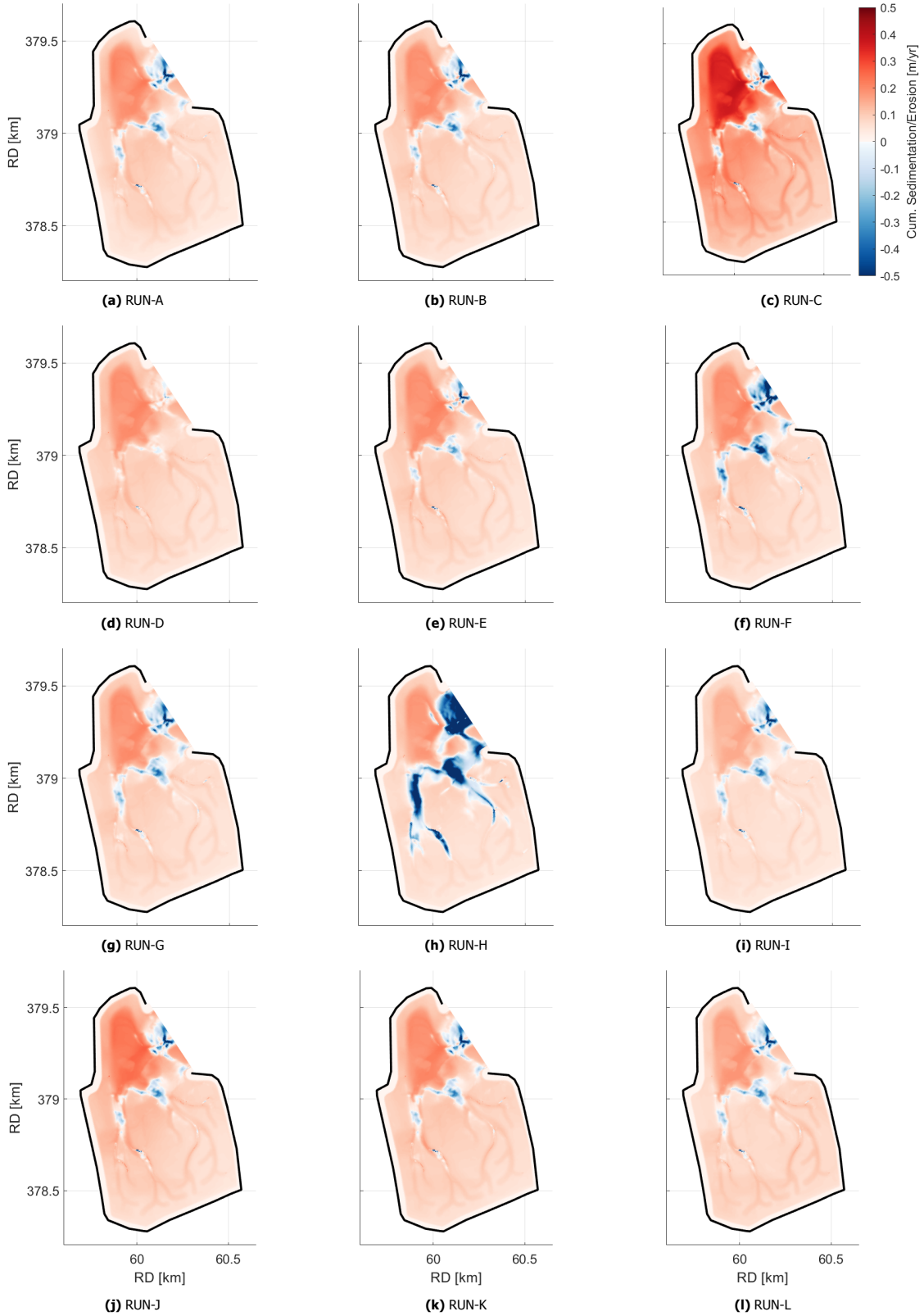

Figure G.3: Cumulative sedimentation/erosion of model runs (RUN-A to RUN-L). The model is run for one month and the cumulative erosion/sedimentation is scaled to a year.

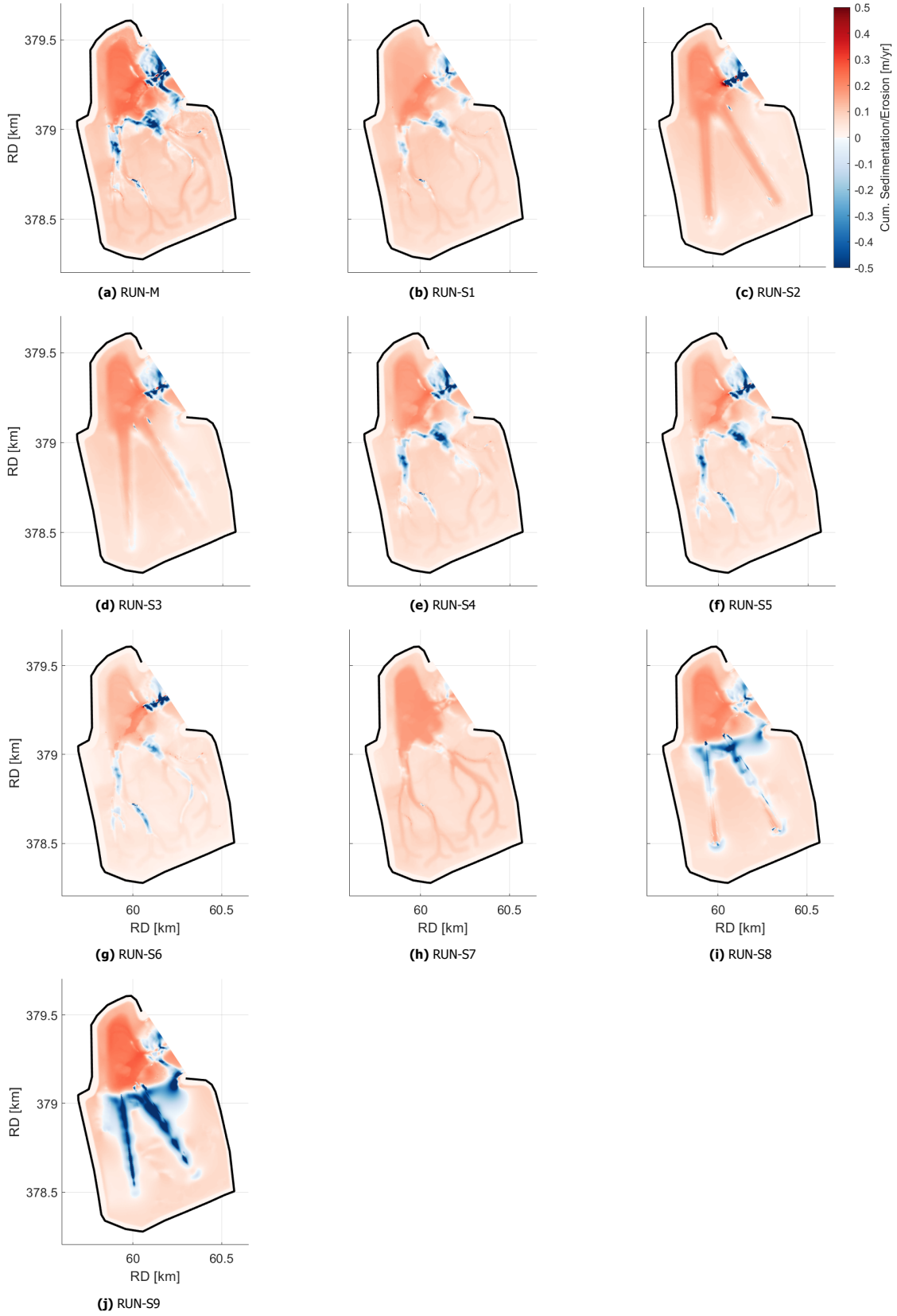

Figure G.4: Cumulative sedimentation/erosion of model runs (RUN-M, RUN-S1 to RUN-S9). The model is run for one month and the cumulative erosion/sedimentation is scaled to a year.

Table G.2: Numerical results of cumulative sedimentation/erosion of each run.

RUN	Erosion volume [m^3]	Accretion volume [m^3]	Net volume [m^3]	Mean bed level of intertidal area [cm/yr]
RUN-BASE	$4.41 \cdot 10^3$	$9.45 \cdot 10^4$	$9.01 \cdot 10^4$	6.03
RUN-A	$4.43 \cdot 10^3$	$9.21 \cdot 10^4$	$8.76 \cdot 10^4$	5.82
RUN-B	$4.45 \cdot 10^3$	$9.44 \cdot 10^4$	$9.00 \cdot 10^4$	6.03
RUN-C	$2.67 \cdot 10^3$	$1.82 \cdot 10^5$	$1.79 \cdot 10^5$	12.59
RUN-D	$1.53 \cdot 10^2$	$9.92 \cdot 10^4$	$9.91 \cdot 10^4$	7.15
RUN-E	$2.63 \cdot 10^3$	$9.77 \cdot 10^4$	$9.51 \cdot 10^4$	6.56
RUN-F	$1.06 \cdot 10^4$	$9.28 \cdot 10^4$	$8.22 \cdot 10^4$	4.99
RUN-G	$5.69 \cdot 10^3$	$9.23 \cdot 10^4$	$8.66 \cdot 10^4$	5.66
RUN-H	$3.97 \cdot 10^4$	$7.40 \cdot 10^4$	$3.43 \cdot 10^4$	-0.39
RUN-I	$5.19 \cdot 10^3$	$7.33 \cdot 10^4$	$6.81 \cdot 10^4$	4.44
RUN-J	$3.80 \cdot 10^3$	$1.16 \cdot 10^5$	$1.12 \cdot 10^5$	7.63
RUN-K	$4.11 \cdot 10^3$	$1.05 \cdot 10^5$	$1.01 \cdot 10^5$	6.95
RUN-L	$4.81 \cdot 10^3$	$9.32 \cdot 10^4$	$8.84 \cdot 10^4$	6.02
RUN-M	$1.55 \cdot 10^4$	$1.10 \cdot 10^5$	$9.43 \cdot 10^4$	5.34
RUN-S1	$3.79 \cdot 10^3$	$9.21 \cdot 10^4$	$8.83 \cdot 10^4$	6.12
RUN-S2	$8.07 \cdot 10^3$	$9.53 \cdot 10^4$	$8.72 \cdot 10^4$	5.88
RUN-S3	$5.01 \cdot 10^3$	$8.73 \cdot 10^4$	$8.23 \cdot 10^4$	5.45
RUN-S4	$1.05 \cdot 10^4$	$8.14 \cdot 10^4$	$7.09 \cdot 10^4$	4.09
RUN-S5	$1.13 \cdot 10^4$	$7.00 \cdot 10^4$	$5.87 \cdot 10^4$	3.14
RUN-S6	$7.20 \cdot 10^3$	$5.72 \cdot 10^4$	$5.00 \cdot 10^4$	2.85
RUN-S7	$1.02 \cdot 10^2$	$9.60 \cdot 10^4$	$9.59 \cdot 10^4$	6.85
RUN-S8	$1.44 \cdot 10^4$	$8.02 \cdot 10^4$	$6.59 \cdot 10^4$	3.11
RUN-S9	$3.87 \cdot 10^4$	$8.69 \cdot 10^4$	$4.82 \cdot 10^4$	-0.66